THE MODULATION OF CORTICAL DENDRITES DURING SENSORY PERCEPTION AND LEARNING

Luca Godenzini

(ORCID ID: 000-0001-9060-8500)

The Neural Networks Laboratory
The Florey Institute of Neuroscience and Mental Health
The University of Melbourne

September 2020

This thesis is being submitted in total fulfilment of the requirements of the degree of Doctor of Philosophy

THESIS ABSTRACT

Sensory perception arises in the cortex by integrating external information from the environment with internal representations and the current brain state. This process is supported by the structure of the neocortex and the organisation of excitatory inputs onto its core computational element: the pyramidal neuron. In layer 2/3 pyramidal neurons, external (feedforward) information mainly target the somatic region, while internal (feedback) information runs through layer 1 and lands onto distal tuft dendrites. Cortical dendrites have active properties that could be important for sensory processing and could provide a cellular mechanism to support the flexibility of sensory representations during learning.

In this thesis, I addressed the role of L2/3 pyramidal neuron dendrites during sensory perception and learning in three parallel studies that investigated: 1) how inputs from another sensory area affect early stages of sensory processing; 2) the modulation of sensory processing in dendrites of the auditory cortex following fear conditioning; 3) changes in dendritic activity during perceptual learning of an auditory discrimination task. To tackle these questions, a combination of two photon Ca^{2+} imaging and whole cell patch clamp electrophysiology in vivo, together with behavioral testing and optogenetics manipulation, was used.

The results presented here confirm that dendrites encode sensory information and show that they can undergo plastic changes during learning. The findings also illustrate the existence of compartmentalised activity in L2/3 pyramidal neurons and of a cellular mechanism for the control of action potential generation that involve dendritic integration. The results presented in this thesis highlight the importance of the upper layers of the cortex for flexible sensory representation through the integration of feedback and feedforward information.

DECLARATION

I declare the following to be true:

- This thesis is composed only by original work that was produced for the completion of the Doctor of Philosophy;

- This thesis conforms with the relevant policies and procedures and the words count is within the limit;

- Due acknowledgments and other contributions were listed in each section;

- Permission to use data in the manuscript with multiple authors is included;

Luca Godenzini

PREFACE

None of the work presented in this thesis has been submitted for other qualifications or carried out prior to enrolment in the degree.

The work presented in Chapter 3 was initially submitted for publication to Nature Neuroscience in March 2019 and, underwent two rounds of peer reviewing process according to the journal standards and policies. In August 2020, the manuscript was submitted to Nature Communications.

The study presented in Chapter 4 was submitted for publication in April 2020 to Cell Reports and underwent one round of review.

I acknowledge the financial support of the Australian Government Research Training Program Scholarship, of the National Health and Medical Research Council through the research training program scheme and the project grants (APP1086082, APP1063533, APP1085708), of the Australian Research Council (DP160103047) and of the Sylvia and Charles Viertel Charitable Foundation.

ACKNOWLEDGMENTS

Pursuing a PhD in Neuroscience has been one of the clearest decisions of my life so far. However, when I decided to move to Melbourne, to join the Neural Network Lab at the Florey as a PhD candidate, I felt that I had made huge bet.

My first and most important acknowledgment is towards the person that constantly proved to me that it was the right one: my supervisor, Dr. Lucy Palmer. Lucy is an exceptional mentor and offered me invaluable support throughout these years. Under her guidance I learned what it really means to be a Neuroscientist. Lucy showed me that positive attitude and hard work are powerful allies, especially when things do not go your way. She taught me to trust myself, and to push the boundaries of what I could achieve. Lucy introduced me to her neuroscience "family" making me feel welcomed and empowered. For all of these and more, I will always be grateful. To all the members of the Neural Network Lab, past and present. From the beginnings, when a bunch of us were learning how to patch every day, rig-by-rig, next to each other, to the diverse and interesting group of people and projects that the lab is today. Thanks for the great science and non-science talk, the help with experiments and analysis, the moral support and the occasional karaoke night. I especially want to thank Danilo La Terra as a lab mate and, more importantly, as a friend. Dani's work ethic and dedication have been a constant source of inspiration for me.

They say that PhD life is made of highs and lows. They are not wrong. I am lucky to have amazing friends next to me in both situations: to Federico, Natasha and to all my Aussie family. Thanks to the Florey and particularly to my fellow students for creating a fun and relaxed environment. To the University of Melbourne Ultimate Frisbee team and the Chilly family for providing me with a great distraction from science and many incredible experiences.

All of this made my PhD an adventure way more exciting and stimulating than I could have ever imagined.

Finally, and most importantly, my deepest gratitude and love goes to my family at home: my mother, father and my sister. Since I can remember, you have given me unconditional love and the support to pursue my lifegoals, even when they were taking me far away from you.

No word is enough, all of this is thanks to you.

TABLE OF CONTENTS

TABLE OF FIGURES

CHAPTER 1

GENERAL INTRODUCTION

CHAPTER 1

SENSORY PROCESSING IN THE NEOCORTEX

Understanding how the brain processes sensory information and drives behavior is currently one of the most important questions in neuroscience. The ability to extract information from sensory signals in the world around us is fundamental to survival and is a driving force for evolution. The brain has to coherently combine an incredible amount of information to be able to source food, find a partner, learn how to use tools or develop a phone app that can do all these things. It is of course not an easy feat to determine how sensory perception arises in the brain, however decades of research have indicated that part of the answer may lie in the functional properties of neurons and their connectivity[3-6]. These are the key principles that coordinates how the brain is able to sense and interact with the world. Moreover, prior experience plays a fundamental role in shaping neural activity and perception to allow us to fit into an ever-changing environment[7,8].

So, how do we make sense of the world around us? At a very fist stage, sensory signals are captured by the peripheral nervous system through a specialised set of sensory receptors and conveyed via specific sensory streams up to the brainstem. From here, through the thalamus and other subcortical structures, sensory information reaches the neocortex. Traditionally sensory processing in the neocortex follows a hierarchical pathway where information is processed starting from low-level physical attributes up to building complex features of the sensory percept. This information is then used to guide choices and actions.

Primary sensory areas are the first stage of neocortical processing as they are the main recipient of sensory information from the primary nuclei of the thalamus. These thalamic projections carry information about the external sensory environment to primary sensory areas and are defined as feedforward inputs. Therefore, primary sensory areas are highly organised according to a specific sensory modality and selectively process the physical attributes of sensory signals such as orientation (visual)[9,10], frequency (auditory)[11-13] or vibration (touch)[14,15]. As

information moves forward in the processing stream to secondary and association areas, a unified percept is built, and sensory perception arises. However, in recent years, neuroscientists started to realise that this view is far too simplistic. Once the tools to record with single cell precision in the awake brain became available (i.e. single unit recordings and two photon microscopy)[16-18] it was clear that something more complex was going on in primary sensory areas. Indeed, evidence of higher order integration and modulation in primary sensory cortices has been recently accumulating. Multisensory integration[19,20], sensory-motor integration[21,22], experience dependent plasticity[23], memory[24], expectation[25], attention[26] and locomotion[27-29] are all aspects of a sensory percept that can be already encoded in primary sensory areas. Moreover, what has in the past been considered as noise (i.e. spontaneous activity) may actually reflect dynamics of brain-wide activity underlying spontaneous behavior[30,31]. All this information reaches sensory areas through feedback inputs, that carry internal signals such as the current brain states or previous experiences. Feedback inputs to primary cortices runs mostly through the upper layer of the cortex, in particular in layer 1 (L1), and are carried by the efferent axons of other cortical areas or sub-cortical structures (i.e. higher order thalamus)[32]. As such, top-down input exerts an important control over sensory processing in primary areas and heavily contributes to the building of sensory representations. It seems that, in an effort towards optimisation, the brain creates an internal representation of the world (feedback) which is constantly updated by our current experience (feedforward). In this model, the integration of feedforward and feedback information is of key importance to sensory processing and in advancing our understanding of how the brain works.

CHAPTER 1

The architecture of the neocortex

The neocortex is a thick layer of cells that constitutes a large and outmost portion of the mammalian brain. It is a layered structure which follows a highly organised and specialised architectural principle. Understanding the different functions of each cortical layer and how they are integrated to form sensory perception is of great importance and yet is still, for the most part, uncharted territory[4].

Each cortical layer is composed of various cell types which are locally connected according to a rule which defines the flow of information: sensory input from the thalamus lands in layer 4 (L4) and propagates to layer 2/3 (L2/3) and then layer 5 (L5). In addition, the distribution of feedforward and feedback input into the cortex is laminar specific (Figure 1.1). The central layer, specifically L4, receives most of the feedforward inputs from primary thalamic nuclei which carries external information about the sensory world[33]. Feedback inputs from other cortical or subcortical areas instead brings internal information about the past or current brain state, and runs horizontally to the surface of the brain within L1[32].

L1 is an enigmatic and interesting region of the cortex as, different to all other layers, it contains very few cell bodies, most of which are inhibitory, in addition to long range axonal projections[34,35]. Here also lie the distal tuft dendrites of L2/3 and L5 pyramidal neurons which indeed receive synaptic inputs from both inhibitory interneurons and excitatory axons. Importantly, local and long range connections within L1 can modulate the activity of the lower layers of the cortex[5,26,36,37,38]. As a result, it is believed that L1 has an important role in top-down control of sensory activity in the cortex.

Organisation of excitatory inputs onto a pyramidal neuron

The pyramidal neuron is considered the main computational unit of the cortex. Although there are other cell types within the cortex, pyramidal neurons make up for the vast majority (70-

85%) of cell types in the cortex[39]. Despite different morphological and functional differences according to their laminar location, pyramidal neurons are all excitatory and possess a well described sets of dendrites. In most pyramidal neurons a single apical dendrite projects from the soma towards the surface of the brain (could be two in the case of some L2/3 pyramidal neurons). At the most distal region in L1, the apical dendrite branches into thinner dendritic arborisations which are called tuft dendrites. In addition, dendritic arborisations called basal dendrites project radially from the soma. The location of these two sets of dendrites within the cortical layers defines an organising principle for excitatory inputs into a pyramidal neuron (Figure 1.1). Tuft dendrites are found in the upper L1 of the cortex where long range projections land and therefore will receive mostly feedback inputs. The vast majority of synapses onto tuft dendrites come from long range projecting axons[32]. In contrast, basal dendrites, which reside deeper in the cortex, are typically targeted by feedforward inputs. This wiring diagram (Figure 1.1) has been supported by functional studies that have mapped the organisation of excitatory inputs onto pyramidal neurons[40]. Here, it is highlighted that, while in L5 there is some overlap of the two streams, an actual neat segregation of feedback and feedforward input onto tuft and basal dendrites respectively is present in L2/3 pyramidal neurons[41]. This suggests that the pyramidal neuron in itself could have an important role in integrating feedback and feedforward information.

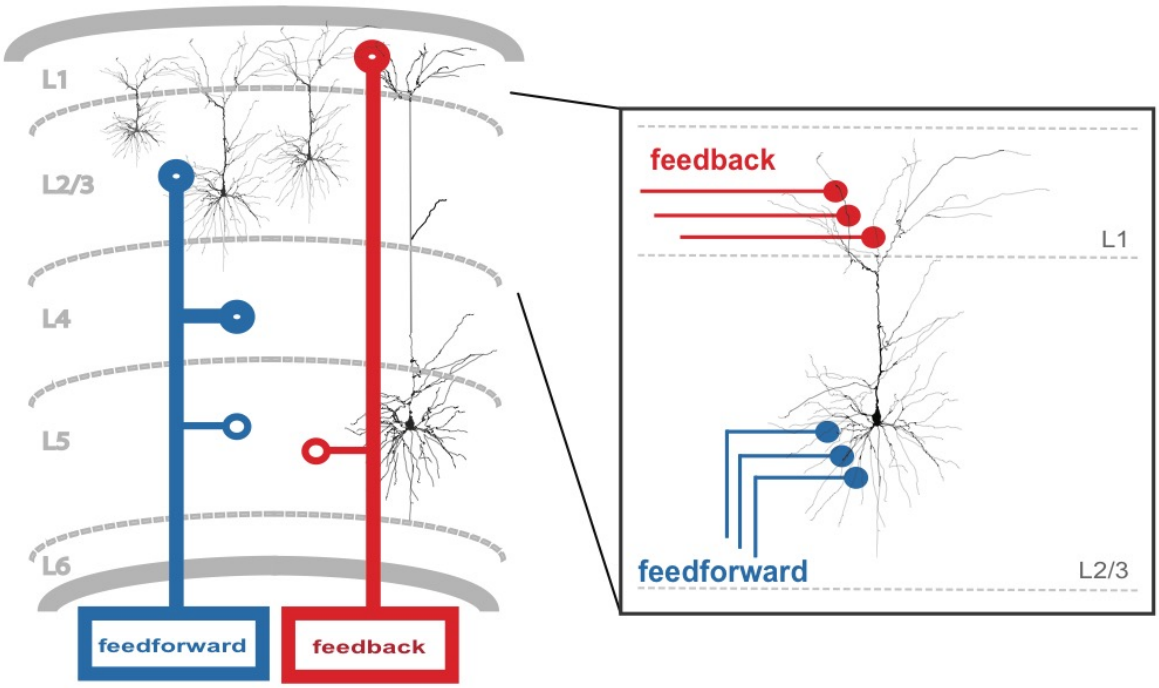

Figure 1.1 | Architectural organisation of inputs into primary sensory areas of the neocortex. The feedforward pathway conveys sensory information about the external world which mainly target layer 4 (L4) of primary sensory cortices. The local recurrent network defines a feedforward flow of information from L4 up to L2/3 and finally to L5. Feedback information are long range projections from sub-cortical and other cortical regions which land, for the majority, on L1. This wiring diagram also define the organisation of excitatory input onto the L2/3 pyramidal neurons (inset): feedforward inputs target basal dendrites and the peri-somatic region in L2/3, while feedback inputs land on tuft dendrites in L1.

CHAPTER 1

A cellular model for the integration of synaptic inputs

The ability to make predictions about the world by using past experiences to guide our current perceptions is a key feature of the brain, however, it can be argued that such a complex mechanism would only emerge at a large scale. Why would a system, so complex in its entirety, already need to integrate so much information in its single unit component? It is not the intention of this paragraph is to answer this spiny question, however, decades of evidence about the functional properties of pyramidal neurons have highlighted its incredible computational power and ability of integrating information. It is now clear that neurons should be considered as a single unit compartment and that what happens in distal sub-compartments (i.e. dendrites) can drastically affect the output of a cell.

We have highlighted how the wiring diagram of the cortex and the morphological properties of pyramidal neurons suits each other beautifully to enable the integration of different streams of information at a cellular level. However, in the upper layer of the cortex, where feedback inputs mainly arrive, only few cell bodies (mostly interneurons) and the tuft dendrites of L2/3 and L5 pyramidal neurons are found. Tuft dendrites are spatially quite far from the action potential initiation zone in the axon hillock[42]. If dendrites are cables that passively conduct currents, tuft dendrites would be electrically isolated from the rest of the cell as any distal inputs would be greatly attenuated before reaching the soma. This would basically mean that all feedback information in tuft dendrites do not contribute to somatic output. It seems reductive to think that so much important information would not be transferred to synaptically coupled cells. Indeed, dendrites have active properties and can generate all-or-none events, termed dendritic spikes, which extend the influence of distal dendritic compartments to the somatic region[43-46]. Dendritic spikes are complex phenomena that have been widely investigated in vitro and recently, also in vivo.

Pyramidal neurons possess a second action potential initiation zone, close to the apical dendritic bifurcation[47]. This area is enriched with calcium channels that when activated can depolarise the compartment to a threshold level and generate non-linear events, namely Ca^{2+} spikes [43,47]. The occurrence of a Ca^{2+} spike causes a sustained depolarization (plateau potential) in the dendrites which can spread to the somatic region and cause bursts of action potentials. In addition, when a Ca^{2+} spike is triggered at the same time as an action potential, the somatic output is increased[32]. Furthermore, the generation of an action potential at the soma can lower the threshold for initiating a Ca^{2+} spike[47]. This phenomenon is called backpropagating action potential and defines a bidirectional flow of information in the pyramidal neuron[48]. In this way, both action potential initiation zones can influence each other creating a perfect built-in mechanism for coincidence detection. According to its biophysical properties, a pyramidal neuron could therefore detect and integrate inputs arriving at different locations and combine feedback with feedforward information. In addition, dendrites can compute information locally and independently. In fact, an incoming input onto distal tuft dendrites produces an excitatory post synaptic potential (EPSP) which by itself has a small effect on both spike initiation zones[49]. However, the presence of active conductances in the more distal tuft dendrites contribute to the generation of local, non-linear, events which are NMDA dependent and have been therefore termed NMDA spikes[42,50]. These types of dendritic spikes can influence the Ca^{2+} initiation zone and further increase the somato-dendritic coupling[50]. NMDA spikes can occur also in basal dendrites although they seem to follow slightly different rules[51,52]. Basal dendrites receive a vast amount of synaptic inputs from other local pyramidal neurons and primary nuclei of the thalamus[41,51,52] as part of the feedforward pathway. Their role has been less explored, nonetheless, being much closer to the action potential initiation zone, there is no doubt that they have an important role in the integration of synaptic inputs and controlling the somatic output. This further highlights the importance of both feedback and feedforward inputs

in shaping pyramidal neuron activity and the presence of a cellular mechanism for coupling different streams of information.

Dendritic integration during sensory perception

Despite playing a clear role in the cellular integration of synaptic inputs, whether dendrites have an important role during sensory perception is still hotly debated. Indeed, while dendritic activity has been extensively studied in vitro, their role during sensory perception and behavior has only recently been investigated. The development of two photon microscopy and calcium sensors were of great importance for these studies[16-18]. These techniques allow us to look inside the brain of an awake behaving animal and record activity of neurons and dendrites with unprecedent spatial resolution. Notably, dendritic spikes were recorded in vivo in L2/3 pyramidal neurons with both optical and electrophysiological techniques[50,53]. Studies with simultaneous recording of dendritic and somatic activity have provided a direct evidence of local dendritic spiking[50,53-55]. NMDA spikes occur in vivo not only spontaneously but also during sensory stimulation, both in presence and absence of somatic action potentials[50]. Importantly, when an NMDA spike is triggered during sensory stimulation the somatic output is increased. Dendritic spikes are tuned to the orientation of visual stimuli and their disruption decrease the orientation selectivity of pyramidal neurons[53]. Moreover, non-linear dendritic integration is involved in active somatosensation and the processing of sensory-motor signals[22]. Recently, Takahashi et al. have provided evidence that calcium signals in apical dendrites of somatosensory L5 pyramidal neurons are causally linked with the threshold for sensory detection of whiskers stimulation[56]. This study is the first to show the direct involvement of dendritic activity in a perceptual task. Active dendrites have also been linked to complex network representation further highlighting the importance of such mechanisms in sensory perception[57]. Dendrites can also encode aspects other than sensation and motion, such as

reward[58] and space representation[59,60 61]. The functional and anatomical properties of dendrites suggest that they can support different types of plasticity. For example, the simultaneous occurrence of dendritic EPSPs with backpropagating action potentials increases the amplitude of the synaptic potential, in a process termed long-term potentiation (LTP)[62] . A similar mechanism has been observed by Gambino et al. where NMDA-evoked dendritic plateau potentials underlined the formation of LTP in vivo[63]. Performing whole cell recordings in vivo, they further show that rhythmic stimulation of whiskers can induce the formation of LTP in L2/3 pyramidal neurons of the primary somatosensory cortex and that this is dependent on the presence of NMDA-mediated dendritic plateau potentials. Therefore, it is clear that dendritic active properties can provide a substrate for learning mechanisms involved in sensory perception.

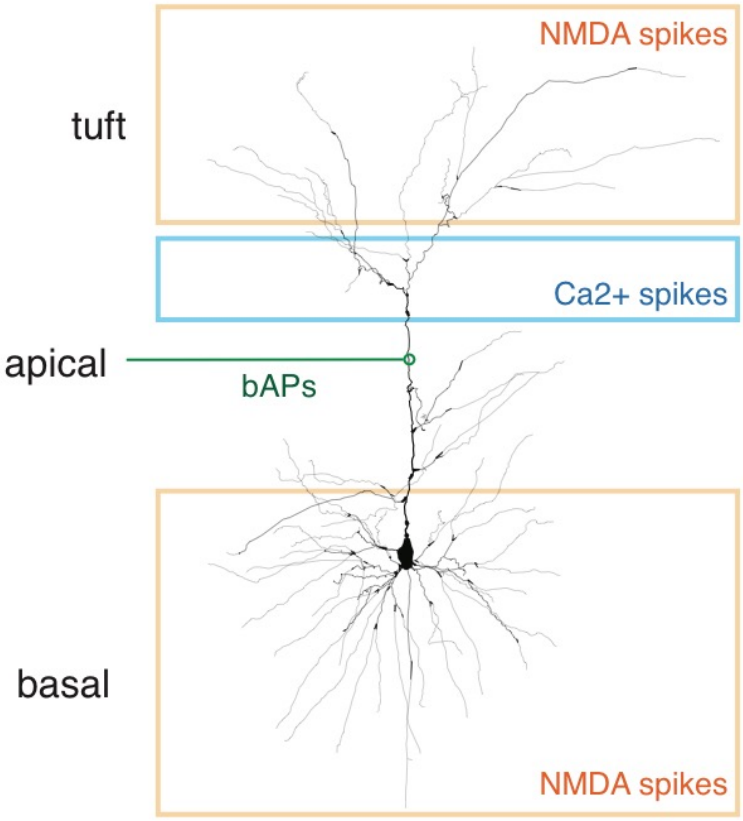

Figure 1..2| Compartmentalisation of dendritic spikes in a L2/3 pyramidal neuron. Sub-compartments of L2/3 pyramidal neurons can generate different types of dendritic spike according to the local distribution of conductances. Tuft and basal dendrites support the generation of local NMDA spikes, whereas Ca2+ spikes are generated at the main bifurcation of the apical dendrite. The apical dendrite is also endowed with Na+ channels that allow the backpropagation of somatic action potentials (bAPs). Adapted from Palmer et al., 2012[2].

CHAPTER 1

BEYOND A SIMPLE VIEW OF PRIMARY SENSORY AREAS

As mentioned in the previous paragraphs, a traditional view of sensory processing in the cortex suggests that information follows a hierarchical stream of processing, from low level features to higher association areas. This view was consolidated by neurological studies which described people with lesions of higher order cortical areas, who acquired very peculiar deficits. A very famous example is that narrated, amongst others, by Oliver Sacks in his book "The man who mistook his wife for a hat". The patient suffered of a peculiar type of visual agnosia, prosopagnosia (face blindness), which is described as the inability to recognise faces. This condition was due to a lesion of a brain region called the fusiform gyrus, which has now been linked with face recognition in humans. Although the patient retained an intact visual system, and no particular sight impairments, the brain of this patient was not able to combine the information that represented his wife's face: "he reached out his hand and took hold of his wife's head, tried to lift it off, to put it on". He could remember her, he could see her, but he was not able to perceive and recognise her face. This, and many other cases of visual agnosia, have been correlated with lesions of higher order associative areas of the cortex. However, we know that primary sensory cortices are specialised to extract low level features of the percept. This concept was accepted by neuroscientists since the pioneering studies of Hubel and Wiesel in the visual cortex[9,10]. It is therefore reasonable to believe that the cortex has a compartmentalised structure, each with its specific functional role. However, the more neuroscientists have looked into cortical structure, activity and function, the more they realised that things are much more complicated. Although it remains ground truth that the primary visual cortex processes basic features of the visual scene such as orientation and direction, it became clear that motion, attention, learning and many other factors can be encoded here as well. Furthermore, recent studies have challenged the role of the cortex by showing that, in many cases, it was dispensable for solving and acquiring sensory-based tasks[64].

The idea that the cortex operates as multiple independent modules does not seem to fit the picture. Investigating the modulation of primary sensory cortices to extend our view of how they work might also be a first, very small step towards a better understanding of how the entire brain works.

The forepaw primary somatosensory cortex

It is believed that somatosensation has an important ethological role for rodents. Mice and rats can discriminate different textures and vibrations or assess the distance of objects around them through their whiskers and limbs[65,66]. Traditionally, most studies of the mouse somatosensory system have focused solely on the whiskers[67-69]. This is because the rodent whisker system has a peculiar cortical organisation. Indeed, a region of the rodent primary somatosensory cortex is organised in structures called barrels that are spatially set to reflect the organisation of the whisker pad[70]. In contrast, much less is known about the organisation of the mouse somatosensory area that represents the limbs and processes touch. Most of this knowledge comes from a study that investigated the representation of touch in the brain[14] with flutter stimuli. Flutter sensation arises from vibration applied to the surface of the skin. Although not as neatly organised as the barrel cortex, the forepaw primary somatosensory cortex of the mouse has a functional role in encoding vibrations[15]. Indeed, mice can detect a flutter stimulus with their forepaw[71,72]. Pacinian corpuscle, located deeply in the forepaw of the mouse, mediate the activation of neurons in the cortex in response to vibrating stimuli[15]. From the periphery, this sensory information is channelled into the ventral posterior lateral nucleus of thalamus (VPL) and, from here, it is relayed to the region of the somatosensory cortex representing the forepaw. Here, cells are activated by feature selectivity of the stimulus as a function of frequency and intensity of the vibration. Within the forepaw area of the somatosensory cortex, vibrations are represented similarly to frequency in the auditory cortex. In other words, neurons

in the forepaw primary somatosensory cortex can be tuned to a preferred vibration frequency. However, it is still unclear how these cells are organised within the primary somatosensory cortex or what is their function is during behavior.

Early cortical integration of multisensory information

The brain has to combine information from different modalities in order to achieve a unified sensory percept. While this can happen in integrative areas such as the posterior parietal cortex[73,74], evidence of multisensory integration in primary sensory areas has been abundantly accumulating in recent years[20,75]. Furthermore, primary sensory cortices are widely inter-connected [76]. These functional connections can be different according to the area and modality[76,77]. It is also possible for sensory information from a different modality to reach primary sensory areas through the thalamus or other subcortical structures[76]. All of this evidence supports the idea that multisensory integration could happen already at lower level of cortical processing. Importantly, multisensory integration in association and primary areas could follow very different rules and principles[78]. For example, tactile stimulation can induce a hyperpolarization of L2/3 pyramidal cells in the auditory cortex and similarly, auditory stimulation can hyperpolarise neurons within the somatosensory cortex[77]. This suggests that connections between primary cortices also occur in the upper layers of the cortex, where they can synapse onto inhibitory interneuron or tuft dendrites. While a cross-modal input onto tuft dendrites by itself may not be enough to generate dendritic spikes, the concurrent activation of somatic input through the feedforward pathway may lower the threshold for triggering a dendritic spike. In this way single pyramidal neurons in a primary area could integrate multisensory information. Indeed, Ibrahim et al. reported a sharpening of orientation tuning in the visual cortex when an auditory stimulus was played at the same time. This mechanism

involved the activation of axonal projections from the auditory cortex to the visual cortex through L1[20]. Although the authors do not directly test the involvement of tuft dendrites, they highlight the importance of L1 as a top down modulation hub for the integration of cross modal information in a primary sensory area. Whether dendrites can support the integration of multisensory signals is still unknown.

The functional organization of the mouse auditory cortex

The first cortical stage of auditory processing occurs in the primary auditory cortex. Similar to other sensory areas, many studies have characterized its functional and spatial organization according to basic principles[12]. The central layers of pyramidal neurons in the primary auditory cortex receive their main feedforward input from the medial geniculate nuclei (MGN) of the thalamus and further project to the upper cortical layers. The spatial organization of these connections define two principles of organization that can be identified. One, vertical, reflects the laminar organization of the inputs and the other, horizontal, follows the spatial organization of the thalamic inputs. Neurons in the primary auditory cortex encode the basic feature of sounds such as frequency and intensity. In this sense, the organization of the auditory cortex is precisely defined by the functional properties of the cells in a tonotopic map. However, in the mouse auditory cortex the question of whether and how such an organization is still debated. Large-scale analysis of the auditory cortex has provided evidence for a precise spatial map while response properties seem to follow less strict rule at a local level[11]. However, it is still possible to identify different regions of the auditory cortex according to their tonotopic organisation. The primary auditory cortex has differences in the functional properties of its local elements (i.e. interneurons)[79]. In addition to thalamic inputs, local inhibition plays an important role in shaping the frequency and intensity tuning of pyramidal neuron[13,80].

Besides encoding basic features of stimulus information, the auditory cortex is also involved in a more complex cognitive aspect. For example, the auditory cortex is part of a distributed neural circuitry that processes threat memory[24,81]. The auditory cortex has also been shown to be important for the discrimination of complex sounds[82] and decision making[83]. The auditory cortex is also peculiarly modulated by motor action as feedback input from the motor cortex to the auditory cortex suppresses neural activity[84]. It is believed that corollary discharge is important to suppress self-generated sound during motion/locomotion and increase signal to noise ratio of environmental (or more relevant) stimuli[85].

Perceptual learning in primary sensory areas

Previous experience plays a fundamental role in shaping neural activity and perception to allow us to adapt to an ever-changing environment[86]. Indeed, animal behavior is constantly modified by experience and so is the underlying neural activity. The processes that underlie such changes in sensory signalling are defined as perceptual learning. In this way, sensory signals can acquire relevance and be used for the selection and execution of appropriate actions. To serve this role, sensory coding needs to be efficient. During perceptual learning different strategies could be implemented by the sensory system to achieve such efficiency[7]. For example, signals can be enhanced in their single element components: perceptual learning can increase the selectivity of neurons for specific features of the stimulus by modulation of its firing rate[87,88]. In addition, perceptual learning enhances stimulus selectivity and discriminability[89]. During learning, this allows for the emergence of stable and reliable patterns of activation which facilitate sensory processing and the transfer of information to other areas[67]. Another example mechanism is sparse coding, which plays an important role by optimising the number of cells or action potentials needed to encode a sensory signal[7]. Indeed, learning increases sparse coding in sensory cortices[90] suggesting that the inhibitory control of neural activity in sensory areas is

very important during learning. Interneurons can follow different rules of experience-dependent plasticity, allowing the emergence of another key aspect of perceptual learning: flexibility. In the real world, the behavioral relevance of a sensory stimulus can change and so the neural activity underlying it should follow bidirectional changes[91]. Indeed, even passive exposure to sensory stimulation can induce perceptual changes in neuronal representation which can be quickly reversed once the same stimulus acquires a different relevance[91]. As highlighted in the previous section, dendrites could play an important role in sensory perception and are placed in an important hub for the modulation of sensory processing during learning. Dendrites could provide an additional cellular mechanism to enhance the efficiency and flexibility of sensory representation within perceptual learning. However, whether and how dendritic activity undergoes changes during learning remains unclear.

The role of the auditory cortex during fear learning

Fear learning is a specific type of associative learning resulting from the association of a sensory cue to a threat. As such, fear conditioning has the ability to update the perceptual representation of sensory information and supporting adaptive behaviors. For example, sensory discrimination of odor cues is enhanced following fear learning, lowering the threshold for discrimination[92,93]. In support of this, much evidence illustrates that sensory evoked responses are altered following fear conditioning at different stages of the involved circuitry, which have been extensively studied. For example, fear conditioning alters the encoding of sensory information in the amygdala [94], prevents habituation in response to conditioned stimuli[95] and can induce quick and long lasting receptive field plasticity in the auditory cortex[96]. In this paragraph we focus on the changes that occur following fear learning in the auditory cortex. In a recent study, Yang and colleagues report a new amygdalocortical pathway that undergoes selective remodelling of synapses following auditory fear conditioning protocol. Here, fear

learning caused an increase in the formation of both amygdala axonal boutons and dendritic spines of L5 pyramidal neurons in the auditory cortex[97].

Fear conditioning-related structural changes could enhance neuronal responses by increasing coincident inputs in the auditory cortex. The investigation of functional properties and circuits in this area are have recently shown consistent results. Letzkus et al have identified a disinhibitory circuit that enhances the activity of pyramidal neurons by transiently shifting the balance of excitation and inhibition within the auditory cortex[98]. Acetylcholine mediates the recruitment of an inhibitory circuit that blocks paravalbumin positive (PV^+) interneurons control over pyramidal cells. Interestingly, interfering with this mechanism showed impairment in fear learning, suggesting its importance not only for sensory processing but also for memory acquisition and expression. Indeed, more recently it has been proved that the auditory cortex plays a fundamental role in the processing of threat memory[81]. In addition, the upper layer of the cortex seems to be critically involved in such mechanism as well. A specific interneuron type, which targets distal dendrites in L1 of the auditory cortex, undergoes plasticity changes following fear leaning[99]. Other evidence has pointed at the importance of dendritic inhibition in supporting fear learning in the hippocampus[100]. However, the plasticity of cortical dendrites in the auditory cortex during fear learning remains unexplored.

Of plasticity and dendrites

As mentioned in the previous paragraphs, dendrites could support the emergence of local plasticity. What mechanisms could provide plasticity of dendritic activity? A well-studied form of plasticity is spike-timing-dependent-plasticity (STDP), which involves pairing of a single action potential in the pre- and post-synaptic cells[101,102]. The timing of spiking in the two neurons determines the direction and the amplitude of the change in synaptic strength[103]. If a synaptic event is evoked just before a post synaptic action potential, the synapse will be

potentiated. However, if an EPSP arrives after an action potential on the post-synaptic cell, the synapse will be depressed[103]. Because most inputs onto a neuron arrive at the dendrites, changes in the strength of these synapses could change local dendritic activity.

One mechanism that allows the coupling of pre and postsynaptic activity is the backpropagation of the somatic action potential (bAP) into the dendritic arbour[49,104]. bAPs locally depolarize the synapse and, if it encounters an incoming EPSP, allow the formation of LTP[49,62,105]. According to this, the time window for STDP is defined by the occurrence of a somatic action potential. In this way, STDP is a mechanism for the coincidence detection of feedforward and feedback inputs[106]. This model, however, fails to explain the complete scenario. In fact, as previously mentioned, most synapses are located on distal dendrites and backpropagation of somatic action potential is limited by passive properties, hence failing to successfully conduct signals to synapses in remote compartments[107]. Dendritic active properties are a candidate mechanism for the formation of LTP on distal dendrites[106,108]. Bursts of action potentials at the soma are known to elicit dendritic spikes that involve a large depolarization of the dendritic region[107,108]. Indeed, inhibition of dendritic spikes through the application of a voltage gated calcium channel antagonist blocks the occurrence of STDP[109]. Other evidence suggests that bursts of action potentials at the soma need to reach a certain threshold in order to form STDP in distal dendrites. However, thanks to dendritic spikes, a single burst of action potentials is sufficient to form LTP[109]. On the other hand, dendritic spikes can occur also independently from the somatic action potential. Recently, Brandalise and co-workers have identified a causal relation between NMDA dendritic spikes and the formation of LTP at synapses of hippocampal CA3 pyramidal cells. They showed that NMDA spikes provide the postsynaptic depolarization necessary for the formation of STDP at distal synapses[110]. The location of synaptic inputs plays an important role in the induction of plasticity[107]. Inputs on a pyramidal neuron are spatially organised according to the information

that they carry. Sandler et al. have recently identified a novel form of plasticity in tuft (distal) dendrites of L5 pyramidal neurons that depends on NMDA receptor and provides a mechanism to bind proximal and distal activity and integrate feedforward and feedback inputs[111]. Importantly, dendritic plasticity can also be quickly induced by behavior[61] and motor learning[112]. However, whether plasticity can also occur in dendrites during sensory processing is currently unknown.

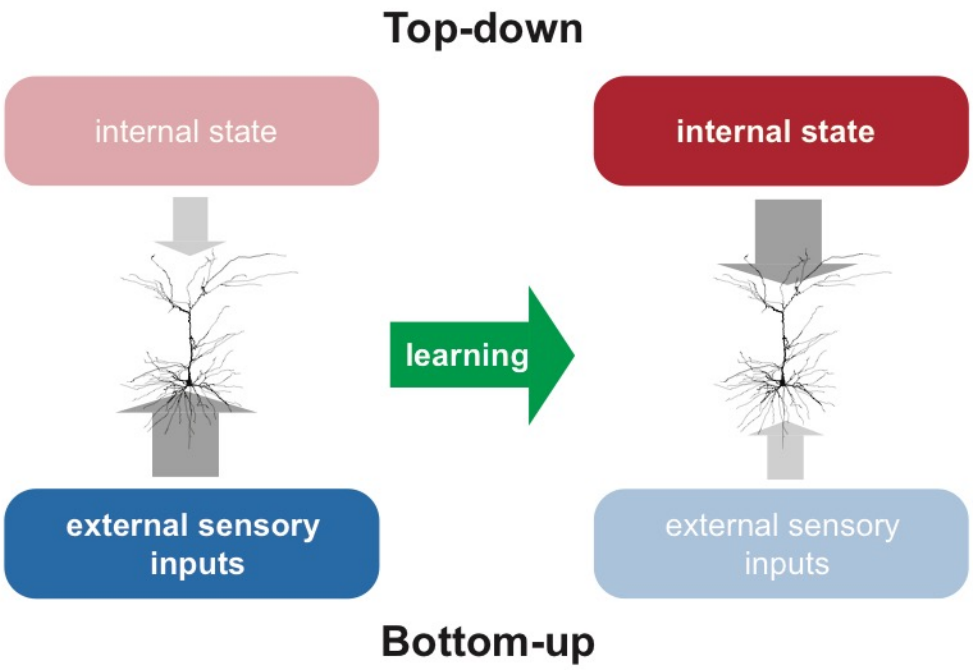

Figure 1.3 | Dynamic shift of sensory processing during learning in primary areas. Neural activity in the naïve condition (left) is mostly driven by external sensory inputs through the feedforward (bottom-up) pathway. These inputs mainly target basal dendrites of L2/3 pyramidal neurons. During learning, feedback inputs in L1 are enhanced as is the impact of top-down modulation in sensory processing. Feedback inputs mostly target distal tuft dendrites of L2/3 pyramidal neurons. Adapted from Makino and Komiyama, 2015[1].

CHAPTER 1

AIMS OF THE THESIS

Sensory perception arises by integrating external information (feedforward) from the environment with the internal representation and the current brain state (feedback). Interestingly, this can already happen at early stages of sensory processing. Here, the structure of the cortex and the organization of inputs onto the pyramidal neuron grant the possibility to perform such integration at the cellular level.

The tuft dendrites of cortical pyramidal neurons reside in the upper layers of the cortex and are the first point of contact for feedback inputs in sensory areas. Given the vast literature about active dendritic properties, it is reasonable to think that tuft dendrites could play an important role in integrating long range inputs carrying feedback information. By looking at dendritic activity in vivo, the overall Aim of this thesis is to investigate the modulation of cortical dendrites during sensory perception and learning. Specifically, in three parallel sets of experiments, this thesis Aims to:

1. **Investigate the influence of auditory input on sensory encoding and tactile goal-directed behavior.** Primary areas of different sensory modalities are widely interconnected. This could provide a mechanism to enhance coding efficiency during behavior by integrating cross-modal sensory information at the first stage of cortical processing. With a combination of two photon calcium imaging, whole cell patch clamp recordings in vivo, behavior and optogenetic manipulation I aim to reveal the role of synaptic input from the auditory cortex in modulating sensory encoding in the primary somatosensory cortex and the related behavioral output in a sensory-based task.

2. **Investigate the influence of fear learning on tuft dendritic activity in the auditory cortex.** Fear learning modulates the functional activity and spine morphology of

pyramidal neurons in the auditory cortex. Is dendritic activity also shaped by fear learning? If so, does this modulation have an effect on the neuronal output? I aim to answer these questions using an auditory fear conditioning protocol in combination with dendritic (two-photon imaging) and somatic (whole cell patch clamp) recordings in anaesthetised mice

3. **Investigate the dynamics of dendritic activity during learning of a sound discrimination task.** Perceptual learning rearranges sensory representations to improve efficiency. I aim to investigate the changes in encoding of sensory information in cortical dendrites during learning of a discrimination task. I addressed this by performing longitudinal two-photon imaging of dendritic activity in the auditory cortex of awake behaving mice engaged in a sound discrimination task

CHAPTER 2

GENERAL METHODS

This chapter describes the main surgical preparations, experimental procedures and data analysis that were used throughout the thesis. Each results chapter also has a dedicated methods section with further specific details.

Ethics

All experiments were conducted in strict accordance with the Code of Practice for the Care and Use of Animals for Scientific Purposes (National Health and Medical Research Council, Australia) and guidelines given by the veterinary office of The Florey Institute of Neuroscience and Mental Health.

Virus injections

Mice (C57BL/6; P30 - 55) were anaesthetised with isoflurane (1 - 3 % in 0.75 L/min O_2) and body temperature was maintained at 36 - 37 °C through a closed loop heating-pad. Eye ointment was applied to prevent dehydration and meloxicam (1 - 3mg/kg, Ilium) was intraperitoneally injected for anti-inflammatory action at the beginning of the surgery. After the fur was removed with scissors, the skin was disinfected with ethanol 70 % and betadine and a small slit was made in the skin to expose the skull. A microcapillary pipette was previously backfilled with the viral construct of (specific details included in Chapters 3, 4, 5; a list of all the constructs used can be found at the end of this paragraph) and a layer of mineral oil (Sigma) through a 1 ml syringe. A plunger was then inserted to push the virus front to the tip of the pipette. The pipette was centred over bregma and the coordinates for the injections were identified with a stereotaxic manipulator (Narishige) (all coordinates used are listed at the end of this paragraph). A small craniotomy (0.5 x 0.5 mm) was then made over the brain region of interest with a dental drill. The pipette was inserted into the brain at the depth of interest, allowing time for the brain to adapt to the applied pressure, and the virus was slowly injected with an oil hydraulic injector (Narishige). The pipette was left in position for at least 5 minutes after the injection and slowly retracted. The skin was sutured, and the mouse was able to recover for at least 3 days prior to any further experimental procedures.

Stereotaxic coordinates for viral injections (from bregma):

Auditory cortex

- L2/3: Anterior Posterior (AP): -2.5 mm; Medio Lateral (ML): 4.5 mm; Dorso-Ventral (DV): - 0.45 mm; (Chapter 4 and 5)
- L5: AP: -2.5 mm; ML: 4.5 mm; DV: - 0.7 mm; (Chapter 3)

Forepaw primary somatosensory cortex:

- L2/3: AP: 0 mm; ML: 2 mm; DV: - 0.45 mm; (Chapter 3)
- L5: AP: -0 mm; ML: -2mm; DV: - 0.7 mm (reached by moving the pipette 1.4 mm with an angle of 30°, starting at AP: -1.2 mm, ML: 2mm; to avoid "spilling" in the upper layers; (Chapter 3)

Viral constructs

- AAV1.hSyn.Cre.WPRE.hGH (Chapter 3, 4 and 5)
- AAV1.Syn.Flex.GCaMP6f.WPRE.SV40 (Chapter 3, 4 and 5)
- AAV1.Syn.Flex.GCaMP7f.WPRE.SV40 (Chapter 5)
- AAV1.CAG.ArchT.GFP.WPRE.SV40 (Chapter 3)

Sparse labelling

To perform dendritic imaging using two photon microscopy in vivo, we used a sparse labelling techniques. This strategy was used to optimise dendritic imaging in vivo, as a dense labelling of the cortical tissue would result in a higher background noise and put a great constrain on the possibility of demixing the dendritic signals.

To achieve sparse labelling of the forepaw primary somatosensory cortex (Chapter 3) or the auditory cortex (Chapter 4 and 5) with a Ca^{2+} indicator, a mix of Cre-dependent genetic Ca^{2+} indicator GCaMP6f (AAV1.Syn.Flex.GCaMP6f.WPRE.SV40) and diluted Cre (AAV1.hSyn.Cre.WPRE.hGH) was injected in either L2/3 (at a depth of 450 μm) or L5 (at a depth of 700 μm). The rationale behind this strategy is that GCaMP6f will be expressed only in those cells that were also transfected by Cre. Using a dilution of 1:6000 (in distilled water)

of the Cre virus we were able to achieve labelling of around 20-40 neurons in the brain region of interest. One limitation of our approach is that we used a non-specific promoter, which would also label interneurons. However, being the percentage of interneurons in layer2/3 of the cortex much lower compared to pyramidal neurons, very rarely we observed labelling of interneurons. In addition, the small fraction of cell labelled allow to visually identify the cell types that were imaged as pyramidal neurons.

Finally, a common problem with adeno-associated virus is the risk of overexpression, which usually occurs after a couple of months from transfection of the cells. To avoid this, all experiments were performed between 3 - 9 weeks from the injection of the viral construct.

Head-post implantation and cranial window surgery

To surgically implant the head-post for recordings in the awake state, mice were anaesthetized with isoflurane (1 – 3 % in 0.75 L/min O_2) and intraperitonially injected with Meloxicam (1 – 3 mg/kg, Ilium). Throughout the surgery, body temperature was maintained at 36 - 37 °C. Lidocaine (20mg/ml, Ilium) was topically injected around the surgical site before the skin was cut to expose the skull. The skull was carefully scraped with a razor blade to clean the entire surface and increase adhesion. For Ca^{2+} imaging experiments, a craniotomy was performed (3 mm diameter) over the virus injection site. The craniotomy was made using a dental drill with a 0.5 mm tip. Once the bone flap was carefully removed with a surgical tweezer, sterile sodium chloride was applied to keep the brain hydrated. If blood was present in the craniotomy, it was cleaned and removed with a hemostatic sponge. A circular coverslip (3 mm diameter, size #1) was placed over the craniotomy, and sealed with glue. In some cohort of mice, a double window was used by putting together two coverslip of different sizes (3-3.5 mm) using UV curable glue. This helps reducing motion artifacts and stabilizing the cranial window implant. Finally, a custom-made metal head-bar was then attached to the skull using dental cement (C&B

Metabond®, Parkell) and the entire skull surface was covered. Mice were returned to their home cage for at least 3 days before imaging or behavioral training commenced.

Two photon calcium imaging in vivo

Two-photon imaging was performed through the cranial window implanted in mice previously transfected with the Ca^{2+} indicator. Prior to each imaging session the cranial window was carefully cleaned with ethanol. Mice were positioned in a head-fixation frames with a tube to help contain them. The objective was positioned parallel to the cranial window at a distance of roughly 1 cm before applying either water or imaging gel for the objective immersion. The surface of the brain was identified via a camera, using the brightfield path of the microscope. After this, the dichroic mirror was slide in to perform scanning imaging with a two photon laser (see below). The craniotomy was explored to identify the cells expressing the Ca^{2+} indicator. Ca^{2+} transients were then recorded from the dendrites of layer 2/3 or L5 pyramidal neurons at a depth of 50-100 μm from the pia surface. Images were acquired at a frequency of 30 Hz (512 x 512 pixels) using ScanImage software (Vidrio Technologies). GCaMP6f or 7f was excited at 940 nm (~30 mW at the back aperture) with a titanium sapphire laser (140 fs pulse width; SpectraPhysics MaiTai Deepsee) and imaged on a Sutter MoM through a 16x Nikon objective (0.8 NA). Emitted light was passed through a dichroic filter (565dcxr, Chroma Technology) and short-pass filtered (ET525/70-2p, Chroma Technology) before being detected by a GaAsP photomultiplier tube (Hamamatsu).

The images were motion corrected with a custom written MATLAB script (kindly provided by Naoya Takahashi). Region of interest (ROI) were manually drawn on ImageJ and fluorescence signal extraction was performed with a custom MATLAB script (kindly provided by Pedro Garcia Da Silva). All trials with motion in the z axis were manually excluded from the analysis.

Calcium transients analysis

Custom-written MATLAB (MathWorks) codes were used for analysis of Ca^{2+} imaging data (see code for DF/F calculation in the Appendix). The relative fluorescent signals were measured by subtracting the median value of the baseline during the pre-stimulus interval. Calcium transients were then detected, during each trial, when they crossed a threshold value of 3 standard deviations of the noise of the (pre-stimulus) baseline. The amplitude and duration of each calcium transient were measured as the maximum peak and half width at half maximum of the detected event. Calcium responses were smoothed using a Savitzky-Golay filter with a 2nd order polynomial and a 7 sample window and only transients longer than 250 ms were included in analysis. Unless differently specified, the amplitudes and durations are reported as the mean value of the detected events for each ROI. The probability of occurrence of calcium transients was measured as the number of events divided by the total number of trials. All calcium data were analysed with custom scripts in MATLAB written by me (see code for Ca^{2+} events detection in the Appendix).

Whole cell patch clamp in vivo (under anaesthesia)

Mice (C57BL/6; P42-63) were initially anaesthetised with isoflurane (3% in 0.75 L/min O_2) before urethane anaesthesia (intraperitoneal, 1.6 g/kg, Sigma) was administered. Anaesthesia was monitored throughout the experiment, and a top-up dose of 10% of the initial urethane dose was administered when necessary. Body temperature was maintained at 36-37 °C with a closed loop system. Lidocaine (20mg/ml, Ilium) was injected around the surgical site on the scalp and the head was stabilized in a stereotaxic frame by a head-plate attached to the skull with dental cement (paladur, Heraeus). A craniotomy (~1.5 x 1.5 mm^2) was performed over the region of interest, measured in stereotaxic coordinates from bregma. After the bone flap was carefully removed with surgical tweezers, the dura was surgically removed and the brain

was constantly bathed with normal rat ringer (135 mM NaCl, 5.4 mM KCl, 1.8 mM CaCl2, 1 mM MgCl2, 5 mM HEPES) throughout the experiment. Whole-cell *in vivo* patch clamp recordings were performed using a patch pipette (resistance 6-9 MΩ) filled with an intracellular solution containing 115 mM potassium gluconate, 20mM KCl, 10 mM sodium phosphocreatine, 10 mM HEPES, 4 mM Mg-ATP, 0.3 mM Na-GTP, adjusted to pH 7.3-7.4 with KOH. The patch pipette was inserted into the brain at an angle of 30°- 40° relative to the cortical surface, to a depth of ~200 μm (to target layer 2/3 neurons). The pipette was then advanced in steps of 1 μm (to a maximum distance of 300 μm in the hypotenuse trajectory) until a neuron was encountered. Pressure was released to obtain a gigaseal and a gentle suction was applied to open the cell membrane. Whole-cell voltage recordings were performed from the soma using Dagan BVC-700A amplifiers and were filtered at 10 kHz. Once a whole-cell recording was obtained, the voltage response to incremental current steps (50 pA; 800 ms) was recorded to characterize the neuron. Custom-written Igor software was used for the acquisition of whole-cell recordings (kindly provided by Matthew Larkum).

Voltage and action potentials analysis

Custom-written Igor Pro (Wavemetrics) software was used for the acquisition and analysis of whole-cell recordings. For evoked subthreshold responses, the integral of the evoked potentials were calculated in Igor. Membrane potential measures were made to the millivolt. The peak amplitude of the subthreshold response was measured using the “findpeaks” function in a custom Matlab script, written by me. The firing rate was measured in a 500 ms window from sensory stimulation onset and calculated with a custom written MATLAB script that measured the total number of spikes within the detection window divided by the total number of trials. The threshold for spike detection was absolute and visually determined for each recording.

CHAPTER 3

AUDITORY INPUTS ENHANCES SOMATOSENSORY ENCODING AND TACTILE GOAL-DIRECTED BEHAVIOR

The work presented in the following Chapter was submitted for publication. The format was slightly adapted to fit the thesis requirements. References have been collated at the end of the thesis.

CHAPTER 3

Auditory input enhances somatosensory encoding and tactile goal-directed behavior

Godenzini, L[1*]., Alwis, D[1*]., Guzulaitis, R[1]., Honnuraiah, S[2]., Stuart, G.J[2]., Palmer, L.M[1]

[1]Florey Institute of Neuroscience and Mental Health, University of Melbourne, Victoria, Australia 3052

[2]Eccles Institute of Neuroscience, John Curtin School of Medical Research, Australian National University, Canberra, ACT, Australia 0200

[*]These authors contributed equally to this work

Author Contributions

I performed and analysed all of the two-photon Ca^{2+} imaging experiments and behavioral experiments.

Dasuni Alwis and Robertas Guzulaitis performed and analysed the anaesthetized and awake in vivo patch clamp recordings respectively. Suraj Honnuraiah performed and analysed the in vitro patch clamp recordings.

Acknowledgements

I would like to thank Dan Scott for providing the AAV1/2-muGFP GFP. This work was supported by the NHMRC (APP1086082, L.M.P and G.J.S; APP1063533, L.M.P), the Sylvia and Charles Viertel Charitable Foundation (L.M.P) and the ARC Centre of Excellence for Integrative Brain Function.

CHAPTER 3

ABSTRACT

The capacity of the brain to encode multiple types of sensory input is key to survival. However, how neurons integrate information from multiple sensory pathways and to what extent this influences behavior is largely unknown. Here, we report the influence of auditory input on sensory encoding in the somatosensory cortex and its effect on tactile goal-directed behavior. Using two-photon Ca^{2+} imaging, optogenetics and electrophysiology *in vivo* and *in vitro*, we show that monosynaptic input from the auditory cortex enhances dendritic Ca^{2+} responses and somatic action potential output in layer 2/3 (L2/3), but not layer 5 (L5), pyramidal neurons in forepaw somatosensory cortex (S1). During a tactile-based goal-directed task, auditory input increased distal dendritic activity in L2/3 pyramidal neurons and reduced reaction time, which was abolished by photoinhibition of auditory cortex projections to forepaw S1. Taken together, these results indicate that distal dendrites of cortical L2/3 pyramidal neurons encode multi-sensory information, leading to enhanced neuronal output and response latencies during goal-directed behavior.

INTRODUCTION

One of the fundamental tasks of the brain is to make sense of the world. This requires the concurrent integration of different sensory information streams, which are constantly changing as an animal moves through its environment. During sensory-guided behaviors, the integration of multiple sensory pathways (multi-modal integration) typically results in shorter reaction times, lower sensory-detection thresholds and enhanced object recognition [73,113-118]. Such changes in behavior are believed to be driven, in part, by the modulation of sensory processing within the cortex [119]. Consistent with the complex connectivity within the brain [120], there is an increasing body of literature demonstrating the convergence of multisensory projections in primary sensory cortex [75,121,122]. For example, in the visual cortex, multi-modal input results in

altered encoding and cortical processing of sensory input [20,77,123]. Despite the known influence of cross-modal input on overall neural activity, information about the cellular mechanisms leading to changes in cortical processing and sensory-based behavior is limited. In the cortex, the integration of multisensory information requires the combination of top-down input from different sensory brain regions with the bottom-up input from the primary sense [124]. This integration can occur at the level of single cortical neurons, often resulting in dendritic electrogenesis[46].

Dendritic integration ultimately influences neuronal firing[38,50,124-130] which are crucial for sensory encoding and perception of a single sense [56,131]. However, our external world is sensory-rich and therefore individual sensory modalities are usually not sensed in isolation. Cortical layer 2/3 (L2/3) pyramidal neurons are perfectly positioned to act as a hub for multisensory information. They directly influence cortical output neurons [132-134], and also send and receive long-range projections from other cortical and subcortical areas [135,136]. However, how individual L2/3 pyramidal neurons integrate signals from multiple sensory pathways and the impact this has on somatic output is largely unknown. Here, we used a combination of Ca^{2+} imaging, patch-clamp electrophysiology, and optogenetics during goal-directed behavior to investigate the influence of the activation of one sense, in this case the auditory system, on sensory processing in the somatosensory cortex (S1). We find that the integration of auditory input on tuft dendrites of L2/3, but not layer 5 (L5), pyramidal neurons in forepaw S1 leads to enhanced sensory encoding and faster reaction times during tactile goal-directed behavior.

CHAPTER 3

RESULTS

Auditory stimulus enhances sensory encoding in tuft dendrites of L2/3 pyramidal neurons in S1

To assess the influence of auditory input on somatosensory processing in S1, we first characterized whether the auditory cortex sends direct axonal projections to forepaw S1. Using dual fluorescence imaging to label both auditory cortex projections and the somatosensory cortex, we visualized a high density of axons projecting from the auditory cortex within forepaw S1 (Supplementary Figure 3.1). These auditory axons were predominately restricted to the upper cortical layers of forepaw S1 (Figure 3.1a). Since the tuft dendrites of pyramidal neurons stratify in the upper layers of the cortex, we investigated the influence of auditory input on somatosensory processing in the tuft dendrites of pyramidal neurons in the forepaw S1 of awake mice (Figure 3.1a). We first targeted L2/3 pyramidal neurons as they send and receive projections from other cortical and subcortical areas, making them ideally positioned for encoding multi-sensory information. L2/3 pyramidal neurons were sparsely transfected with the Ca^{2+} indicator, GCaMP6f, and following expression, Ca^{2+} activity was recorded from tuft dendrites that were located between 50 and 100 μm below the pia using two-photon microscopy. In naïve mice, tactile stimulation (Tac) of the contralateral forepaw (200 Hz, 500 ms) evoked large Ca^{2+} transients (> 3 s.d. of the baseline fluorescence) in L2/3 tuft dendrites (Figure 3.1b; 2.39 ± 0.14 ΔF/F; n = 110 dendrites, 11 mice).

To test the influence of auditory input, mice were presented with a broadband auditory stimulus (Aud, 2 - 50 kHz, 60 dB, 500 ms) which evoked activity in the auditory cortex (Supplementary Figure 3.2). Surprisingly, this broadband auditory stimulus also evoked Ca^{2+} transients in tuft dendrites of L2/3 pyramidal neurons in forepaw S1 (Figure 3.1b; 2.86 ± 0.15 ΔF/F; n = 110 dendrites, 11 mice). In fact, auditory Ca^{2+} transients in L2/3 pyramidal neuron tuft dendrites were significantly larger than those evoked by tactile stimulation (Figure 3.1c; p = 0.0014).

Furthermore, when auditory and tactile stimulus were presented simultaneously (AudTac), there was a further increase in the amplitude of evoked Ca^{2+} responses (Figure 3.1b, c; 3.29 ± 0.16 ΔF/F; n = 110 dendrites, 11 mice; $p < 0.0001$). Likewise, there was also a significant increase in the rate of evoked Ca^{2+} responses during paired tactile and auditory stimulus (Figure 3.1d; Tac, 0.09 ± 0.008; AudTac, 0.12 ± 0.01; n = 110 dendrites, 11 mice; $p < 0.0001$). Auditory-evoked Ca^{2+} transients were not due to a startle response as the presentation of the auditory stimulus was not associated with movement detected by EMG recordings from the neck muscles (Supplementary Figure 3.3). Additionally, pupil dilation was similar during auditory and tactile stimuli (Aud, 0.056 ± 0.02 mm; Tac, 0.059 ± 0.02 mm; n = 6 mice, p = 0.56), suggesting there was no effect of the auditory stimulus on the saliency of the tactile stimulus or the arousal state (Supplementary Figure 3.4). These data indicate that when paired together, the auditory stimulus increased the dendritic response to tactile stimuli, highlighting a potential role of auditory input to forepaw S1 in the dendritic integration of multi-sensory information.

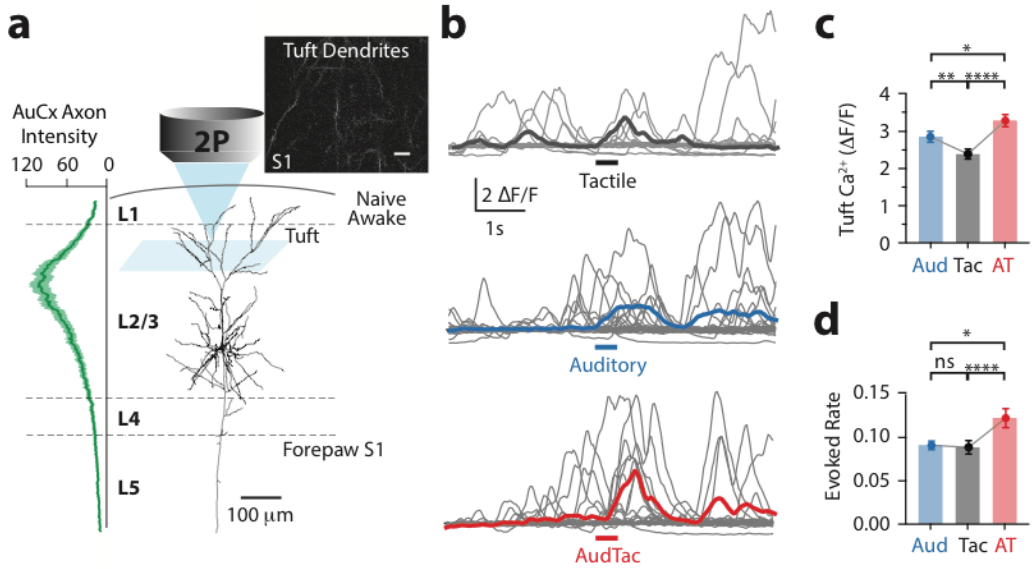

Figure 3.1 | Auditory stimulus enhances sensory encoding in tuft dendrites of layer 2/3 pyramidal neurons in the primary somatosensory cortex. a. (Left) The maximum relative optical density of axonal projections from the auditory cortex within the forepaw S1. (Right) Schematic of experimental design. In vivo two-photon Ca^{2+} imaging was performed in the tuft dendrites of L2/3 pyramidal neurons previously injected with the genetic Ca^{2+} indicator, GCaMP6f. Inset, two photon image of tuft dendrites recorded 90 μm below pia. Inset scale, 10 μm. b. Typical evoked Ca^{2+} responses recorded in an example tuft dendrite during tactile (black), auditory (blue) and paired tactile and auditory (red) stimuli. c. The amplitude of sensory-evoked Ca^{2+} transients during tactile (black), auditory (blue) and paired tactile and auditory (red) stimuli (One-way ANOVA Friedman test, $p < 0.0001$; Dunn's multiple comparisons test, n = 110 dendrites, 11 mice). d. The rate of sensory-evoked Ca^{2+} transients during tactile (black), auditory (blue) and paired tactile and auditory (red) stimuli (One-way ANOVA Friedman test, $p < 0.0001$; Dunn's multiple comparisons test, n = 110 dendrites, 11 mice). Error bars represent S.E.M. * $p < 0.05$, ** $p < 0.01$, **** $p < 0.0001$.

Auditory stimulus enhances tactile-evoked action potentials in L2/3 pyramidal neurons in S1

Does the enhanced multi-sensory integration in tuft dendrites during auditory input influence somatic output and the transfer of somatosensory information in L2/3 pyramidal neurons? To investigate this, whole-cell patch clamp recordings were made from the soma of L2/3 pyramidal neurons in forepaw S1 of awake mice (Figure 3.2a). In response to tactile stimulation of the forepaw, L2/3 pyramidal neurons reliably evoked action potentials above baseline (Figure 3.2b; Baseline, 1.05 ± 0.23 Hz vs Tactile, 2.29 ± 0.59 Hz; n = 17 neurons, 8 mice; $p = 0.027$). Likewise, when tactile stimulation was paired with an auditory stimuli, the evoked firing rate was also significantly increased above baseline (Figure 3.2c; Baseline, 1.11 ± 0.22

Hz vs AudTac, 2.61 ± 0.63 Hz; n = 17 neurons, 8 mice; p = 0.008). This is in contrast to the evoked firing rate in response to an auditory stimulus on its own, which did not differ significantly from baseline (Figure 3.2d; Baseline, 1.16 ± 0.27 Hz vs Aud, 1.20 ± 0.31 Hz; n = 17 neurons, 8 mice; p = 0.75). These data suggest that auditory input alone does not result in action potential generation, and that co-activation with other pathways are required to influence somatic output. Indeed, when the tactile stimulus was paired with an auditory stimulus there was a significant increase in the evoked firing rate compared to tactile stimulus alone (Figure 3.2e; n = 17 neurons, 8 mice; p = 0.013). Similar to previous studies, this enhanced somatic output during paired auditory and tactile input was not reflected in the somatic membrane potential. Tactile stimuli evoked a robust voltage response at the soma, which had a similar amplitude when combined with an auditory stimulus (Figure 3.2f; 7.1 ± 1.0 mV vs 7.2 ± 0.8 mV; n = 17 neurons, 8 mice; p = 0.644). Similar results were obtained in L2/3 pyramidal neurons in the anaesthetized state, where paired tactile and auditory simulation had no discernible effect on the amplitude of the subthreshold voltage response compared to tactile stimulation alone (18.4 ± 1.6 vs 18.4 ± 1.7 mV; p = 0.525), but significantly increased the number of evoked action potentials (Supplementary Figure 3.5; p = 0.049; n = 15 neurons, 12 mice). Overall, these results show that auditory input only

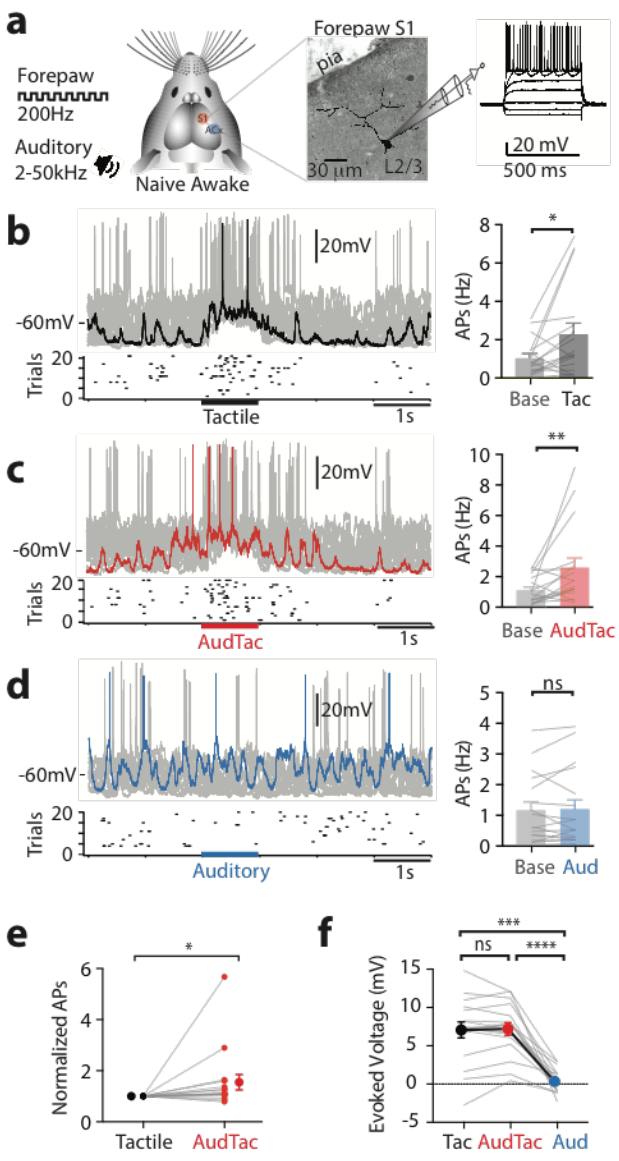

enhances action potential output in forepaw S1 when paired with tactile stimulation, suggesting that activation of one primary sensory area can alter the somatic output in another primary sensory area during sensory encoding. Furthermore, the negligible influence of auditory stimuli on its own suggests that the influence of auditory input on somatic output may involve active dendritic integration rather than summation of synaptic input at the soma.

Figure 3.2 | Auditory input enhances tactile-evoked somatic action potentials in layer 2/3 pyramidal neurons in vivo. a. Left, Schematic of experimental design. Mice were previously habituated to headfixation before whole-cell patch clamp recordings were performed from L2/3 pyramidal neurons in forepaw S1 in the awake state. Right, L2/3 pyramidal neuron filled with fluorescence biocytin for reconstruction and example voltage response to injected current steps (50 pA). **b-d.** (left) Overlay of individual trials and raster of action potentials from a typical neuron and (right) average evoked action potentials per trial in all recorded neurons in response to (**b**) tactile stimulus (Wilcoxon matched-pairs signed rank test; $p = 0.027$; $p_{shuffled} = 0.782$; 27 $trials_{av}$), (**c**) auditory stimulus (Wilcoxon matched-pairs signed rank test; $p = 0.75$; $p_{shuffled} = 0.41$; 21 $trials_{av}$) and (**d**) paired auditory and tactile stimulus (Wilcoxon matched-pairs signed rank test; $p = 0.008$; $p_{shuffled} = 0.927$; 28 $trials_{av}$). n = 17 neurons, 8 mice. Colored trace, single example voltage traces for tactile (black), paired auditory and tactile (red), auditory (blue) stimulus. **e.** Average evoked action potentials during paired auditory and tactile stimulus (red) normalized to tactile stimulus (black). Wilcoxon matched-pairs signed rank test. n = 17 neurons, 8 mice. **f.** Mean somatic voltage response during tactile (black), paired auditory and tactile (red), and auditory (blue) stimulus (n = 17 neurons, 8 mice; One-way ANOVA Friedman test, $p < 0.0001$; Dunn's multiple comparisons test). Error bars represent S.E.M. * $p < 0.05$, ** $p < 0.01$, *** $p < 0.001$,

Auditory cortex directly projects to L2/3, not L5, pyramidal neurons in S1

Is the influence of auditory input on somatosensory encoding due to direct monosynaptic connectivity between the forepaw S1 and auditory cortex? To examine this, we turned to the brain slice preparation where synaptic inputs and cellular excitability can be precisely controlled. The photo-active opsin ChR2 (AAV1.hSyn.ChR2(H134R)-eYFP.WPRE.hGH) was injected into the auditory cortex (200 - 500 μm below pia) and following expression, somatic whole-cell recordings were made from L2/3 pyramidal neurons in forepaw S1 in vitro (Figure 3.3a). Auditory cortex axons containing ChR2 were activated by brief LED pulses (470 nm; 2 ms) and slices were bathed in TTX plus 4-AP to determine if evoked responses were monosynaptic (Supplementary Figure 3.6). Photo-activation of axonal projections from auditory cortex generated robust EPSPs in 76% (22 / 29 neurons) of L2/3 pyramidal neurons in forepaw S1, which increased in amplitude as the intensity of the LED stimulus was increased (Figure 3.3b; 0.2 - 1.0 mW; n = 16 neurons). These responses were abolished by inclusion of DNQX and AP5 in the bath, illustrating they were mediated by AMPA/NMDA receptors (Figure 3.3c) and remained in the presence of TTX plus 4-AP, indicating that they are monosynaptic (Supplementary Figure 3.6). These data indicate that the auditory cortex provides direct synaptic input onto L2/3 pyramidal neurons in forepaw S1. To investigate the influence this monosynaptic auditory input has on firing properties of L2/3 pyramidal neurons, brief somatic current pulses (100 ms) were paired with LED activation (Figure 3.3d). Photoactivation of auditory cortex axons significantly decreased rheobase (Figure 3.3e; control, 291 ± 30 pA; LED, 208 ± 55 pA; n = 6 neurons, p = 0.03), however, had no effect on action potential threshold (Figure 3.3f; Control, -38.9 ± 2.1 mV; LED, -40.7 ± 1.6 mV; n = 6 neurons, p = 0.12). Since both L2/3 and L5 pyramidal neurons have their tuft dendrites stratifying in the upper layers of the cortex where auditory projections are predominately located, we also tested whether auditory cortex makes monosynaptic input onto L5 pyramidal

neurons in forepaw S1. Whole-cell patch clamp recordings were made from L5 pyramidal neurons in the same brain slices as L2/3 neurons to control for different axonal densities and/or expression in different slices/preparations (Figure 3.3g). In contrast to L2/3 pyramidal neurons, photoactivation of auditory cortex projections (470 nm; 2 ms) did not generate detectable somatic voltage responses in L5 pyramidal neurons in S1 (Fig. 3h and i; n = 18 neurons). Consistent with this observation, photoactivation of auditory input during somatic current injection did not alter rheobase (Figure 3.3j and k; Control, 529 ± 51.7 pA; LED, 517 ± 47.9 pA; n = 9 neurons, p = 0.41) or action potential threshold (Fig. 3l; Control, -43.2 ± 1.4 mV; LED, 43.0 ± 1.4 mV; n = 9 neurons, p = 0.56). To rule out the possibility that voltage responses in L5 neurons were absent because the apical dendrites had been severed during the slicing procedure, the dendritic tree of recorded L5 pyramidal neurons were morphologically reconstructed and shown to be intact (Supplementary Figure 3.7). Together, these data indicate that monosynaptic axonal projections from auditory cortex to S1 evoke somatic voltage responses in L2/3, but not L5, pyramidal neurons in forepaw S1.

Figure 3.3 | Auditory cortex directly projects to layer 2/3, and not layer 5, pyramidal neurons in the primary somatosensory cortex. a. Schematic of experimental paradigm. The photoactivatable opsin, pAAV-Syn-ChR2(H134R)-GFP, was injected into the auditory cortex (~100 nl; 200 - 500 μm below pia) and brain slice recordings were subsequently performed in the primary somatosensory cortex (S1). Auditory cortex axonal projections were visualised in the upper layers of the primary somatosensory cortex (green). **b**. Example of voltage responses in a layer 2/3 (L2/3) pyramidal neuron in S1 to photo-activation of auditory cortex axons with 15 increasing power (470 nm, 2 ms, 0.16 to 5 mW). Inset, Average synaptic response to increasing LED Power (n = 16 neurons). **c**. Example synaptic responses in a L2/3 pyramidal neuron in S1 to photo-activation (470 nm; 2 ms) of auditory cortex axons in control (black) and during bath application of DNQX+AP5 (orange).

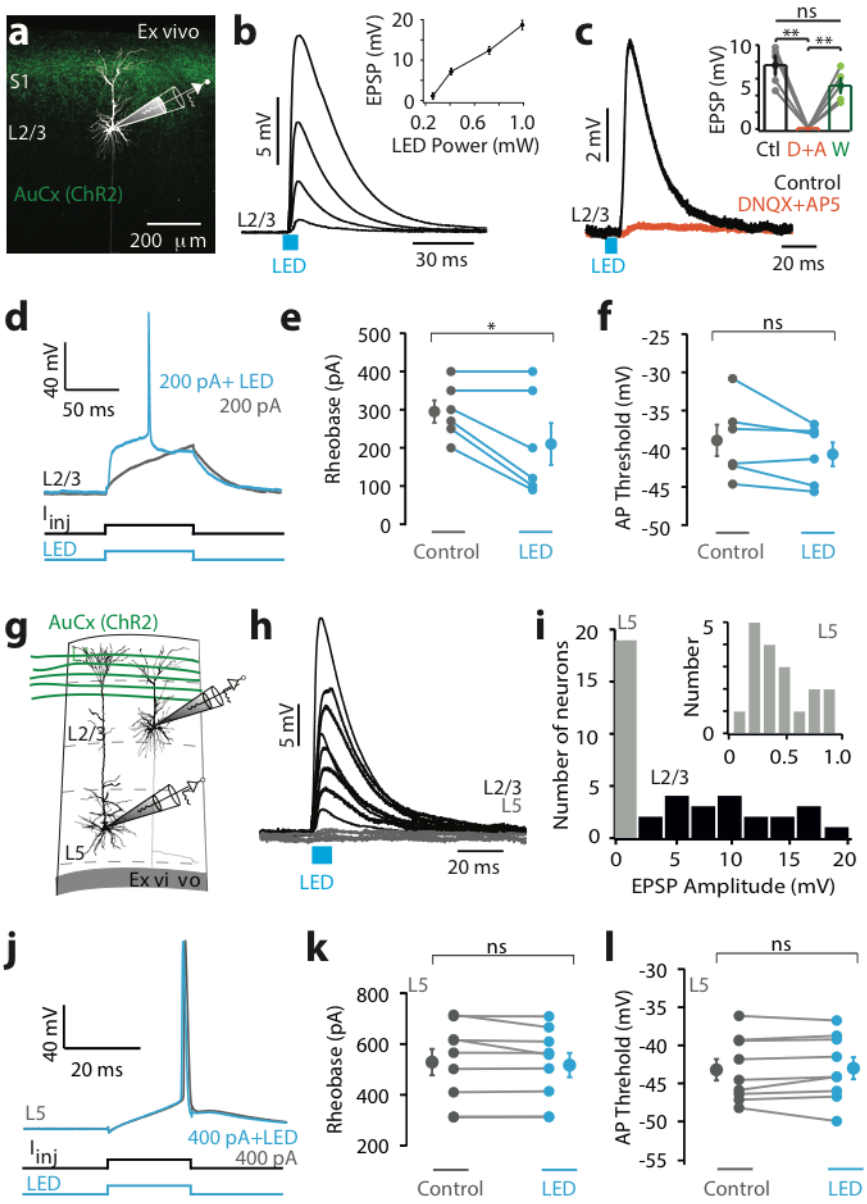

Inset, Average light evoked voltage responses in control (Ctl, black) DNQX+AP5 (D+A, orange), and washout (W, green; n = 5 neurons). **d.** Example of evoked action potentials in a L2/3 pyramidal neuron in S1 to somatic current pulse alone (grey; 200 pA, 100ms) and paired with photo activation of auditory cortex axons (blue; 470 nm; 2 ms). **e.** Rheobase during control current injection (grey) and paired with photo-activation of auditory cortex axons (blue; 470 nm; 2 ms) in L2/3 pyramidal neurons (n = 6 neurons; p = 0.03; $p_{shuffled}$ = 0.813).

f. Action potential (AP) threshold during control somatic current injection (grey) and current injection paired with photo-activation of auditory cortex axons (blue; 470 nm; 2 ms) in L2/3 pyramidal neurons (n = 6 neurons; p = 0.12; $p_{shuffled}$ = 0.313). **g.** Schematic of experimental paradigm. Patch clamp recordings were performed in L2/3 and layer 5 (L5) pyramidal neurons in the same somatosensory brain slice. **h.** Average light-evoked synaptic responses to photo-activation of auditory cortex axons (470 nm, 2 ms) in different L2/3 (black) and L5 (grey) pyramidal neurons in S1. **i.** Histogram of peak amplitudes of lightevoked synaptic responses to photo-activation in L2/3 pyramidal neurons (black) and L5 pyramidal neurons (grey). Inset, Histogram of L5 pyramidal neuron responses. **j.** Example of evoked action potentials in a L5 pyramidal neuron in S1 to somatic current pulse alone (grey; 200 pA, 20 ms) and paired with photo-activation of auditory cortex axons (blue; 470 nm; 2 ms). **k.** Rheobase during control current injection (grey) and paired with photo-activation of auditory cortex axons (blue; 470 nm; 2 ms) in L5 pyramidal neurons (n = 8 neurons; p = 0.41; $p_{shuffled}$ = 0.297). **l.** AP threshold during control somatic current injection (grey) and current injection paired with photo-activation of auditory cortex axons (blue; 470 nm; 2 ms) in L5 pyramidal neurons (n = 8 neurons; p = 0.56; $p_{shuffled}$ = 0.0.570). Error bars represent S.E.M. * $p < 0.05$.

Auditory input does not influence dendritic integration nor somatic output in L5 pyramidal neurons

While L5 pyramidal neurons do not receive direct monosynaptic input from the auditory cortex, we nevertheless tested whether auditory input can indirectly influence the encoding of somatosensory information in L5 pyramidal neurons during a forepaw stimulus in vivo. Using two-photon Ca^{2+} imaging, responses to sensory input were recorded in awake mice sparsely transfected with the Ca^{2+} indicator GCaMP6f in layer 5 of forepaw S1 (Figure 3.4a). Large

Ca^{2+} transients were evoked in tuft dendrites of L5 pyramidal neurons in response to tactile stimuli (Figure 3.4a and b; 2.56 ± 0.113 ΔF/F; n = 112 dendrites, 4 mice). Unlike L2/3 neurons, the amplitude of these tactile-evoked responses was not significantly altered when paired with auditory input (Figure 3.4c; AudTac; 2.507 ± 0.112 ΔF/F; n = 106 dendrites, 4 mice; p = 0.794). Ca^{2+} transients were also evoked in the main apical dendrites of L5 pyramidal neurons in response to tactile input (Fig. 4d and e; 3.25 ± 0.21 DF/F; n = 44 dendrites). Similar to L5 tuft dendrites, the amplitude of tactile-evoked responses were not significantly different when paired with auditory input (Figure 3.4e and f; AudTac; 3.10 ± 0.18 ΔF/F; n = 44 dendrites, 4 mice; p = 0.755). These results illustrate that auditory input does not influence sensory integration in L5 pyramidal neuron dendrites. Compared to L2/3 pyramidal neurons, the normalized amplitude of sensory-evoked Ca^{2+} responses in the dendrites of L5 pyramidal neurons was significantly smaller in amplitude (Figure 3.4g; $p < 0.0001$). Likewise, the probability of evoking Ca^{2+} responses in the dendrites of L5 pyramidal neurons was significantly different to L2/3 pyramidal neurons ($p < 0.0001$; Figure 3.4h). To test whether auditory input impacts on somatic output of L5 pyramidal neurons, we performed whole-cell recordings from the soma of L5 pyramidal neurons in forepaw S1 of awake mice (Figure 3.4i). These experiments indicated that tactile stimulation of the forepaw alone reliably evoked a subthreshold voltage response (3.9 ± 0.62 mV) and action potential firing (Figure 3.4j and k; 4.77 ± 1.20 Hz; n = 16 neurons, 5 mice). In contrast, auditory input did not significantly alter the tactile-evoked subthreshold voltage response (AudTac, 3.97 ± 0.61 mV; n = 16 neurons, 5 mice; p = 0.43) or action potential output (Figure 3.4j and k; AudTac, 5.09 ± 1.15 Hz; n = 16 neurons, 5 mice; p = 0.81). Furthermore, auditory input had negligible impact on the voltage response at the soma (Figure 3.4j; peak, 0.63 ± 0.23 mV; n = 16 neurons, 5 mice;) and no significant impact on action potential output (Figure 3.4j and k; baseline, 2.60 ± 0.65 Hz vs auditory, 2.85 ± 0.72 Hz; n = 16 neurons, 5 mice; p = 0.83). These results show that, unlike

L2/3 pyramidal neurons, auditory input to forepaw S1 has minimal impact on dendritic activity and does not alter somatic action potential output of L5 pyramidal neurons.

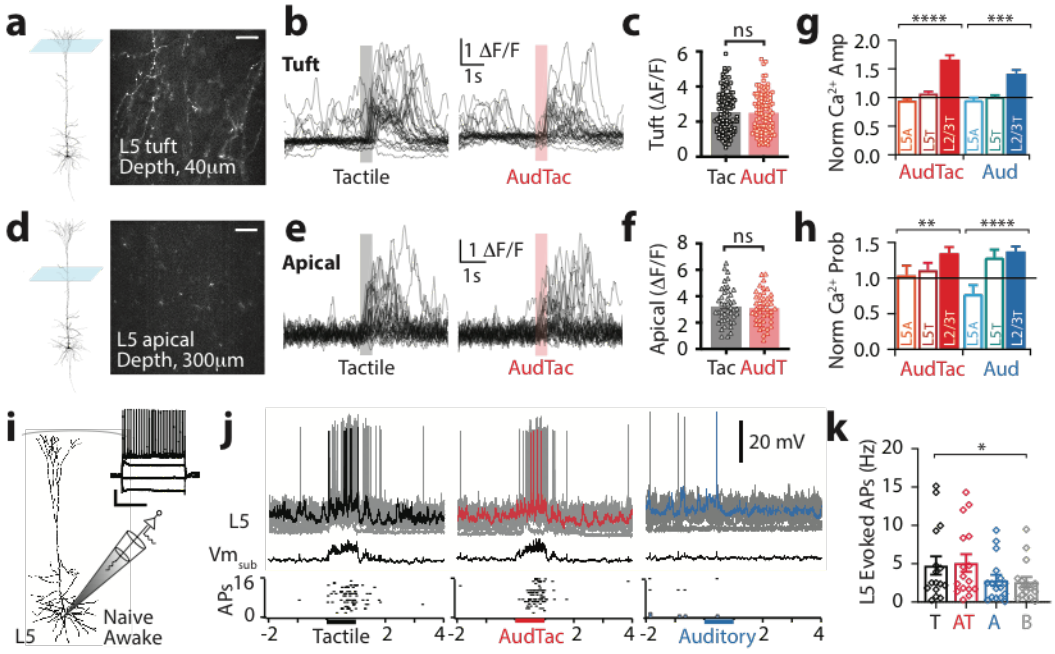

Figure 3.4 | Auditory input does not influence dendritic integration, nor somatic output, in layer 5 pyramidal neurons. a. Left, Schematic of experimental paradigm. Right, Two-photon Ca^{2+} imaging was performed in the tuft dendrites of L5 pyramidal neurons previously injected with GCaMP6f. Imaging depth, 40 µm below pia. Scale bar, 10 µm. **b.** Overlay of Ca^{2+} transients from a tuft dendrite shown in (a) during tactile stimulus alone (black) and paired with auditory stimulus (AudTac, red). **c.** The amplitude of Ca^{2+} transients in L5 tuft dendrites during tactile stimulus (black; n = 112 dendrites, 4 mice; 27 $trials_{av}$) and paired auditory and tactile stimulus (red; n = 106 dendrites, 4 mice; 24 $trials_{av}$; p = 0.794; $p_{shuffled}$ = 0.960; Mann Whitney test). **d.** Left, Schematic of experimental paradigm. Right, Two-photon Ca^{2+} imaging was performed in apical dendrites of L5 pyramidal neurons previously injected with GCaMP6f. Imaging depth, 300 µm below pia. **e.** Overlay of Ca^{2+} transients from an apical dendrite shown in (d) during tactile stimulus alone (black) and paired with auditory stimulus (AudTac, red).

f. The amplitude of Ca^{2+} transients in L5 apical dendrites during tactile stimulus (black; n = 44 dendrites, 4 mice; 26 $trials_{av}$) and paired auditory and tactile stimulus (red; n = 44, 4 mice; 26 $trials_{av}$; p = 0.755; $p_{shuffled}$ = 0.931; Mann Whitney test). **g.** Comparison of the amplitude of Ca^{2+} transients in L5 apical (L5A), L5 tuft (L5T) and L2/3 tuft (L2/3T) dendrites during AudTac stimulus (red) and auditory stimulus (blue) normalized to the response to tactile stimulus. One-way ANOVA Friedman test, **** p < 0.0001, *** p = 0.0005. **h.** Comparison of the probability of evoked of Ca^{2+} transients in L5 apical (L5A), L5 tuft (L5T) and L2/3 tuft (L2/3T) dendrites during AudTac stimulus (red) and auditory stimulus (blue) normalized to the response to tactile stimulus. One-way ANOVA Friedman test, ** p = 0.0087, **** p < 0.0001. **i.** Schematic of experimental paradigm. Patch clamp recordings were performed from L5 pyramidal neurons in forepaw S1 from naïve mice in the awake state. Inset, example voltage response to injected 50 pA steps of current. Scale, 20 mV, 400 ms. **j.** (Top) Overlay of individual trials, (middle) average subthreshold voltage, and (bottom) raster of action potentials from a typical neuron (left) in response to tactile stimulus (black), paired auditory and tactile stimulus (red) and auditory stimulus (blue). Grey traces, all trials overlaid. Colored trace, single example voltage trace. **k.** Comparison of the evoked action potentials in response to tactile (black), paired auditory and tactile (red), auditory (blue) and baseline (grey) in L5 pyramidal neurons (n = 16 neurons, 5 mice; 17 $trials_{av}$; One-way ANOVA Friedman test. Error bars represent S.E.M. * p < 0.05.

Auditory stimulus enhances dendritic tuft activity during tactile goal-directed behaviour

We next asked whether auditory input can impact somatosensory-based behavior. To investigate this, we trained mice in a tactile-based Go/NoGo goal-directed task (see methods). Here, mice rested their contralateral forepaw on a vibrating button which provided a nonnoxious tactile vibration stimulus (200 Hz, 500 ms; Tactile-trial). If mice licked the sensor

within one second of receiving the tactile stimulus, then a sucrose water reward was delivered. Once trained in this task, mice were then randomly presented with an auditory stimulus (broadband noise, 2 - 50 kHz, 75 dB, 500 ms) either alone (Auditory-trial) or simultaneously with the tactile stimulation (AudTac-trial). Mice were trained to ignore the auditory stimulus and only received a water reward after the tactile stimulus was presented alone or when paired with the auditory stimulus (Figure 3.5a; see Methods). Mice rapidly learnt the task and were considered expert when they had greater than 80% correct responses to Tactile-trials and less than chance response to Auditory-trials (Supplementary Figure 3.8). To test whether, similar to naïve mice, dendritic activity was altered by auditory input during sensory-based behavior, we performed Ca^{2+} imaging in tuft dendrites of L2/3 pyramidal neurons in forepaw S1 while mice performed the goal-directed tactile task (Figure 3.5b). Large Ca^{2+} transients were evoked during rewarded trials in approximately 40% of all active tuft dendrites (75/190 dendrites from 6 mice). During Tactile-trials, Ca^{2+} transients were evoked in 15.68 ± 2.05 % of correct trials (Figure 3.5c). When paired with an auditory stimulus, the proportion of tactile-trials with a Ca^{2+} response was significantly increased to 21.1 ± 2.6 % (Figure 3.5d and e; $p < 0.0001$). The peak amplitude of Ca^{2+} transients evoked in tuft dendrites with increased activity was also significantly increased during AudTac-trials by on average 71 ± 31 % (Figure 3.5f; n = 58 dendrites, 6 mice; $p = 0.0025$). In contrast, there was no difference in the duration (Tactile trials, 221 ± 21 ms; AudTac-trials, 241 ± 15 ms; Auditory-trials, 237 ± 19 ms), onset (Tactile-trials, 350 ± 7 34 ms; AudTac, 406 ± 38 ms) or variance (Tactile-trials, 3.49 ± 0.59 ΔF/F; AudTac-trials, 3.87 ± 0.64 ΔF/F) of Ca^{2+} transients in tuft dendrites during these rewarded trials. These tactile-evoked dendritic Ca^{2+} events require NMDA receptor activation as they were abolished in 86% of dendrites by local application of the NMDA channel blocker APV (n = 18/21 dendrites, 3 mice), suggesting they represent NMDA spikes. During the goal-directed task, auditory stimuli were randomly presented to expert mice (Figure 3.5g). Similar

to the naïve state (Figure 3.1), auditory input alone evoked significantly larger Ca^{2+} transients in tuft dendrites compared to tactile-trials (Figure 3.5h; Auditory-trial, 3.26 ± 0.30 ΔF/F; Tactile-trial, 2.61 ± 0.32 ΔF/F, n = 58 dendrites, 6 mice; p = 0.018), however, these events were evoked in significantly less trials (7.5 ± 0.8% trials; p = 0.0006). Taken together, these results illustrate that dendritic Ca^{2+} activity is enhanced when auditory input is paired with Tactile-trials in a goal-directed task.

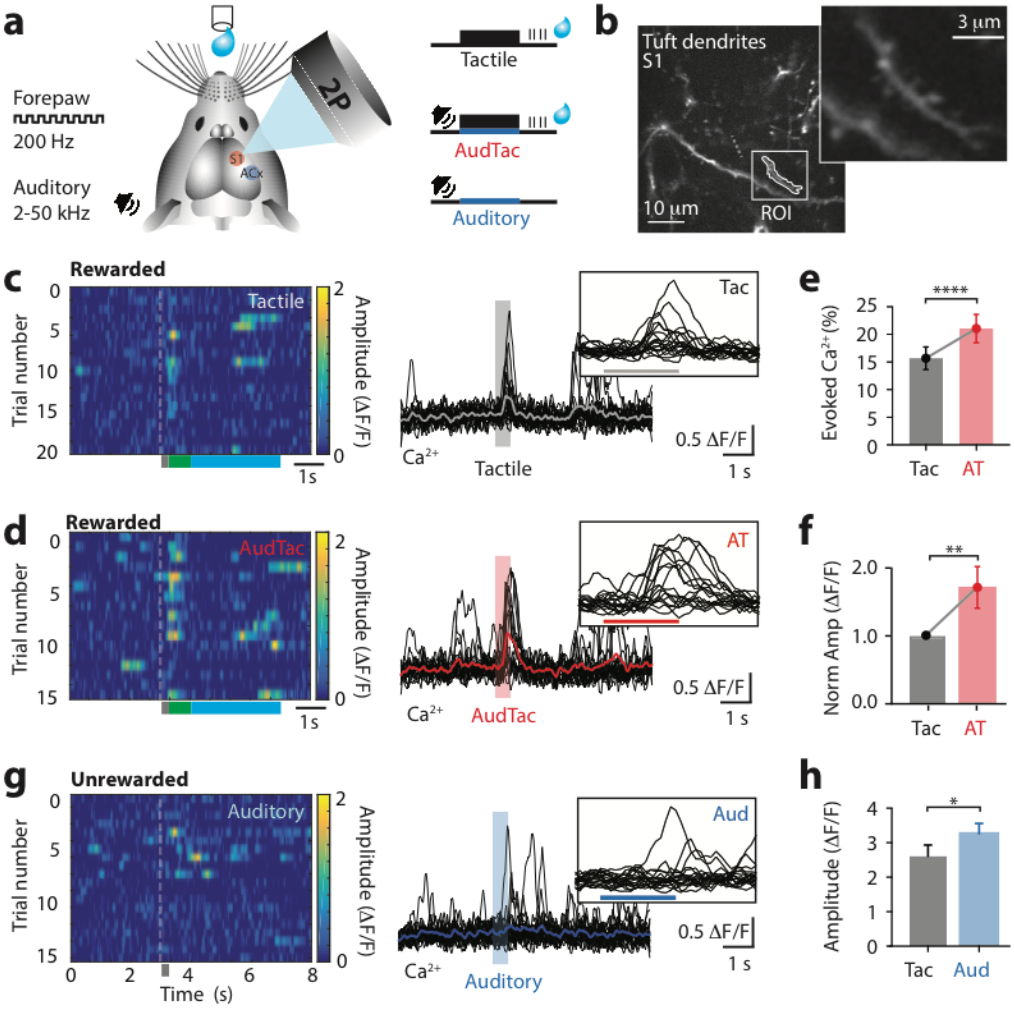

Figure 3.5 | Auditory input during tactile goal-directed behavior enhances tuft Ca^{2+} activity. a. Schematic of tactile-based goal directed behavior paradigm. Mice received a water reward if they licked in response to tactile stimulus alone (tactile-trial; 200 Hz, 500 ms) and paired tactile and auditory stimulus (AudTac-trial). On random trials, mice were also presented with auditory stimulus alone (Auditory-trial; 2 – 50 kHz; 500 ms) which was not rewarded. **b.** Ca^{2+} activity from the tuft dendrites of L2/3 pyramidal neurons within the primary somatosensory cortex was recorded during task performance. Inset, zoom of dendrite from boxed region. **c.** (left) Colour heatmap of Ca^{2+} signals from an example tuft dendrite during correct HIT performance in Tactile-trials. (right) Overlay of Ca^{2+} traces during Tactile-trials. Inset, zoom of evoked Ca^{2+} responses. **d.** (left) Color heatmap of Ca^{2+} signals from an example tuft dendrite during correct HIT performance in AudTac-trials. (right) Overlay of Ca^{2+} traces during AudTac-trials. Inset, zoom of evoked Ca^{2+} responses. **e.** Percentage of trials with evoked Ca^{2+} activity during Tactile-trials (black) and AudTac-trials (red). n = 75 dendrites, 6 mice; 39 $trials_{av}$; $p < 0.0001$; $p_{shuffled} = 0.850$; Wilcoxon matched-pairs signed rank test). **f.** Average peak amplitude of Ca^{2+} responses during AudTac-trials (red) normalized to Tactile trials (black). n = 58 dendrites, 6 mice; p = 0.0025; Wilcoxon matched-pairs signed rank test. Only dendrites with evoked Ca^{2+} transients during both Tactile- and AudTac- trials are included in the analysis. **g.** (left) Colour heatmap and (right) overlay of Ca^{2+} signals during Auditory-trials from the example tuft dendrite in (**a**) and (**b**). Auditory-trials are not rewarded. Inset, zoom of evoked Ca^{2+} responses. **h.** Average peak amplitude of Ca^{2+} responses during Tactile-trials (black) and Auditory-trials (blue). n = 58 dendrites, 6 mice; p = 0.0025; Wilcoxon matched-pairs signed rank test. Error bars represent S.E.M. * $p < 0.05$, ** $p < 0.01$, **** $p < 0.0001$.

Auditory stimulus decreases the reaction time during tactile goal-directed behavior

The presentation of auditory stimuli during this tactile-based goal directed behavior did not influence task-related attention or arousal state as determined by pupillometry (Figure 3.6a), with the relative change in pupil diameter not significantly different during correct performance in Tactile-trials (0.130 ± 0.02 mm) and AudTac-trials (Figure 3.6b; 0.122 ± 0.02 mm; n = 6 mice; p = 0.22). Pupil responses during Tactile-trials and AudTac-trials were both significantly larger than those during Auditory-trials (0.03 ± 0.01 mm; n = 6 mice; p < 0.0001), further illustrating that the auditory stimulus alone does not alter attentional state during this goal directed task. To test whether auditory input during Tactile-trials alters behavior, we analysed lick responses during correct performance (Hit trials) in expert mice (Figure 3.6c). On average, expert mice reported the detection of the tactile stimulus by licking the port with an overall latency of 460 ± 33 ms (n = 18 mice). During the same session, when the auditory stimulus was paired with a tactile stimulus (AudTac-trails), the lick latency was significantly reduced (Figure 3.6d; 433 ± 33 ms; n = 18 mice; p = 0.0002). This decrease in response latency was not due to session differences, as mice reliably and robustly performed the task with only a 4.5 ± 2.5 ms difference in response latency between consecutive sessions (Tactile-trials, n = 18 mice). Furthermore, the decrease in response latency did not occur if the auditory stimulus was presented 200 ms before the tactile stimulus (p = 0.34; n = 8 mice) and was not correlated with the Tactile-trial reaction time in different mice (Supplementary Fig 3.9; R_2 = 0.14). Despite decreasing reaction time, there was no significant difference in the percentage of rewarded (HIT) Tactile-trials (90.49 ± 1.27 %) and AudTac-trials (Fig. 6e; 91.94 ± 1.42 %; n = 18 mice; p = 0.327).

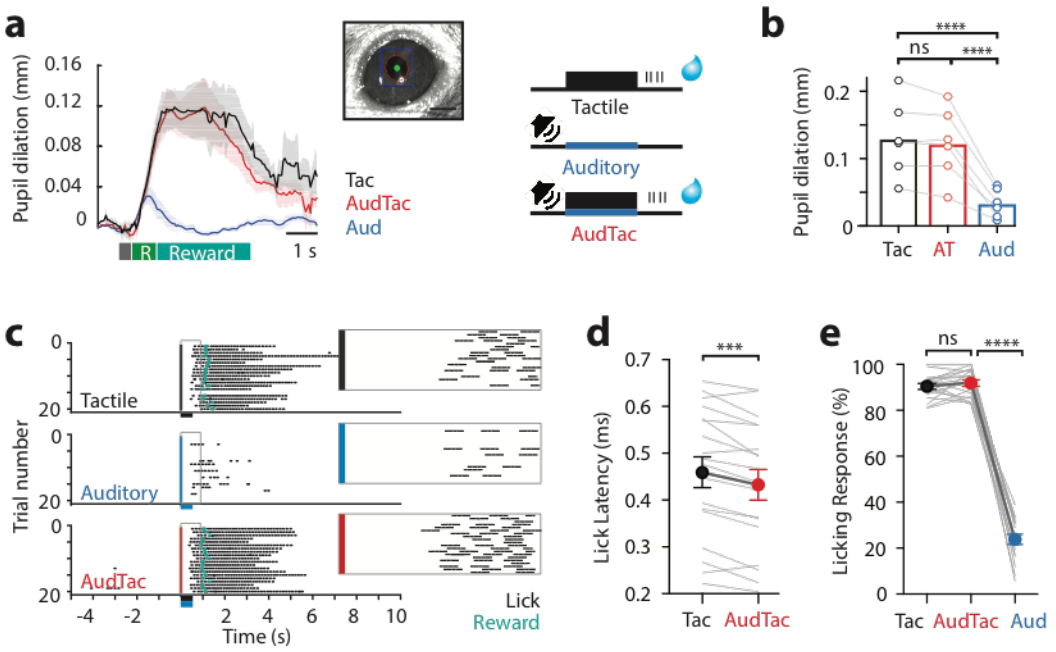

Figure 3.6| Auditory input during tactile goal-directed behavior decreases reaction time. a. Tactile goal-directed task: Mice were trained to receive a water reward if they licked a reward port in response to tactile stimulus alone (Tactile-trial; 200 Hz, 500 ms) and paired tactile and auditory stimulus (AudTac-trial). On random trials, mice were also presented with auditory stimulus alone (Auditory-trial; 2 – 50 kHz) which was not rewarded. Pupil diameter was 17 measured during task performance illustrating Tactile-trials (black) and AudTac-trials (red) had similar dilation. Grey, stimulus; Green, response; Blue, reward. Inset, eye pupil ROI. **b.** Pupil dilation during Tactile-trials was not significantly different to AudTac-trials (AT; n = 6 mice; 17 $trials_{av}$; p = 0.31 p = 0.22; $p_{shuffled}$ = 0.563; Wilcoxon matched-pairs signed rank test). However, pupil dilation during both Tactile-trials and AudTac-trials was significantly greater than Auditory-trials (n = 6 mice; 10 $trials_{av}$; p = 0.031; $p_{shuffled}$ = 0.156; Wilcoxon matchedpairs signed rank test). **c.** Licking activity in an example mouse performing the goal directed task during tactile-trials (black), AudTac-trials (red) and Auditory-trials (blue). Dots, detected licks on lick port. Reward delivery, blue. Inset, expanded view of grey boxed region highlighting licking response from stimulus onset (coloured line).

d. The licking response in AudTac-trials was faster than Tactile-trials (n = 18 mice; 50/61 $trials_{av}$; p = 0.0002; $p_{shuffled}$ = 0.610; Wilcoxon matched-pairs signed rank test). **e.** Percentage of trials with a lick in the response window during Tactile-trials (black), AudTac-trials (red) and Auditory-trials (blue). There was no significant difference in performance between Tactile-trials and AudTac-trials (p = 0.327; $p_{shuffled}$ = 0.229; n = 18 mice; 61/50 $trials_{av}$; Wilcoxon matched-pairs signed rank test). Error bars represent S.E.M. *** p < 0.001, **** p < 0.0001.

Photo-inhibition of axonal input in S1 abolishes the decrease in reaction time during tactile goal-directed behaviour

Is this enhanced behavioural response due to axonal projections from the auditory cortex to forepaw S1? To test this, we silenced these auditory axonal projections in forepaw S1 during the goal-directed behavior. To achieve this, mice were transfected with the inhibitory opsin, Archaerhodopsin (AAV1.CAG.ArchT.GFP.WPRE.SV40) in the auditory cortex (Figure 3.7a and Supplementary Figure 3.10). Following expression, axonal projections from the auditory cortex were photoinhibited by a LED (590 nm) focused on the surface of forepaw S1 while mice performed the goal-directed task (Figure 3.7b). Axonal photo-inhibition abolished the decrease in response latency observed when auditory input was paired with tactile input (Figure 3.7c; Tactile-trial, 417 ± 38 ms vs AudTac-trial, 408 ± 41 ms; n = 6 mice; p = 0.563). Light activation alone did not alter lick latency, as the decrease in reaction time observed during 0.0312; n = 6 mice) and in mice where light penetration into the cortex was blocked (Supplementary Figure 3.11; p = 0.03; n = 6 mice;). Similar to control animals, input from the auditory cortex to forepaw S1 did not alter the percentage of correct responses, as mice performed at near perfect performance during photo-inhibition of auditory input (Figure 3.7d and Supplementary Figure 3.11; LED ON, 91.54 ± 3.44 %; LED OFF, 99.01 ± 0.62; p = 0.44;

n = 6 mice). These findings suggest that inhibiting the direct axonal projection from the auditory cortex to forepaw S1 abolishes the capacity of auditory input to enhance somatosensory encoding during tactile goal-directed behavior.

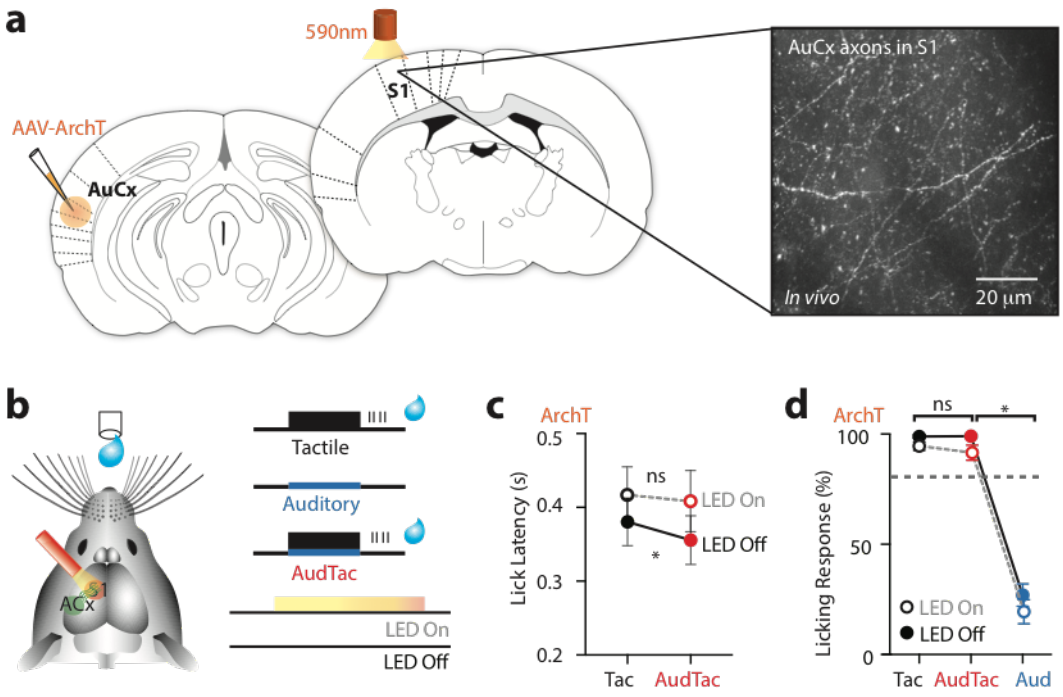

Figure 3.7 | Photo-inhibiting the direct axonal projection from the auditory cortex to forepaw S1 abolishes the capacity of auditory input to decrease the behavioral response latency during tactile goal-directed behavior. a. The inhibitory opsin, Archaerhodopsin, was injected into the auditory cortex and axonal projections in forepaw S1 were photo-inhibited (590 nm) during the goal-directed behavior. Image of auditory-cortex axons transfected with Archaerhodopsin in forepawS1 (~50 µm below pia). **b.** Schematic of experimental paradigm. Mice previously injected with Archaerhodopsin were trained to receive a water reward if they licked a reward port in response to tactile stimulus alone (Tactile-trial; 200 Hz, 500 ms) and paired tactile and auditory stimulus (AudTac-trial).

On random trials, mice were also presented with auditory stimulus alone (Auditory-trial; 2 – 50 kHz) which was not rewarded. LED (590 nm) was either focused on the surface of forepaw S1 (LED On) or not (LED Off) while the mouse performed the goal-directed task. **c.** The lick latency during Tactile-trials and AudTactrials were not significantly different during photo-inhibition of auditory axons in forepaw S1 (LED On; n = 6 mice; 37/33 $trials_{av}$; p = 0.563; $p_{shuffled}$ = 0.688; Wilcoxon matched-pairs signed rank test). **d.** Percentage of trials with a lick in the response window during LED On (orange) and LED Off (black). There was no significant difference in performance during LED On (n = 6 mice; 37/33 $trials_{av}$; p = 0.44; $p_{shuffled}$ = 0.844;). Error bars represent S.E.M. * p < 0.05, *** p < 0.001, **** p < 0.0001.

DISCUSSION

The function of the primary sensory areas of the cortex in information processing is unclear. Historically, primary sensory areas of the cortex were seen to play an important role in the processing and encoding of sensory information necessary for perception of a single sense[137-139]. This, coupled with early work showing a lack of evidence of direct projections between primary sensory areas[140], supported the view that primary cortical areas were involved solely in unimodal stimulus processing. Here, we illustrate that the primary somatosensory cortex plays a more complex role in the processing of information, and combines sensory information from various modalities to directly impact sensory-based behavior. Specifically, the auditory cortex sends direct projections to the primary somatosensory cortex, resulting in auditory evoked activity in tuft dendrites of L2/3 pyramidal neurons in S1. This monosynaptic auditory input enhanced sensory encoding by increasing the Ca^{2+} response in tuft dendrites as well as the number of action potentials evoked during tactile stimulation. Furthermore, we show that auditory input impacts tactile-based behavior, decreasing the reaction time during a goal-

directed task. Photoinhibition of axonal projections from the auditory cortex to forepaw S1 abolished the impact of auditory input on reaction speed, illustrating the importance of this input during a tactile task.

In contrast to our findings in somatosensory cortex, a previous study found a hyperpolarizing (inhibitory) influence of auditory input in primary visual cortex[77]. Response suppression to multiple unimodal stimuli has also been demonstrated in other primary cortices and cell types[141,142]. These contrasting results illustrate the complexity of cross-modal communication, which targets different cell types as well as different cortical layers, leading to both excitatory and inhibitory cell-specific changes in cellular processing. Indeed, our results highlighted the different influence of auditory input on sensory processing in L2/3 and L5 pyramidal neurons in forepawS1. Although both L2/3 and L5 tuft dendrites generate auditory-evoked responses, neural output during tactile-encoding was not modulated by auditory input in L5 pyramidal neurons. This is in contrast to L2/3 pyramidal neurons, and may result from the increased electrotonic remoteness of L5 apical tuft dendrites from the soma compared to L2/3 pyramidal neurons [143,144]. Selectivity of multi-modal information processing has also been reported in auditory projections to the visual cortex[20], where orientation selectivity of layer 2/3, not layer 4, excitatory neurons were sharpened by the presence of sound. This is in contrast to the impact of visual information on coding in auditory cortex, which is almost exclusively found in deeper infragranular layers[145]. Despite L2/3 pyramidal neurons controlling the gain of L5 pyramidal neuron output[132], there was no influence of auditory input on tactile-evoked action potential output in L5 pyramidal neurons in our study. Although known to directly influence cortical output neurons [132-134], L2/3 pyramidal neurons also send long-range projections to other cortical and subcortical areas [135,136]. This connectivity strategy provides the entire cortex with an intermediate stage of processing where, due to the integration of internal feedback, representations are constantly updated, potentially enhancing flexibility of behavioral outputs.

Paradoxically, auditory stimulation evoked a larger Ca^{2+} transient in tuft dendrites of L2/3 pyramidal neurons in forepaw S1 than tactile stimulation. This is likely to be a consequence of where these different sensory inputs synapse onto pyramidal neurons. In the cortex, bottom-up sensory information typically targets the middle cortical layers, whereas top-down information usually courses through the upper cortical layers where the distal dendrites of pyramidal neurons stratify[33,139,146]. Using fluorescence imaging, we illustrated that auditory input is predominately restricted to upper cortical layers, with the maximum relative optical density occurring in layer 1. Therefore, auditory input would primarily synapse onto distal tuft dendrites in S1, whereas tactile somatosensory input would primarily target basal dendrites[41]. In contrast to Ca^{2+} transients in tuft dendrites, the soma of L2/3 pyramidal neurons fired more action potentials during tactile stimulation compared with auditory stimulation. Again, this is likely to be a consequence of the location of synaptic input, as more proximal tactile input onto basal dendrites is electrotonically closer to the soma than the more distal input from auditory cortex. The relative influence of different sensory modalities on neural activity would be dependent on the strength of the stimulus [114] with different intensities leading to different sensory integration at the level of a single neuron.

Despite auditory input causing a significant increase in the tactile-evoked firing in L2/3 pyramidal neurons, there was no measurable influence of auditory input on the subthreshold responses to the tactile stimuli. This disconnect between subthreshold responses and enhanced action potential output has been reported previously in hindpaw S1[147] and is likely to be due to the generation of dendritic spikes in the distal apical dendrites, which can have a direct impact on action potential generation[50,124,126,148,149]. Consistent with this idea, auditory input increased tactile-evoked Ca^{2+} transients in the distal tuft dendrites of L2/3 pyramidal neurons. This may result from the active integration of synaptic input from the two different pathways, or possibly from passive boosting of the tactile-evoked Ca^{2+} transient by auditory input. Since auditory

input also increased the probability of evoking Ca^{2+} activity during the tactile-based behavior, this suggests auditory input actively integrates with tactile input to generate a new detectable event. Evoked Ca^{2+} events were completely abolished by the NMDA antagonist APV, consistent with the idea that they represent NMDA spikes [129,149-151]. Taking these results together, they suggest a non-linear interaction between intra-cortical and bottom-up inputs reminiscent of back-propagating action potential activated Ca^{2+} spike firing (BAC firing) observed in L5 pyramidal neurons[124]. Finally, it is worth noting that the long duration of NMDA spikes[150] would ensure there is an extended time window for multi-sensory integration. Integrating information from multiple senses is crucial to survival. The cortex is central to this process, connecting information from different senses in a layer and neuron specific manner. Here, we demonstrate that this can occur at the level of single neurons as the auditory cortex sends direct projections to primary somatosensory cortex, resulting in auditory evoked activity in tuft dendrites of pyramidal neurons. Since feedback contextual information is dampened under anaesthesia [152], auditory responses in both the awake and anaesthetized preparation further illustrate the direct nature of the auditory input. This monosynaptic auditory input enhanced sensory encoding of somatosensory information and decreased reaction time by ~30 ms during a tactile goal-directed task. Taking into account a minimum reaction time in sensory decision-based behaviors [153], this equates to an increased reaction time by 10-20 %. This small, but robust behavioral effect could have a profound influence on behavior in a multi-sensory environment, and may also be influenced by the specific training paradigm [154,155] and stimuli used [15,114]. Modulation of reaction times during photo-inhibition of the primary somatosensory cortex have also been observed in a texture discrimination task, however, in this case reaction time was driven by the recruitment of cortical inhibition by layer 5 pyramidal neurons [156]. This illustrates the complexity of the neural networks underlying sensory-based behavior, and the important role the primary somatosensory cortex plays in the reaction time of a behavioral

response. Since its development [157], the inhibitory opsin Archaerhodopsin has been frequently used to investigate the role of specific neural networks. Despite being a powerful approach [158], the effectiveness of photoinhibition may not be complete therefore potentially explaining the variability of the results.

In summary, our study adds to an increasing body of literature demonstrating that primary cortical areas process information from multiple senses. These studies, combined with our findings, challenge the classic view of information processing in the cortex as being mainly hierarchical and segregated.

METHODS

All experiments were conducted in strict accordance with the Code of Practice for the Care and Use of Animals for Scientific Purposes (National Health and Medical Research Council, Australia) and guidelines given by the veterinary office of The Florey Institute of Neuroscience and Mental Health and the Animal Ethics Committee of the Australian National University.

Virus injections. Mice (C57BL/6; P30 - 55) were anaesthetised with isoflurane (1 - 3 % in 0.75 L/min O_2) and body temperature was maintained at 36 - 37 °C. Eye ointment was applied to prevent dehydration and meloxicam (1 - 3mg/kg, Ilium) was intraperitoneally injected for anti-inflammatory action. The skin was disinfected with ethanol 70 % and betadine and a small slit was made in the skin to expose the skull. A small craniotomy (0.7 x 0.7 mm) was then made over the brain region of interest and the dura was left intact. For labelling the auditory cortex with channelrhodopsin (ChR2; AAV1.hSyn.ChR2(H134R)-eYFP.WPRE.hGH), 100 nl was injected at 2.5 mm posterior to bregma and 4.5 mm lateral from midline (at a cortical depth from pia of 200 - 500 µm). For sparsely labelling the primary somatosensory cortex (forepaw) with a Ca^{2+} indicator, a mix of Cre-dependent genetic Ca^{2+} indicator GCaMP6f (AAV1.Syn.Flex.GCaMP6f.WPRE.SV40) and diluted Cre (AAV1.hSyn.Cre.WPRE.hGH) was injected in either L2/3 (AP: 0 mm and ML: 2 mm at a depth of 450 µm) or L5 (at a depth of 700 µm, reached by moving the pipette 1400 µm with an angle of 30°, starting at -1.2 mm from bregma and 2 mm from midline). After slowly retracting the microcapillary pipette, the skin was sutured and the mouse was able to recover for at least 3 days prior to any further experimental procedures.

Head-post implantation and cranial window surgery. To surgically implant the head-post for recordings in the awake state, mice were anaesthetized with isoflurane (1 – 3 % in 0.75 L/min O_2) and intraperitonially injected with Meloxicam (1 – 3 mg/kg, Ilium). Throughout the

surgery, body temperature was maintained at 36 - 37 °C. Lidocaine (20mg/ml, Ilium) was topically injected around the surgical site before the skin was cut to expose the skull. A custom-made metal head-bar was then attached to the skull using dental cement (C&B Metabond®, Parkell). For electrophysiological recordings in the awake state, the remaining exposed skull was covered with transparent dental cement and the mouse returned to their home cage for at least 3 days before habituation commenced. For Ca^{2+} imaging experiments, a craniotomy was performed (3 mm diameter) over the virus injection site in the primary somatosensory cortex. A circular coverslip (3 mm diameter, size #1) was placed over the craniotomy, and sealed with glue and dental cement before the entire surface was covered with inert silicon (kwik-cast, WPI). Mice were returned to their home cage for at least 3 days before behavioral training commenced. In one cohort of mice, a double window was used by putting together two coverslip of different sizes (3-3.5 mm) using UV curable glue. This helps reducing motion artifacts and stabilizing the cranial window implant.

EMG recordings. In a subset of experiments, two electrodes were inserted in the neck muscles bilaterally during head-post surgery for nuchal EMG recordings. The EMG signal was recorded using differential amplifier DP-301 (Warner Instruments), band-pass filtered between 300-10000 Hz, digitized and recorded at 20 kHz using custom written Igor Pro (Wavemetrics) software.

Pupil Tracking. In some experiments, the pupil of the mouse was monitored during passive stimulus presentation or task performance, to measure attention level and arousal state. The pupil dilation was tracked using a high-speed CMOS camera (Blaser aCA1300) mounting a 50 mm lens and a custom software provided by Viktor Bahr, Jens Kremkow and Robert Sanchez from Charité University Berlin. The traces were extracted and normalized as the difference from mean baseline value (pre-stimulus). The relative change in pupil diameter during stimulus presentation or task performance was then measured as the maximum value in a window of 1

second following stimulus onset (once the trace crossed 2 standard deviation from baseline activity). Values are reported as mean changes in pupil size (mm) per mouse.

Sensory stimulus. Tactile stimulus was delivered to the contralateral forepaw (200 Hz; 500 ms) via a piezo-electric buzzer (Microdrive). Auditory stimulation was evoked using a broadband noise stimulus (2 - 50 kHz, 75 dB, 500 ms) played through a speaker (Logitech) placed approximately 5 - 10 cm away from the contralateral ear. All experiments were performed within a sound-proofed faraday cage with a white noise ambient sound (~60 dB) constantly played to further isolate and exclude any external sound cue (not relevant to the task). The tactile stimulus produces sound measured at 1-2 dB, which is considerably less than the auditory stimulus and background ambient sound. Both tactile and auditory stimuli were generated and delivered using Arduino micro-processing boards (Arduino Uno) and Bpod (Sanworks) with custom-written MATLAB (MathWorks) software.

Whole-cell recordings in the awake state. Mice (C57BL/6; P25 - 39) which had previously had a head-post implanted (>5 days prior) were gradually habituated to head restriction for 4 to 9 days. Here, mice were fixed to the recording frame and their paws rested unaided on either an active (contralateral) or inactive (ipsilateral) vibrating button. To prevent auditory startle response, the speaker delivering the auditory stimulation was located at a distance > 30cm from the mouse. During habituation, experimental stimuli (auditory broadband noise stimulus (2 - 50 kHz, 50 - 60 dB, 1 s); tactile (200 Hz, 1s) or both together) were presented randomly every 10 to 20 s for at least 3 sessions (30 - 60 min each). Once habituated, a craniotomy (1 x 1 mm) was performed over the forepaw area of the primary somatosensory cortex (AP 0mm; ML, +2.2 mm) under isoflurane anaesthesia (1 – 3 % in 0.75 L/min O_2). The brain was covered with agar and then inert silicon (kwik-cast, WPI). Animals were allowed to recover for at least two hours before whole-cell patch clamp experiments were performed for a maximum of two hours over two consecutive days. During a recording session, mice were placed on the head-fix frame

and their paws naturally rested on a vibrating button. The silicon protective cover was removed, and normal ringer (135 mM NaCl, 5.4 mM KCl, 1.8 mM CaCl2, 1 mM MgCl2, 5 mM HEPES) was used to bathe the craniotomy throughout the experiment. Whole-cell *in vivo* patch clamp recordings were obtained from either layer 2/3 pyramidal neurons (~200 μm below pia) or layer 5 (~600 μm below pia) using a patch pipette (resistance 4 - 6 MΩ) filled with an intracellular solution containing 115 mM potassium gluconate, 20mM KCl, 10 mM sodium phosphocreatine, 10 mM HEPES, 4 mM Mg-ATP, 0.3 mM Na-GTP, adjusted to pH 7.3 - 7.4 with KOH. The patch pipette was inserted into the brain at an angle of 45° relative to the cortical surface, to a depth of ~200 μm. The pipette was then advanced in steps of 1 μm (for a maximum distance of 200 μm in the hypotenuse trajectory) until a neuron was encountered. Whole-cell voltage recordings were performed from the soma using Dagan BVC-700A amplifiers and sampled at 20 kHz. Custom written Igor Pro (Wavemetrics) software was used for both acquisition and analysis and no correction were made for the junction potential. The identity of pyramidal cell in *in vivo* blind recordings was confirmed using the recording depth and voltage response to current steps. Once a whole-cell recording was obtained, the voltage response to current steps (50 pA; 800 ms) was recorded to characterize the neuron. Mice were then exposed to auditory broadband noise stimulus (2 - 50 kHz, 60 dB, 1 s) and/or tactile stimulus (200 Hz, 1 s) at inter-trial intervals of 10s. In a subset of neurons which had a low rate of action potential firing, positive holding current was applied to the neuron via the patch pipette (~50 pA) to provide additional depolarization to lower the threshold for action potential generation. Only recordings where greater than 14 trials of each stimulus were presented to the mouse were included in the analysis. Where reported, neurons were filled with fluorescent biocytin for posthoc cell identification and morphological reconstruction using online software, NeuTube.

Whole-cell recordings in the anaesthetized state. Mice (C57BL/6; P42 - 63) were initially anaesthetised with isoflurane (1 - 3 % in 0.75 L/min O_2) before urethane anaesthesia (intraperitoneal, 1.6 g/kg, Sigma) was administered. Anaesthesia was monitored throughout the experiment, and a top-up dose of 10 % of the initial urethane dose was administered when necessary. Body temperature was maintained at 36 - 37 °C. Lidocaine (20mg/ml, Ilium) was injected around the surgical site on the scalp and the head was stabilized in a stereotaxic frame by a head-plate attached to the skull with dental cement (paladur, Heraeus). A craniotomy was performed over the forepaw area of the primary somatosensory cortex, S1 (~1.5 x 1.5 mm^2), centered at bregma and 2.2 mm lateral from midline. The dura was surgically removed and normal rat ringer (135 mM NaCl, 5.4 mM KCl, 1.8 mM CaCl2, 1 mM MgCl2, 5 mM HEPES) was used to bathe the craniotomy throughout the experiment. Whole-cell *in vivo* patch clamp recordings were performed using a patch pipette (resistance 6 - 9 MΩ) filled with an intracellular solution containing 115 mM potassium gluconate, 20mM KCl, 10 mM sodium phosphocreatine, 10 mM HEPES, 4 mM Mg-ATP, 0.3 mM Na-GTP, adjusted to pH 7.3 - 7.4 with KOH. The patch pipette was inserted into the brain at an angle of 30° relative to the cortical surface, to a depth of ~200 μm (to target layer 2/3 neurons). The pipette was then advanced in steps of 1 μm (for a maximum distance of 200 μm in the hypotenuse trajectory) until a neuron was encountered. Whole-cell voltage recordings were performed from the soma using Dagan BVC-700A amplifiers and were filtered at 10 kHz. Once a whole-cell recording was obtained, the voltage response to current steps (50pA; 800ms) was recorded to characterize the neuron. In a subset of neurons which had a low rate of action potential firing, positive holding current was applied to the neuron via the patch pipette (~50 pA). Custom written Igor Pro (Wavemetrics) software was used for both acquisition and analysis and no correction was made for the junction potential. For post-hoc identification and partial reconstruction of the recorded neurons, the cellular tracer, 5-(and-6)-Tetramethylrhodamine Biocytin (0.01 -

0.02 %) was included in the intracellular solution in a sub-set of experiments. For visualization, brains were sliced via a vibratome into 100 µm sections and fluorescent neurons were visualised using a confocal microscope (561 nm excitation, 566 - 669 nm bandpass emission filter).

Habituation and behavioral training for Ca^{2+} imaging during behavior. Mice which had previously undergone head-bar implantation surgery were water restricted (5 - 2 cycle, 1 ml/day on restriction days; *ad libitum* access to food). After > 2 days of water restriction, mice were gradually habituated to head fixation and the microscope setup for 4 to 9 days. Once habituated to the setup, behavioral training commenced. Here, mice were head-fixed to the recording frame and their paws rested unaided on either an active (contralateral) or inactive (ipsilateral) piezo-electric buzzer (Microdrive). Tactile stimulus was delivered to the contralateral forepaw (200 Hz; 500 ms). Auditory stimulation was evoked using a broadband noise stimulus (2 - 50 kHz, 75 dB, 500 ms) played through a speaker (Logitech) placed approximately 5 - 10 cm away from the contralateral ear. A white noise ambient sound was constantly played during the training session to isolate and exclude from any external sound cue (not relevant to the task). Both tactile and auditory stimuli were generated and delivered using Arduino micro-processing boards (Arduino Uno) and custom-written MATLAB (MathWorks) software. Behavioral training was performed in a systematic manner. 1) The association phase of training involved training the mouse to associate the presentation of the tactile forepaw stimulation with an automatically presented sucrose reward (10 µl, 10 % sucrose in water). 2) Next, the mouse learnt to lick the reward spout for reward delivery. Here, sucrose water reward was only delivered if the mouse licked the reward spout within a 1 - 2 second period following delivery of the tactile stimulus. After the inter trial interval (2-3 seconds), trial initiation was triggered only when the mouse was not spontaneously licking for at least 1-2 seconds. Hit rates were calculated as the number of correct trials where the animal

licked within the response period, divided by the total number of trials in a session. Once a hit rate of 80 % was achieved consistently over a period of 3 consecutive days, animals were moved on to the next phase. 3) The auditory stimulus alone was added, and the mouse learnt to ignore it and withhold licking while continuing to report the detection of the tactile stimulus. Licking after broadband auditory noise stimulus alone incurred a timeout punishment (2 s time-out which was re-triggered if licks were detected). Percentage of correct trials for this phase were calculated as the sum of hit (trials with correct tactile detection, as the previous phase) and correct rejections (trials where the mouse did not lick after presentation of the auditory stimulus) divided by the total number of trials in a session. Also, here, once a hit rate of 80 % was achieved consistently over a period of 3 consecutive days, animals were moved on to the test phase. 4) The testing phase consisted of the delivery of the following stimuli: tactile alone stimulus; auditory alone stimulus; tactile + broadband noise auditory stimulus with a 0 ms temporal offset. Lick responses after tactile stimulus (either alone or paired with auditory stimulus) was rewarded with a 10 µl drop of sucrose water. Licking after broadband auditory noise stimulus alone incurred a timeout punishment (2 s time-out which was re-triggered if licks were detected). Behavioral training and testing protocols were custom-written and presented using BPod (Sanworks), and MATLAB (MathWorks) was used to collect data.

Two-photon Ca^{2+} imaging. Two-photon imaging was performed through the cranial window implanted in mice previously transfected with the Ca^{2+} indicator GCaMP6f (see viral injections section). Once the mice had reached expert level (80 % correct during HIT trials) in the behavioral training, Ca^{2+} transients were recorded from tuft dendrites of layer 2/3 pyramidal neurons within the primary somatosensory cortex at a depth of 50-100 µm from the pia surface. GCaMP6f was excited at 940 nm (~30 mW at the back aperture) with a titanium sapphire laser (140 fs pulse width; SpectraPhysics MaiTai Deepsee) and imaged on a Sutter MoM through a 16x Nikon objective (0.8 NA). Emitted light was passed through a dichroic filter (565dcxr,

Chroma Technology) and short-pass filtered (ET525/70-2p, Chroma Technology) before being detected by a GaAsP photomultiplier tube (Hamamatsu). Images were acquired at a frequency of 30 Hz (512 x 512 pixels) using ScanImage software (Vidrio Technologies). In some experiments, prior to training, mice were placed in the imaging set up for habituation before a naïve imaging session was performed. Here, tactile, auditory or paired tactile-auditory stimulation were randomly presented while the mouse was passively resting under the two-photon microscope and tuft dendrites (50 – 100 µm below pia) were performed. The images were motion corrected with a custom written Matlab script. Region of interest (ROI) were manually drawn on ImageJ and fluorescence signal extraction was performed with a custom MATLAB script. All trials with motion in the z axis were excluded from the analysis.

Optogenetic modulation of auditory inputs. To specifically manipulate auditory projections into the primary somatosensory area (forepaw) we injected 150 nl of the inhibitory opsin ArchT (AAV1.CAG.ArchT.GFP.WPRE.SV40, Addgene pasmid #29777) into the auditory cortex (750 µm below pia) of PN30 mice and placed a cranial window over the primary somatosensory cortex with the same procedures described in the above sections (virus injections and cranial window surgery). The control group was injected with a novel GFP (muGFP, Scott et al., 2017) following the same procedures. After mice reached expert level in the behavioral task, a 590 nm LED (15 mW) was placed over the window for photoinhibition of auditory inputs during behavior. The light was carefully adjusted so that the focal plane would be positioned just underneath the glass window in order to optimally deliver the light into layer 1 of the primary somatosensory cortex. The design of the experiment consisted in a block of trials with no light (LED off) followed by a block of trials with LED on (100 each). In LED on trials the light was constantly delivered from 0.5 seconds before stimulus onset until the end of the trial (~ 5.50 s). During a control session the cranial windows of ArchT cohort was temporary covered with silicon (kiwk-Cast, WPI) to prevent the light to reach and inhibit

auditory inputs. In addition, the control cohort expressing muGFP underwent the same training and testing protocol as the ArchT cohort. Lick latencies were analysed in a window between 0.1-1 s from stimulus delivery with a custom MATLAB script. The injection sites and viral spread were checked post-hoc for the ArchT cohort to confirm no other cortical areas outside of the auditory cortex were transfected.

Whole-cell *in vitro* recordings. Mice (P30 - P35) previously injected with ChR2 in the auditory cortex (>14 days prior) were anaesthetized with isoflurane (3 – 5 % in 0.75 L/min O_2) before decapitation. The brain was then rapidly transferred to ice-cold, oxygenated cutting solution containing (in mM): 110 Choline Chloride, 11.60 Na-ascorbate, 7 $MgCl_2$, 3.1 Na-pyruvate, 2.5 NaH_2PO_4, 0.5 $CaCl_2$, 10 Glucose and 26 $NaHCO_3$. Coronal slices of the primary somatosensory cortex (300 μm thick) were cut with a vibrating microslicer (Leica Vibratome 1000S) and incubated in an incubating solution containing (in mM): 92 NaCl, 2.5 KCl, 1.2 $NaH2PO_4$, 30 $NaHCO_3$, 3 Na-pyruvate, 2 $CaCl_2$, 2 $MgCl_2$ and 25 Glucose at 35 ºC for 30 minutes, followed by incubation at room temperature for at least 30 minutes before recording. All solutions were continuously bubbled with 95%O_2/5%CO_2 (Carbogen). Whole-cell patch clamp somatic recordings were made from visually identified pyramidal neurons using DIC imaging and a CCD camera (PL-B957U, Pixelink). During recording, slices were constantly perfused at ~2ml/min with carbogen-bubbled artificial cerebral spinal fluid (ACSF) containing (in mM): 125 NaCl, 25 $NaHCO_3$, 3 KCl, 1.25 NaH_2PO_4, 2 $CaCl_2$, 1 $MgCl_2$ and 25 Glucose maintained at 30-34 ºC. Patch pipettes were pulled from borosilicate glass and had open tip resistance of 5-7 MΩ filled with an intracellular solution containing (in mM):130 potassium gluconate, 10 KCl, 10 sodium phosphocreatine, 10 HEPES, 4 Mg-ATP, 0.3 Na_2-GTP and 0.3% biocytin adjusted to pH 7.25 with KOH. All recordings were made in current-clamp using a BVC-700A amplifier (Dagan Instruments, USA). To ensure direct comparison, recordings were made from layer 2/3 and layer 5 pyramidal neurons from the same slice. Photoactivation

of axonal projections from the auditory cortex was achieved by briefly passing 470nm LED light (10ms) through a 60X Olympus objective onto the somatosensory cortical slice. To test for monosynaptic callosal input, TTX (1 μM) and 4-AP (100 μM) were added to the bath ACSF.

Drug application – in vivo and in vitro. Blocking the contribution of NMDA receptors during two-photon imaging, was achieved by removing the cranial window and dura under isoflurane anaesthesia (3 – 5 % in 0.75 L/min O_2) to apply APV on the brain surface (outside of the dura: 10 mM, Tocris). The glass coverslip was then immediately resealed to perform imaging.

Data analysis. Custom-written MATLAB (MathWorks) software was used for analysis of Ca^{2+} imaging data. Custom-written Igor Pro (Wavemetrics) software was used for the acquisition and analysis of whole-cell recordings. The data that support the findings of this study are available from the corresponding author on reasonable request. For evoked subthreshold responses, the integral of the evoked potentials were calculated. The latency of tactile response was determined by using the threshold calculated from baseline Vm (mean ± 2 sd). The analysis window for action potential reporting was calculated based on the underlying subthreshold voltage response, which was 700 - 800 ms for all recorded neurons. When represented as normalized, all responses were normalised to the response to 200 Hz tactile only stimulus. Measurement were taken from distinct samples and all numbers are indicated as mean ± SEM. Significance was determined using two-sided non-parametric tests (paired: Wilcoxon matched-pairs signed rank test; unpaired: Mann-Whitney test) at a significance level of 0.05. Calcium events were detected in a 1 second window from stimulus onset, when they crossed a threshold value of 3 standard deviation measured on the baseline (3 s, from trial onset to stim onset). The amplitude and duration of each calcium transient were measured as the peak and half width at half maximum of the event occurred during the detection window. Calcium responses were smoothed using a Savitzky-Golay filter with a 2nd order polynomial and a 7 sample window

and only transients longer than 250 ms were included in analysis. Unless differently specified, the amplitudes and durations are reported as the mean value of the detected events for each ROI. The probability of occurrence of calcium transients was measured as the number of events divided by the number of trials. All calcium data were analysed with custom scripts in MATLAB.

EXTENDED DATA

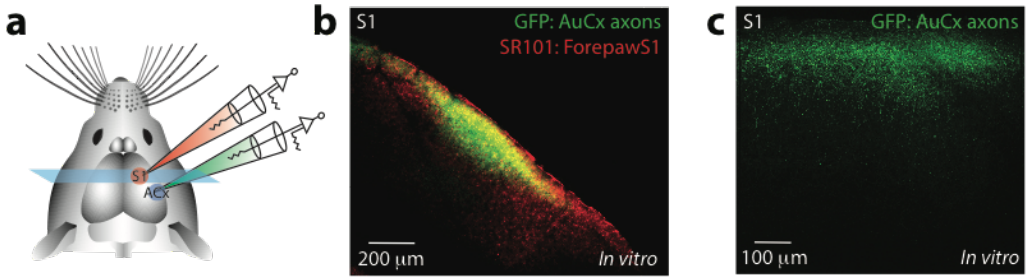

Supplementary Figure 3.1| The auditory cortex sends direct axonal projections to the primary somatosensory cortex. a, Schematic of experimental paradigm. GFP-tagged AAV was injected into the auditory cortex and the glia cell marker SR-101 was injected into forepaw S1. **b**, Example brain slice of the somatosensory cortex from a mouse with dual injections as in (**a**). Green, axonal projections from the auditory cortex. Red, glia cells. **c**, Example illustrating that axonal projections from the auditory cortex (green) targeted the upper layers of the primary somatosensory cortex.

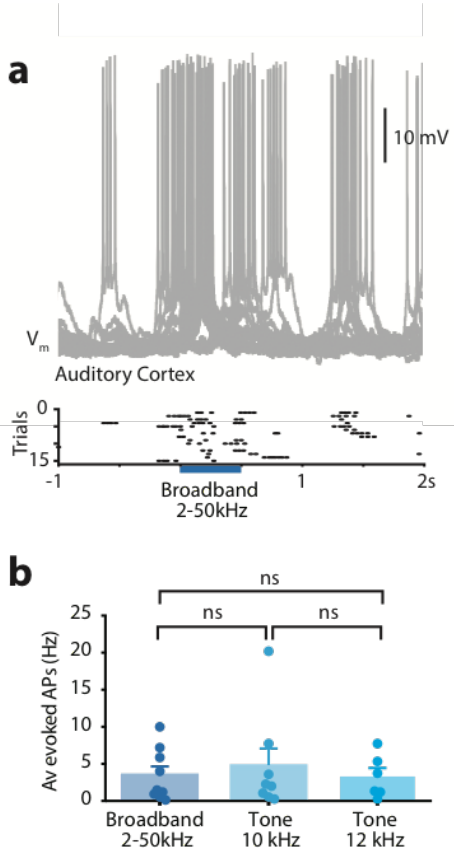

Supplementary Figure 3.2| Neurons within the auditory cortex robustly responded to broadband auditory stimulus. a, Patch clamp electrophysiological recordings were performed from layer 2/3 pyramidal neurons in the auditory cortex of urethane anaesthetized mice. a, Broadband auditory stimuli (2 - 50 kHz, 60 dB, 500 ms) reliably evoked action potentials. Top, Overlay of somatic voltage traces during auditory stimuli. Bottom, Raster of action potentials. **b**, The average evoked action potentials did not significantly differ during the presentation of broadband auditory stimuli (2 – 50 kHz; 3.48 ± 1.17 APs; n = 9 neurons, 3 mice), 10 kHz pure tone (60 dB, 500 ms; 4.71 ± 2.37 APs; n = 8 neurons, 3 mice; p = 0.89) and 12 kHz (60 dB, 500 ms; 3.27 ± 1.18 APs; n = 6 neurons, 3 mice; p = 0.98). Mann-Whitney test. Error bars represent S.E.M.

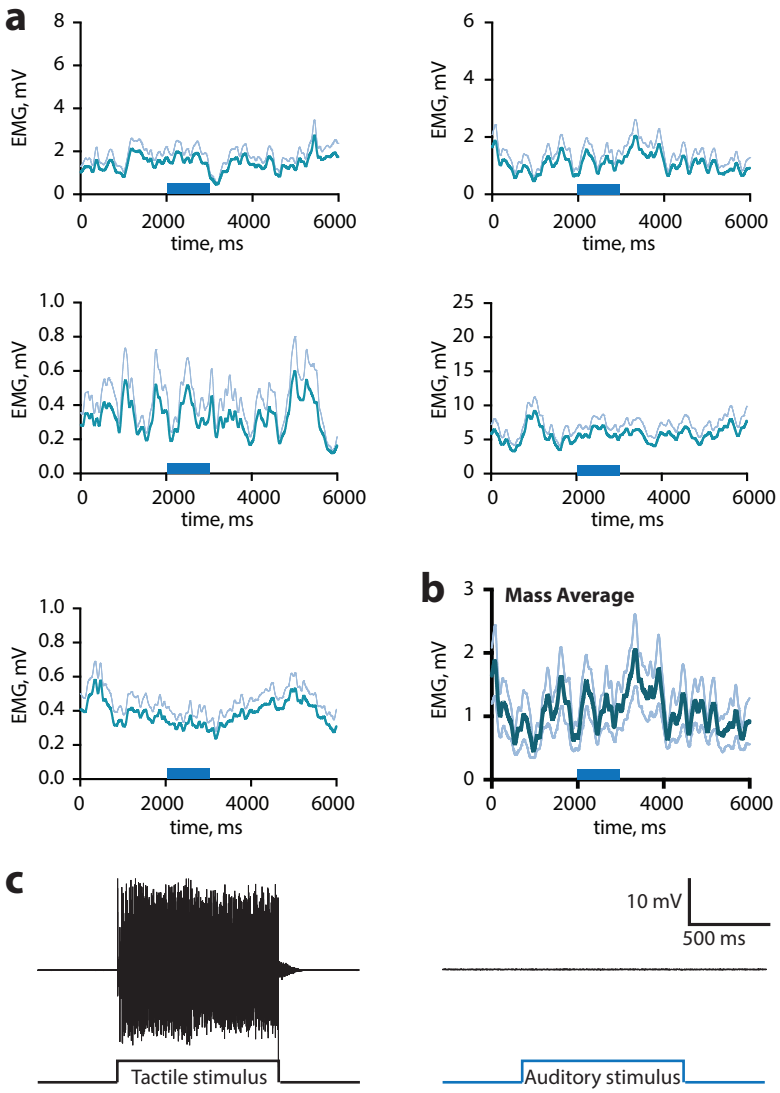

Supplementary Figure 3.3 | Auditory stimulus does not cause body movement (startle response) nor movement of the forepaw stimulator. a, Average examples of nuchal EMG recordings from two electrodes bilaterally inserted in the neck muscles of 5 mice. Auditory stimulus presentation, blue line. **b**, Average EMG recordings during broadband auditory stimuli (2 - 50 kHz, 60 dB; n = 5 mice). Auditory stimulus presentation, blue line. **c**, Vibration of the forepaw stimulator was measured by creating an electrical circuit with the stimulator during (left) tactile stimulus (200 Hz; 1 s) and (right) auditory stimulus (2 - 50 kHz, 60 dB;

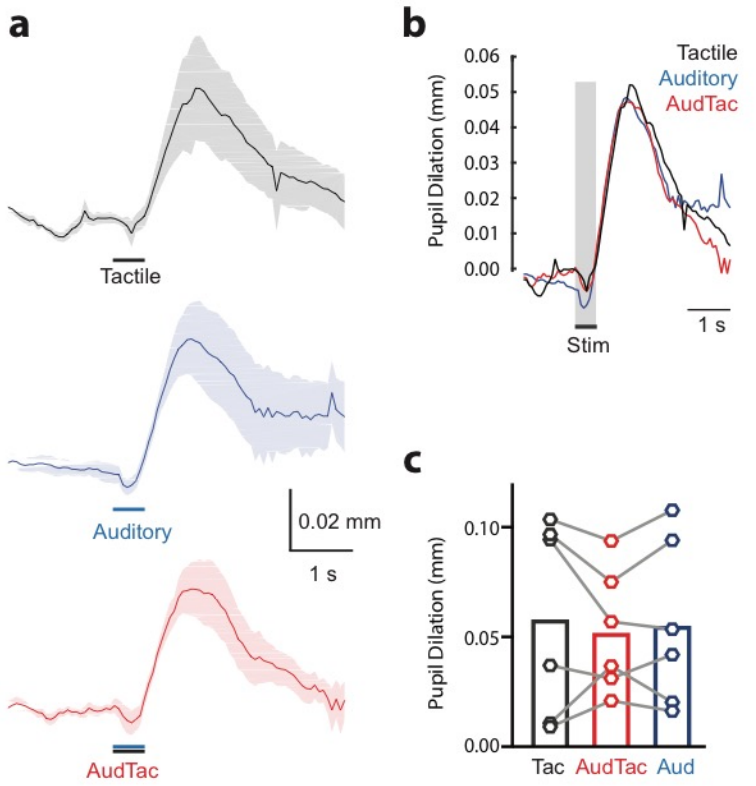

Supplementary Figure 3.4 | Pupil tracking during tactile and auditory stimulus in naïve mice. a, Pupil dilation was measured during tactile (black; 200 Hz, 500 ms), auditory (blue; 2 - 50 kHz, 60 dB, 500 ms) and paired tactile and auditory (red) stimulus. Mean ± s.e.m. **b**, Overlay of average evoked pupil dilation. n = 6 mice. Grey, stimulus delivery. **c**, There was no significant difference between the dilation of the pupil evoked during tactile (black, 0.059 ± 0.02 mm), paired auditory and tactile (red, 0.052 ± 0.01 mm) and auditory (blue, 0.056 ± 0.02 mm). T v AT, p = 0.69; T v A, p = 0.56; TA v A, p = 0.69, n = 6 mice, Wilcoxon matched-pairs signed rank test. Error bars represent S.E.M.

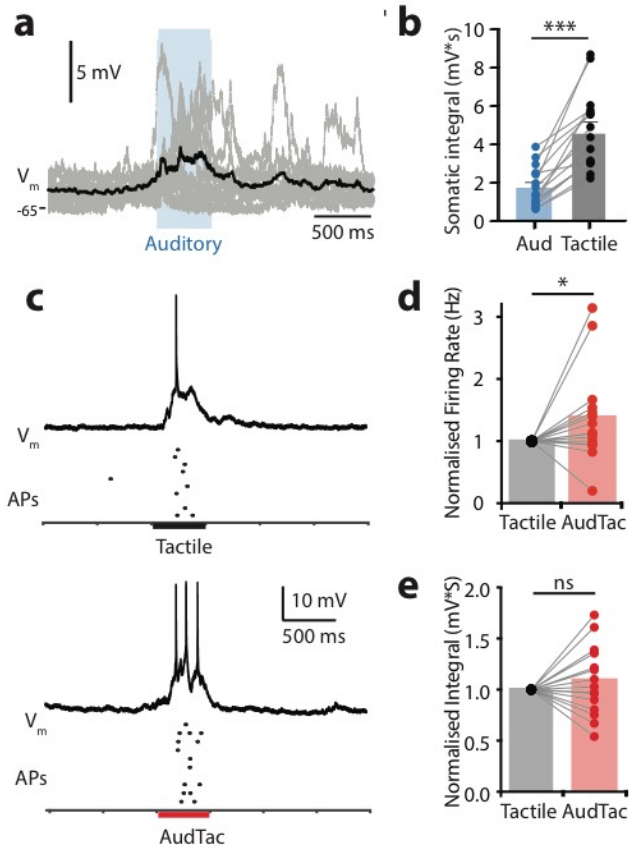

Supplementary Figure 3.5 | Voltage recordings from L2/3 pyramidal neurons in forepaw S1 of anesthetized mice. Patch clamp electrophysiological recordings were performed from layer 2/3 pyramidal neurons in the primary somatosensory cortex of urethane anaesthetized mice. The forepaw stimulation (200 Hz; 500 ms) was either presented alone or paired with auditory stimulation (broadband noise, 2 – 50 kHz, 60 dB, 500 ms).

a, Overlay of somatic voltage traces during broadband auditory stimulation. Black trace, mass average. **b**, The integral of the sensory-evoked somatic voltage responses during auditory stimulus (blue) and tactile (grey). n = 15 neurons, 12 mice; p = 0.0001, Wilcoxon matched-pairs signed rank test. **c**, Example voltage trace and raster plot of action potentials (APs) from a layer 2/3 pyramidal neuron during forepaw tactile stimulation alone (Top; black line) and tactile forepaw stimulation paired with auditory stimulation (Bottom; Tactile + Auditory, red line). **d**, When paired with auditory stimulation, the number of action potentials evoked during tactile stimulation significantly increased by on average 37 ± 19 % (p = 0.049; n = 15 neurons, 12 mice). **e**, Paired auditory stimulation did not alter the tactile-evoked subthreshold voltage response (n = 15 neurons, 12 mice; p = 0.525). Error bars represent S.E.M.

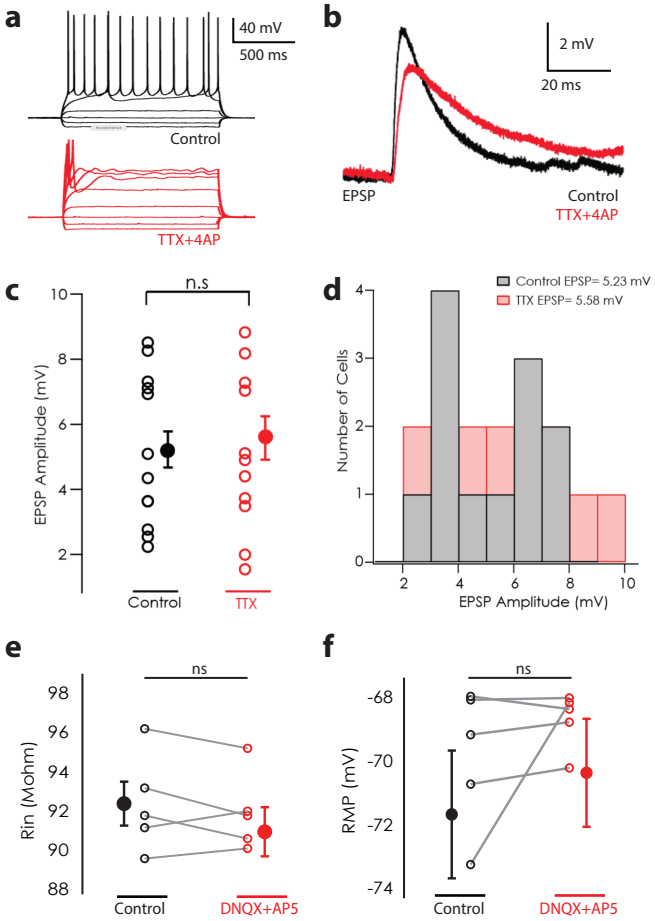

Supplementary Figure 3.6 | Quantification of monosynaptic (TTX- +4-AP) and synaptic (DNQX+AP5) responses. The photoactivatable opsin, ChR2, was injected into the auditory cortex (~100 nl; 200-500 µm below pia). After 10-14 days, patch clamp recordings were performed in layer 2/3 pyramidal neurons from brain slices of the primary somatosensory cortex. **a**, To test whether the layer 2/3 evoked potentials recorded in in the primary somatosensory cortex in response to photo-activation of auditory axons (ChR2, 470 nm) was monosynaptic, the antagonists of sodium (TTX) and potassium (4-AP) channels were bath applied. TTX+4AP (red) prevents action potential generation as illustrated during the current injection step protocol (50 pA, 1200 ms current steps).

b, Example ChR2-evoked potentials in a layer 2/3 pyramidal neuron in the somatosensory cortex before (black, control) and after (red) bath application of TTX- +4AP. **c**, Bath application of TTX+4-AP (red) did not significantly alter the amplitude of the photo evoked (470 nm, 2 ms) potentials compared with control (black; p = 0.69). **d**, Histogram showing the average EPSP amplitudes for neurons during control (black) and TTX+4-AP (red). Bath application of the AMPA and NMDA channel blockers (DNQX and AP5 respectively; red) did not alter **e**) input resistance (Rin) nor **f**) resting membrane potential (RMP).

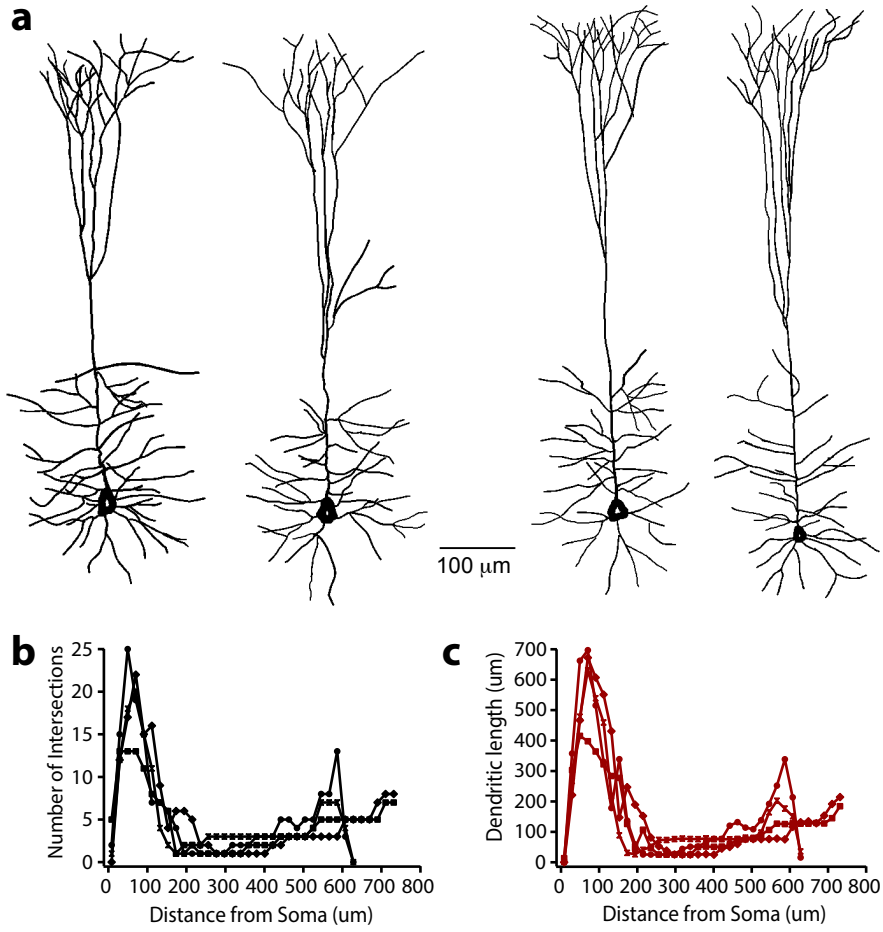

Supplementary Figure 3.7 | Complete morphology of in vitro layer 5 pyramidal neurons. a, Layer 5 pyramidal neurons were filled with biocytin to visualise the dendritic morphology of the recorded neurons. All layer 5 neurons recorded in vitro had intact dendritic arbors. There was no difference between **b**, the number of intersections and **c**, dendritic length. n = 4 neurons, 4 mice.

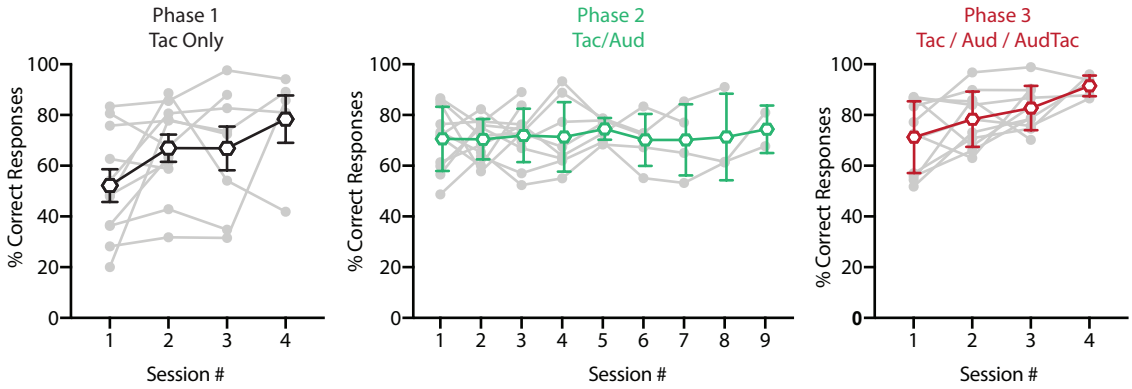

Supplementary Figure 3.8| Behavioral Training Paradigm. Overlay of correct performance during the training paradigm. Mice were trained in phases and only progress to next training phase once criteria (80% correct) has been obtained. 1) Tactile only (grey): mice are trained to associate forepaw tactile stimulation (200 Hz, 500 ms) with water.

2) Tac / Aud (green): mice are trained to withhold licking to auditory stimulus alone (broadband noise, 2 – 50 kHz, 60 dB, 500 ms). 3) Tac / Aud / AudTac (maroon): Paired tactile and auditory stimuli are presented to the mouse. Data points are average values for an entire session for a single mouse. Color line, average for all mice in the training phase.

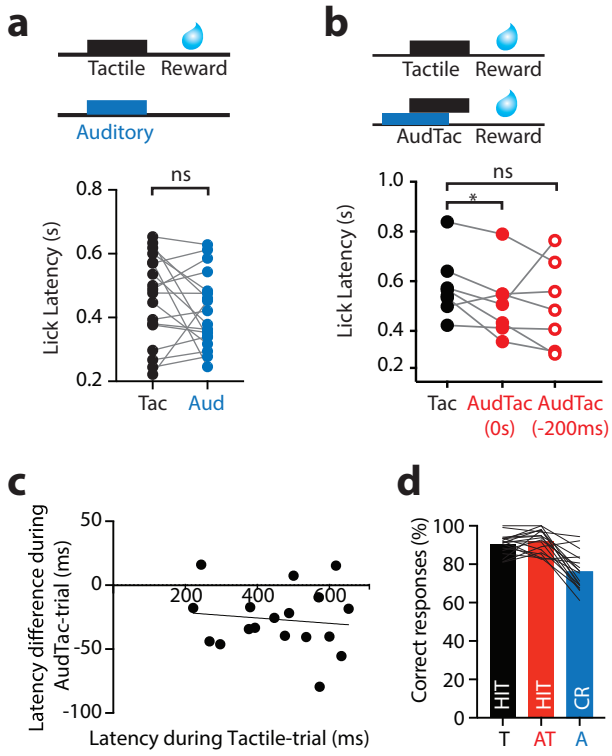

Supplementary Figure 3.9| Behavior controls. a, Top, Experimental paradigm. Bottom, There was no significant difference between the lick latency in response to tactile stimulus alone (black) and auditory stimulus alone ($p = 0.580$; $n = 18$ mice; Wilcoxon matched-pairs signed rank test) in mice which had < 30 % false alarm rate. **b,** Top, Experimental paradigm. Auditory stimulus (blue) was presented 200 ms before tactile stimulus (black). Bottom, Simultaneous auditory and tactile stimulus caused a significant decrease lick latency ($n = 8$ mice, $p = 0.039$; Wilcoxon matched-pairs signed rank test). In contrast, in the same mice, auditory stimulus presented 200 ms before tactile stimulus did not signficantly alter lick latency ($p = 0.34$; Mann Whitney test). **c,** Correlation between the lick latency in tactile-trials and the influence of adding auditory input (Linear Regression, $R_2 = 0.014$; $n = 18$ mice). **d,** Percentage of correct responses in the tactile goal-directed task in mice ($n = 18$ mice).

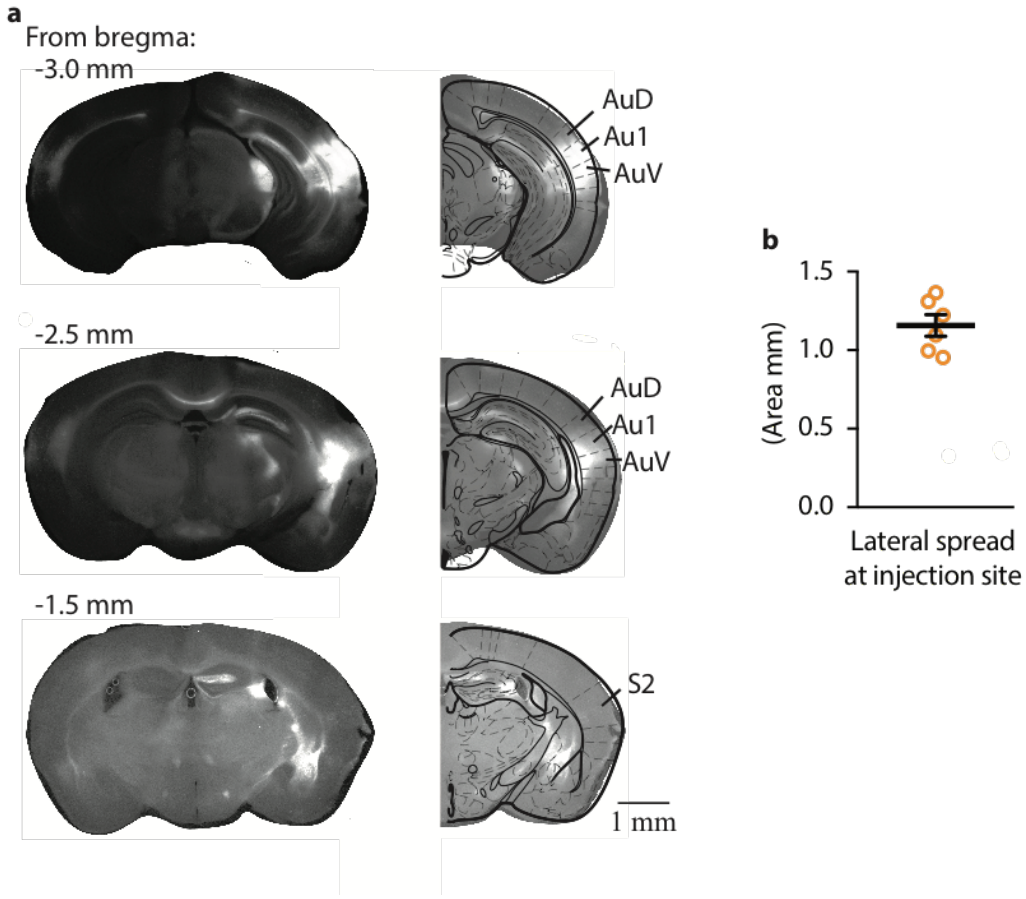

Supplementary Figure 3.10 | Characterization of the viral spread for the ArchT cohort. Mice were injected with the inhibitory opsin ArchT (AAV1.CAG.ArchT.GFP.WPRE.SV40) in the auditory cortex. **a**, Left, Fluorescent images from an example mouse illustrating lateral spread of virus at -3.0, -2.5 and -1.5 mm from bregma. The injection site was at -2.50 mm from bregma. Right, Overlay of fluorescence and brain region categorization (from the Paxinos atlas). The virus did not spread towards S2 or other regions outside of the auditory cortex on the rostro caudal axis. **b**, Lateral spread at the injection site for each mouse of the ArchT cohort (n = 6 mice). The local spread of the virus was contained within the auditory cortex and similar between each mouse. Error bars show mean and S.E.M.

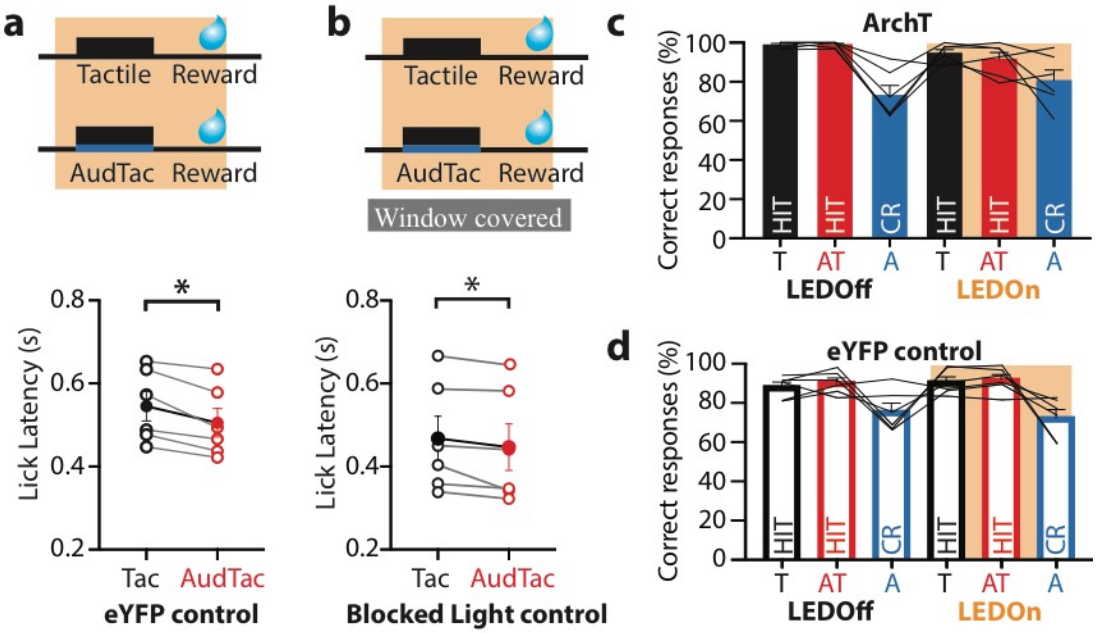

Supplementary Figure 3.11 | Archaerhodopsin Controls. a, Top, Experimental paradigm. A control mus-eYFP was injected into the auditory cortex and the influence of LED was tested as the mouse performed the tactile goal directed behavior. LED exposure in the sham mouse did not influence the enhanced response latency ($p = 0.0312$; $p_{shuffled} = 0.563$; n = 6 mice; 35 trials $_{av}$; Wilcoxon matched-pairs signed rank test). **b,** Top, Experimental paradigm. To test the influence of the LED protocol on behaviour, the chronic window was covered with inert opaque silicone during the LED behavioural paradigm. Bottom, During the blocked LED protocol, the lick latency was significantly decreased, illustrating LED itself did not influence behavior ($p = 0.03$; $p_{shuffled} = 0.438$; n = 6 mice; 35 trials$_{av}$; Wilcoxon matched-pairs signed rank test). **c,** Percentage of correct responses in the tactile goal-directed task in mice previously injected with Archaerhodopsin during LED Off and LED On (n = 6 mice). **d,** Percentage of correct responses in the tactile goal-directed task in mice previously injected with control fluorophore mus-eYFP during LED Off and LED On (n = 6 mice).

Values are shown as mean and error bars represent S.E.M.

CHAPTER 4

FEAR LEARNING ENHANCES TUFT DENDRITIC ACTIVITY IN THE AUDITORY CORTEX

The following work was submitted for publication. The format was slightly adapted to fit in with the thesis. References have been collated at the end of the thesis.

CHAPTER 4

Fear learning enhances tuft dendritic activity in the auditory cortex

Godenzini L[1] and Palmer L.M.[1]

[1]Florey Institute of Neuroscience and Mental Health, University of Melbourne, Victoria, Australia 3052

Author contributions

I performed all of the experiments and analysed the data contributing to this Chapter.

Acknowledgements

I would like to thank all members of the Palmer laboratory for the helpful comments and discussions. In particular Guzulaitis Robertas, La Terra Danilo and Rosier Marius for their feedback on the study. I would also like to thank Jee Hyun Kim for her help in the fear conditioning protocol. This research was funded by the NHMRC (APP1086082, APP1063533, APP1085708), ARC (DP160103047) and the Sylvia and Charles Viertel Charitable Foundation.

CHAPTER 4

ABSTRACT

Neural activity underlying sensory processing in the neocortex is constantly modified by learning. How neurons integrate such dynamic changes during sensory encoding remains unclear. Here, this is addressed by investigating dendritic and somatic activity in the auditory cortex following fear learning. Using whole cell patch-clamp electrophysiology, we recorded auditory-evoked somatic voltage responses in L2/3 (L2/3) pyramidal neurons in the auditory cortex of anaesthetised mice following auditory fear conditioning. The action potential output evoked by CS+ was increased compared to CS- following auditory fear conditioning, despite no changes in the evoked subthreshold voltage response. To investigate whether this discrepancy was correlated with changes in dendritic encoding of the CS+, we next recorded Ca^{2+} responses from both tuft and basal dendrites of layer 2/3 (L2/3) pyramidal neurons. Here, NMDA-dependent Ca^{2+} responses were enhanced in tuft, but not basal, dendrites following auditory fear conditioning. Taken together, these results suggest that fear learning induces experience-dependent plasticity of sensory encoding in tuft dendrites and leads to increased somatic output in the auditory cortex.

INTRODUCTION

The association of sensory information with threat or reward is of fundamental importance to survival. This association involves the neocortex[24,81,82,159] and alters the encoding of sensory information in cortical neurons[91]. Sensory signals acquire relevance through associative learning, a process which can modify neural activity at early stages of cortical processing[7,23,86,160,161] leading to local plasticity[162,163] and refined network activity in primary sensory cortice[1,90,92]. Fear conditioning is a form of associative learning arising from associating sensory information with threat. Requiring the auditory cortex [98], auditory fear conditioning causes rapid and long-term changes in spine dynamics[97,164] and neural

responses[96,99]. These dynamic changes within the auditory cortex have been shown to involve neurons within layer 1[98,99] which concurs with the cortical targeting of long-range feedback projections from the fear pathway [97].

Cortical pyramidal neurons lay at the heart of sensory processing, encoding both feedforward and feedback information. Also residing in the upper layers of the cortex, distal tuft dendrites of pyramidal neurons primarily receive feedback input and therefore play an important role in integrating information from multiple feedback pathways[40]. Conversely, basal dendrites, which project from the soma of pyramidal neurons, largely receive feedforward information and are thought to play an important role in sensory encoding[165]. Both tuft and basal dendrites can generate supra-threshold NMDA-dependent plateau potentials, also known as NMDA spikes[166]. Since NMDA spikes increase the coupling of synaptic input to neuronal output leading to enhanced action potential generation[50,53,151], changes in the dendritic processing of synaptic information can have a dramatic influence on neuronal output. Due to their location and crucial role in the processing and transfer of sensory information, dendrites of cortical pyramidal neurons are prime candidates to drive the dynamic changes in cortical processing required during learning.

To assess the influence of fear learning on dendritic processing and the encoding of sensory information, we used two-photon Ca^{2+} imaging and patch clamp electrophysiology *in vivo* to record auditory-evoked activity in tuft and basal dendrites following fear conditioning. We found that auditory fear learning increases action potential generation and alters tuft, but not basal, encoding of conditioned stimuli in L2/3 pyramidal neurons of the auditory cortex. These experience-dependent changes in sensory-evoked dendritic activity may provide a cellular mechanism for the control of somatic output during learning.

RESULTS

Somatic output is increased following fear learning

To identify learning related changes in the processing of auditory information, we recorded somatic and dendritic activity from L2/3 pyramidal neurons in the auditory cortex of urethane anaesthetised mice following auditory fear conditioning (Figure 4.1a). Mice (P40 - 60) were exposed to a fear conditioning protocol which consisted of trains of pure tones (5 x 500 ms, 5 or 15 kHz) presented with (CS+) or without (CS-) a mild footshock (Figure 4.1b, see methods for details). The auditory stimuli were counterbalanced and randomly allocated as either CS+ or CS-. Behavioural freezing responses to the auditory stimuli were tested the day following conditioning (Figure 4.1a). Conditioned mice discriminated between the two stimuli, with CS+ reliably evoking more freezing compared to CS- (68.5 ± 2.3 % vs 12.3 ± 2.1 %; n = 20 mice; p = 0.0001; Figure 4.1b).

To measure the somatic voltage response to CS+ and CS- auditory stimuli, whole cell patch clamp recordings were performed from L2/3 pyramidal neurons in the auditory cortex of urethane anaesthetised mice following fear conditioning (Supplementary Figure 4.1, n = 13 neurons, 10 mice; see Methods). Here, each tone within CS+ and CS- evoked a robust response consisting of a subthreshold voltage envelope and action potentials (Figure 4.1c). Although both CS+ and CS- had the greatest firing rate in response to the first tone (Figure 4.1c and Supplementary Figure 4.2), the evoked rate was significantly greater during CS+ (CS+ 0.53 ± 0.06 Hz vs CS- 0.44 ± 0.05 Hz; n = 13 neurons, 10 mice; p = 0.01, Figure 4.1d). The evoked subthreshold voltage response to CS+ and CS- was also enhanced during the first tone (Figure 1e and Supplementary Figure 4.2). However, in contrast to the evoked action potentials, there was no significant change in the subthreshold voltage response (CS+, 1.20 ± 0.11 mV/s; CS-, 1.18 ± 0.11 mV/s; n = 13 neurons, 10 mice; p = 0.35; Figure 4.1f). These results illustrate that

following fear conditioning, somatic output, but not subthreshold voltage, is increased in response to CS+.

How can somatic action potentials be enhanced following fear conditioning in the absence of changes in the subthreshold voltage? This discrepancy suggests that the enhanced evoked firing during CS+ is not simply driven by the linear somatic summation of synaptic inputs, and may be due to dendritic electrogenesis. Dendritic electrogenesis, that is, the supra-linear integration of synaptic inputs, has previously been shown to directly generate action potentials without a measurable influence on subthreshold voltage [149,167]. To test whether modulating synaptic activity in the upper cortical layers influences somatic output, we locally applied the NMDA-channel APV (200 µM) onto the cortical surface while recording somatic voltage activity. Block of NMDA-dependent events in the upper cortical layers significantly dampened somatic activity, and abolished the increase in evoked action potentials following fear learning (CS+: 0.06 ± 0.01 Hz vs CS-:0.07 ± 0.01 Hz; p = 0.73 Figure 4.1g).

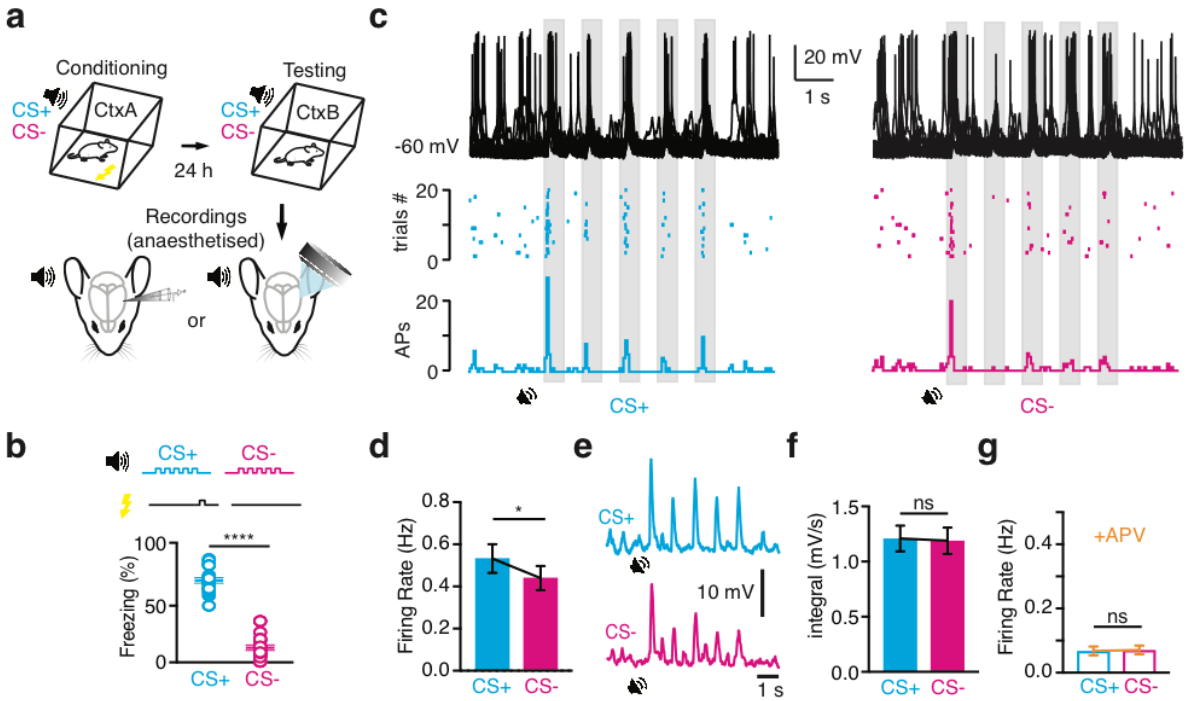

Figure 4.1 | Somatic output is increased following fear learning. a, Schematic of the experiments: 24h after fear conditioning mice were tested for freezing score. After this, whole cell patch clamp or two photon calcium imaging recordings were performed from the auditory cortex of urethane anaesthetised mice **b**, Top: auditory fear conditioning protocol; 5 x 500ms trains of pure tones (either 5 or 15 kHz,randomised) were presented with or without a footshock. Bottom: freezing responses measured 24 h after conditioning. n = 20 mice, Two-tailed paired t-test. **c**, Top: overlay of voltage responses in an example L2/3 pyramidal neuron; middle: raster plot of action potentials; bottom: PSTH of action potentials during CS+ (cyan, left) and CS- (magenta, right). **d**, Analysis of firing rate in response to the tones in the auditory stimuli during CS+ (cyan) and CS- (magenta). Wilcoxon matched-pairs signed rank. **e**, Voltage trace of the subthreshold responses to CS+ and CS- from the same neuron shown in **c**. **f**, Integral value of the voltage response to the tones during CS+ (cyan) and CS- (magenta). Wilcoxon matched-pairs signed rank. **g**, Analysis of the firing rate in response to the tones in the auditory stimuli during CS+ (cyan) and CS- (magenta) following application of the NMDA channel blocker, APV. Wilcoxon matched-pairs signed rank. All values represent mean ± S.E.M, error bars are S.E.M.

Fear learning enhances auditory-evoked responses in tuft dendrites

Since block of NMDA-channels in the upper cortical layers where the distal tuft dendrites of pyramidal neurons reside eliminated the enhanced somatic output following fear learning, we next tested whether dendritic integration is altered following fear learning. L2/3 pyramidal neurons were sparsely transfected with the genetic Ca^{2+} indicator GCaMP6f (see methods). Following expression, auditory-evoked Ca^{2+} transients were recorded from the tuft dendrites of L2/3 pyramidal neurons (<80 μm below pia) using two-photon microscopy (181 responsive dendrites, 9 mice, Figure 4.2a). The Ca^{2+} transients evoked in response to the first tone of CS+ were significantly larger than subsequent tones ($p = 0.0009$; Figure 4.2b and c). This is in contrast to CS- where there was no significant difference between all tones of the auditory stimuli ($p = 0.23$; Figure 4.2b and d). This highlights the specific influence of fear learning on the dendritic encoding of the first tone of CS+. Indeed, the responses evoked by the first tone during CS+ were significantly larger than during CS- (4.19 ± 0.3 ΔF/F vs 2.67 ± 0.2 ΔF/F, n = 65 vs 73 dendrites, 9 mice; $p = 0.002$; Figure 4.2e and f). To further illustrate the learning dependent aspect of this increase, we compared the peak amplitude of the Ca^{2+} response to the first tone in the conditioned stimuli (CS+ and CS-) with a reference stimulus, composed of a train of tones (10 kHz) not previously presented to the mice. Here, the tuft dendritic response to a naïve stimulus (2.93 ± 0.3 ΔF/F; n = 67 dendrites, 9 mice) was not significantly different to CS- ($p = 0.89$) but was significantly reduced in comparison to CS+ ($p = 0.005$; Figure 4.2f). Following fear learning, more dendrites were selectively encoding the CS+ (31%) compared to CS- (22%), while the majority of dendrites responded to both CS+ and CS- (47%, Figure 4.2g). Direct comparison of first tone auditory-evoked Ca^{2+} transients within these dendrites (n = 44 dendrites, 9 mice) also revealed a significant increase in the response duration (CS+: 0.22 ± 0.08 s vs CS-: 0.19 ± 0.07 s; $p = 0.03$; Figure 4.2h), and decrease in the response latency (CS+, 0.54 ± 0.03 s vs CS-, 0.65 ± 0.02 s, $p = 0.007$; Figure 4.2i) during CS+. However, the

evoked rate of these larger dendritic Ca^{2+} events was lower than during CS- (CS+: 0.09 ± 0.01 v CS-: 0.12 ± 0.01; p = 0.004, Figure 4.2l). Local application of the NMDA-channel blocker, APV (10 mM outside the dura) largely abolished evoked dendritic Ca^{2+} transients (5.2 ± 1 % of stimuli, n = 59 dendrites vs 0.01 ± 0 % of stimuli; p = 0.0001; n = 55 dendrites, 3 mice; Supplementary Figure 4.3) illustrating that these auditory-evoked transients were NMDA-dependent. Taken together, fear learning results in an increase in amplitude and duration, and decrease in latency and efficacy, of the first auditory-evoked NMDA-dependent Ca^{2+} transient in tuft dendrites of layer 2/3 pyramidal neurons.

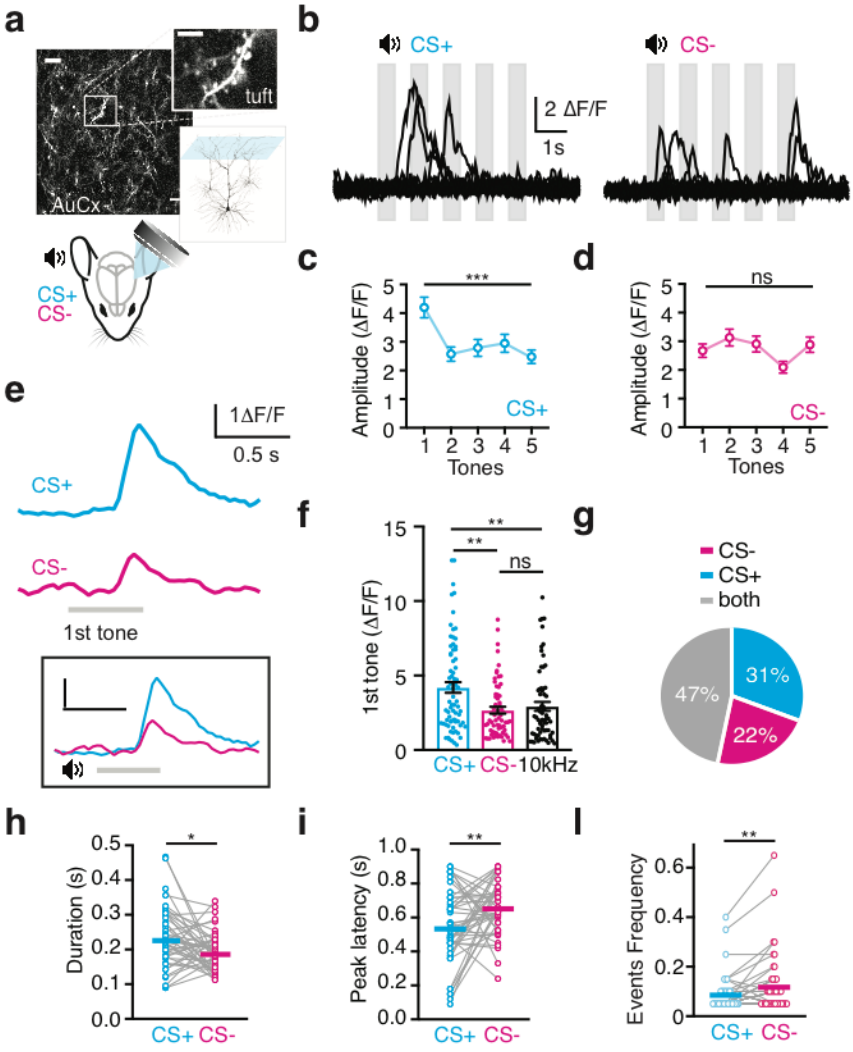

Figure 4.2 | Fear learning enhances auditory-evoked responses in tuft dendrites. a, Schematic of the dendritic recordings. Example field of view of tuft dendrites from layer 2/3 pyramidal neurons expressing GCaMP6f. Scalebar, 10 μm. Inset; Scalebar, 5 μm. **b**, Ca^{2+} transients were recorded in tuft dendrites in response to a train of pure tones (5 x 500ms, 5 or 15 kHz) as either CS+ or CS-. **c**, **d** Peak amplitude (ΔF/F) of Ca^{2+} responses to each tone in the train of CS+ (cyan) and CS- (magenta). Krustal-Wallis test. **e**, Ca^{2+} transients from an example dendrites in response to the first tone during CS+ (cyan) and CS- (magenta). Inset: overlay of the same traces. Scale bar as above. **f**, Analysis of the Ca^{2+} amplitude in tuft dendrites during the first tone of CS+ (cyan), CS- (magenta) and a reference (10 kHz) stimulus (black). Mann-Whitney test. **g**, Percentage of first tone responsive dendrites during CS+, CS- or both. **h**, Paired analysis of the duration of the Ca^{2+} response in tuft dendrites during CS+ (cyan) and CS- (magenta). Paired t-test. **i,** Paired analysis of the peak latency of the Ca^{2+} response in tuft dendrites during CS+ (cyan) and CS- (magenta). Two-tailed paired t-test. **l**, Percentage of conditioned stimuli which evoked a Ca^{2+} response in tuft dendrites during CS+ (cyan) and CS- (magenta). Wilcoxon matched-pairs signed rank test.

All values are means and error bars represent S.E.M.

Fear learning does not alter auditory-evoked responses in basal dendrites

Next we investigated whether fear learning also influences the site of feedforward input (i.e. basal dendrites) in L2/3 pyramidal neurons. Here, Ca^{2+} activity was recorded in visually identified basal dendrites (Figure 4.3a). following fear conditioning. Large Ca^{2+} transients (> 3sd baseline, see methods) were sparsely evoked in basal dendrites (145 responsive dendrites, 8 mice) in response to the conditioned stimuli (Figure 4.3b) . In contrast to tuft dendrites, CS+ and CS- were similarly encoded across the train of tones, with no difference in the peak amplitude evoked by each tone (CS+, $p = 0.30$; CS-, $p = 0.71$; Figure 4.3c and d). Furthermore, there was no significant difference of the auditory-evoked Ca^{2+} response to the first tone following fear learning (CS+, 2.93 ± 0.2 $\Delta F/F$ vs CS-, 3.24 ± 0.2 $\Delta F/F$; $p = 0.13$; n = 75 vs 65 dendrites, 8 mice; Figure 4.3e and f). These findings suggest that, in contrast to tuft dendrites and somatic output, basal dendrites do not encode fear learning. To further illustrate this, we compared the peak amplitude of the Ca^{2+} response to the first tone in the conditioned stimuli (CS+ and CS-) with a reference stimulus, composed of a train of ones (10 kHz) not previously presented to the mice. Here, the basal dendritic response to a naïve stimulus (3.29 ± 0.2 $\Delta F/F$; n = 83 dendrites, 8 mice) was not significantly different to either of the conditioned stimuli (CS+, $p = 0.26$; CS-, $p = 0.84$; Figure 4.3f).

Also in basal dendrites, the majority of dendrites were responsive to both CS- or CS+ (58%, Figure 4.3 g). However, unlike tuft dendrites, there was no difference in the duration (CS+, 0.190 ± 0.006 s; CS-, 0.199 ± 0.008 s; $p = 0.33$; Figure 4.3h), peak latency of the Ca^{2+} response (CS+, 0.60 ± 0.02 s; CS-, 0.60 ± 0.02 s; $p = 0.71$; Figure 4.3i) or evoked frequency (0.17 ± 0.01 vs 0.16 ± 0.01; $p=0.86$; Figure 4.3l) in this subset of basal dendrites (n = 50 dendrites, 8 mice). The auditory-evoked Ca^{2+} transients in basal dendrites were NMDA-dependent as local application of the NMDA-channel blocker (APV, 10 mM outside the dura) significantly decreased the evoked activity by 85 % ($p = 0.0001$; n = 48 dendrites, 3 mice; Supplementary

Figure 4.4). Together, these results illustrate that the auditory-evoked NMDA-dependent Ca^{2+} responses were not altered by fear learning in the basal dendrites of L2/3 pyramidal neurons.

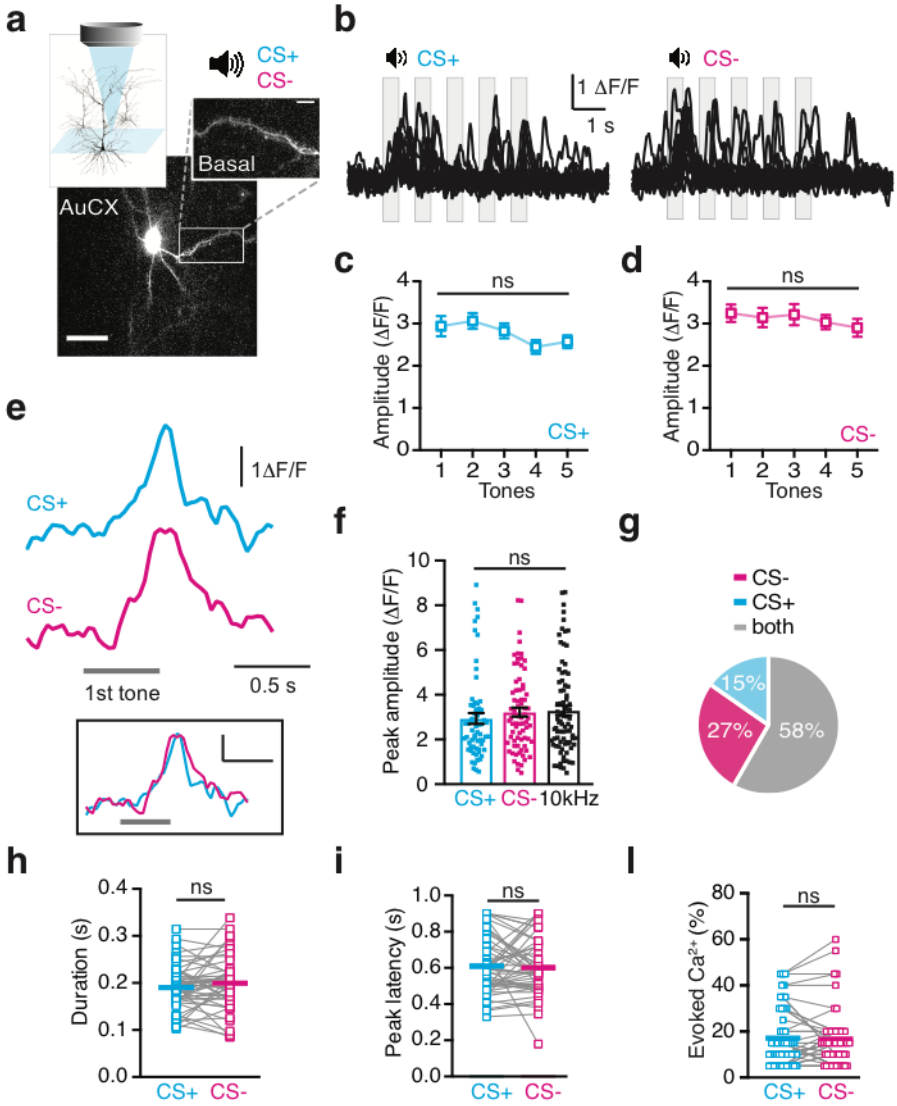

Plasticity of CS+ evoked activity is localised to tuft dendrites

The different encoding following fear conditioning in tuft and basal dendrites suggests that fear learning can induce local changes in different neuronal compartments. We therefore compared tuft and basal dendrites activity during presentation of the conditioned stimuli (CS+ and CS-, Figure 4.4a and b). Consistent with the idea that tuft and basal dendrites receive different source

of inputs (i.e. feedback and feedforward), basal dendrites were differently active compared to tuft dendrites during both CS+ and CS- ($p < 0.0001$, Figure 4.4c).

Figure 4.3 | Fear learning does not alter auditory-evoked Ca^{2+} responses in basal dendrites. a, Top: schematic of the experimental design. Example field of view of basal dendrites from layer 2/3 pyramidal neurons expressing GCaMP6f (located 100 - 250 µm below pia). Scalebar, 10 µm. Inset; scalebar, 5 µm. **b,** Ca^{2+} activity evoked during CS+ (left) and CS- (right) in basal dendrites. **c** and **d,** Peak amplitude ($\Delta F/F$) of the Ca^{2+} responses to each tone during CS+ (cyan) and CS- (magenta). Krustal-Wallis test. **e**, Ca^{2+} transients from an example basal dendrites in response to the first tone during CS+ (cyan) and CS- (magenta). Inset: overlay of the same traces. **f**, Analysis of the peak Ca^{2+} amplitude in basal dendrites during the first tone of CS+ (cyan), CS- (magenta) and a reference stimulus (10 kHz, black). Mann-Whitney test. **g**, Percentage of first tone responsive basal dendrites during CS+, CS- or both. **h**, Paired analysis of the duration of the Ca^{2+} response in basal dendrites during CS+ (cyan) and CS- (magenta). Two-tailed paired t-test. **i,** Paired analysis of the peak latency of the Ca^{2+} response in tuft dendrites during CS+ (cyan) and CS- (magenta). Two-tailed paired t-test. **l**, Frequency of evoked Ca^{2+} response in tuft dendrites during CS+ (cyan) and CS- (magenta). Wilcoxon matched-pairs signed rank test.
All values represent mean ± SEM.

In addition, directly comparing the auditory-evoked Ca^{2+} activity of the first tone in tuft and basal dendrites following fear conditioning illustrates that Ca^{2+} events were overall significantly larger in amplitude ($p = 0.02$, Figure 4.4d) and of longer duration ($p = 0.04$, Figure 4.4e) in tuft dendrites during CS+. On contrary, CS- auditory-evoked Ca^{2+} events were smaller in tuft dendrites ($p = 0.01$; Figure 4.4f) and not different in duration ($p = 0.34$; Figure

4.4g).These results highlight that fear conditioning selectively increased the Ca^{2+} response to CS+ at the site of feedback input in tuft dendrites.

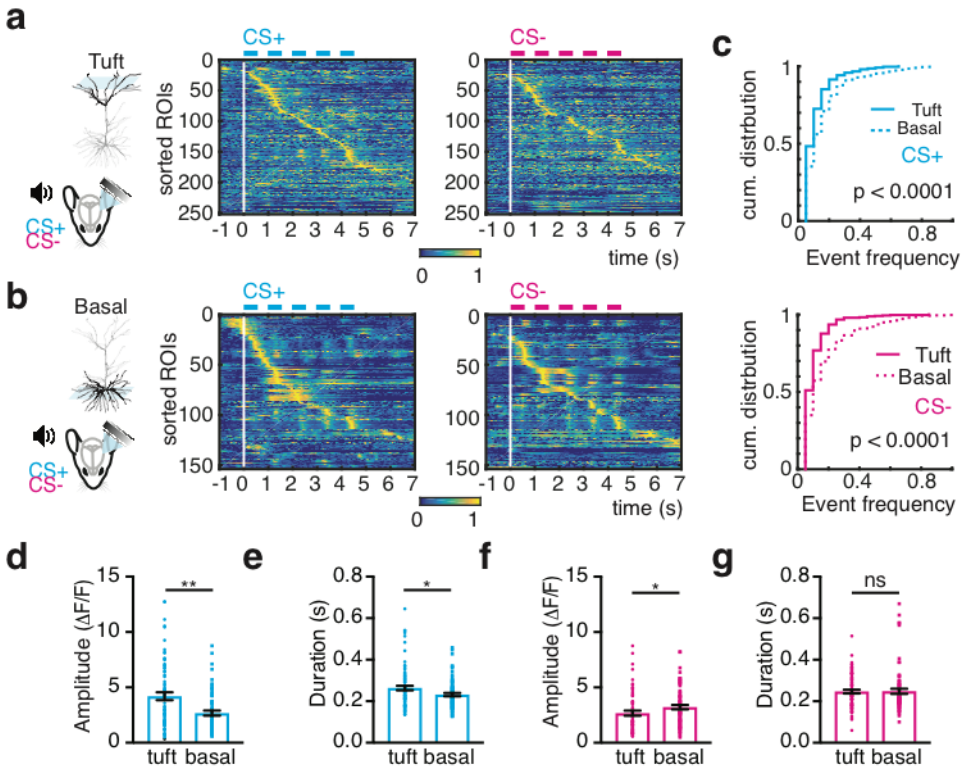

Figure 4.4 | Plasticity of CS+ evoked activity is localised to tuft dendrites. a and **b**, Left: schematic of the recordings. Middle and right: heatmaps showing the PSTH of Ca^{2+} activity pattern for all tuft (**a**) and basal (**b**) dendrites (ROIs) sorted according to the maximum response, during CS+ (cyan, left) and CS- (magenta, right). **c**, cumulative distribution of the Ca^{2+}events frequency during CS+ (top) and CS- (bottom) in tuft (solid line) and basal (dashed line) dendrites. Kolmogorov-Smirnov test. **d** and **f**, Analysis of the amplitude (**d**) and duration (**f**) of the Ca^{2+} transients during CS+ in tuft and basal dendrites. Mann-Whitney test. **e** and **g**, Analysis of the amplitude (**e**) and duration (**g**) of the Ca^{2+} transients during CS- in tuft and basal dendrites. Mann-Whitney test. All values represent mean ± SEM.

Learning dependent modulation of tuft dendrites and somatic output

Is this selective increase of tuft dendrites activity due to learning? To address this, we performed recordings to the same auditory stimuli used as CS+ and CS- (5x 500 ms, 5 or 15 kHz tones) in naïve mice, that were not presented with the fear conditioning protocol. In tuft dendrites, trains of tones of 5 and 15 kHz evoked Ca^{2+} activity that was similar to that of CS- (Figure 4.2), with no difference across the tones ($p = 0.19$ and $p = 0.26$; Figure 4.5a). The amplitude of the evoked Ca^{2+} transients at the first tone was also not different for both 5 and 15 kHz (2.77 ± 0.5 ΔF/F vs 2.43 ± 0.4 ΔF/F; $p = 0.81$; n = 23 vs 29 dendrites, 3 mice; Figure 4.5b). In a similar way, and differently than after fear conditioning, the somatic output of L2/3 pyramidal neurons recorded with whole cell patch clamp in response to the 5 and 15 kHz trains of tones in naïve mice (Figure 4.5c), was not significantly different (0.27 ± 0.04 Hz vs 0.33 ± 0.05 Hz; $p = 0.20$; n = 12 neurons, 8 mice; Figure 4.5d). These data show that in naïve mice the two auditory stimuli used during fear conditioning are similarly encoded. Taken together, these results further illustrate that learning dependent plasticity in tuft dendrites is correlated with an increase in somatic output following fear learning.

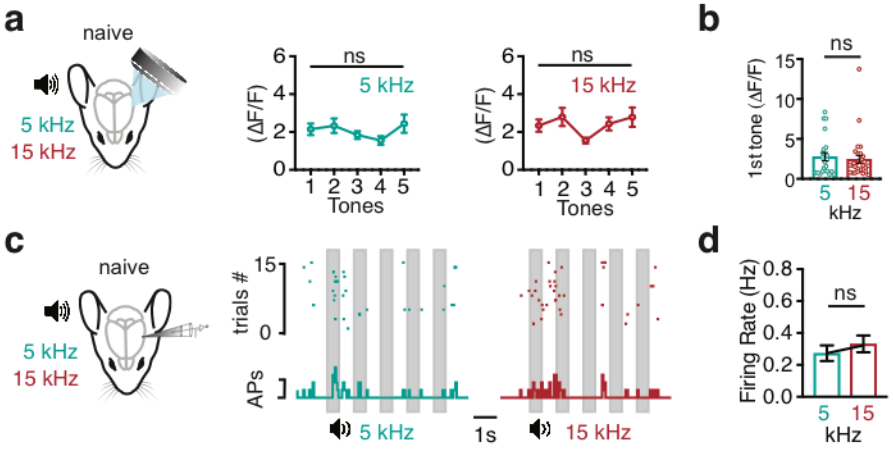

Figure 4.5 | Learning dependent modulation of tuft dendrites and somatic output a, Left: schematic of dendritic recordings in naïve mice. Right: peak amplitude (ΔF/F) of the Ca^{2+} responses in tuft dendrites evoked during 5 (teal) and 15 (red) kHz train of tones in naïve mice. Krustal-Wallis test. **b**, Analysis of the peak Ca^{2+} amplitude in tuft dendrites during the first tone of 5 (teal) or 15 (red) kHz. Mann-Whitney Test. **c**, Left: schematic of whole cell patch clamp recordings in naïve mice. Right: raster plot and PSTH of action potentials, shwing the somatic output from an example L2/3 pyramidal neuron in naïve mice. Scale bar (on the PSTH) = 5 action potentials. **d**, Analysis of the firing rate in response to the train of 5 (teal) and 15 (red) kHz tones. Wilcoxon matched-pairs signed rank. All values reported as mean, error bars show ± S.E.M.

Correlated Ca^{2+} activity is increased in tuft dendrites during CS+

Do all tuft dendritic branches from the same neuron encode fear learning, or is the learning-dependent enhancement computed locally, on a single branch? To address this, we reconstructed L2/3 pyramidal neurons and assessed the auditory-evoked Ca^{2+} responses to conditioned stimuli in tuft dendrites from either the same or different neurons (Figure 4.6a, see methods). Identifying branches from the same neuron illustrated that tuft dendrites typically had similar patterns of activity, although auditory-evoked Ca^{2+} events were occasionally localized to a single branch (Figure 4.6b). Overall, in tuft dendrites from the same neuron auditory-evoked Ca^{2+} transients occurred simultaneously during both CS+ and CS-, whereas this was not the case in tuft dendrites from different neurons (Figure 4.6c). Fear conditioning did not alter the highly correlated activity of sister dendrites as there was no significant difference in the correlation of the number of Ca^{2+} events in tuft dendrites (see methods for details) from the same L2/3 pyramidal neuron in response to CS+ and CS- (0.69 ± 0.07 vs 0.74 ± 0.06; $p = 0.51$; Figure 4.6e). However, during CS+ there was a significantly greater correlation between the number of auditory-evoked Ca^{2+} events in the tuft dendrites from

different neurons (0.27 ± 0.04 vs 0.17 ± 0.04; p = 0.01; Figure 4.6f). These results illustrate that the typically low correlation between auditory-evoked Ca^{2+} activity in the tuft dendrites of neighbouring neurons is increased during presentation of CS+, suggesting fear learning leads to greater overall synchronous activity between neurons within the upper layers of the auditory cortex.

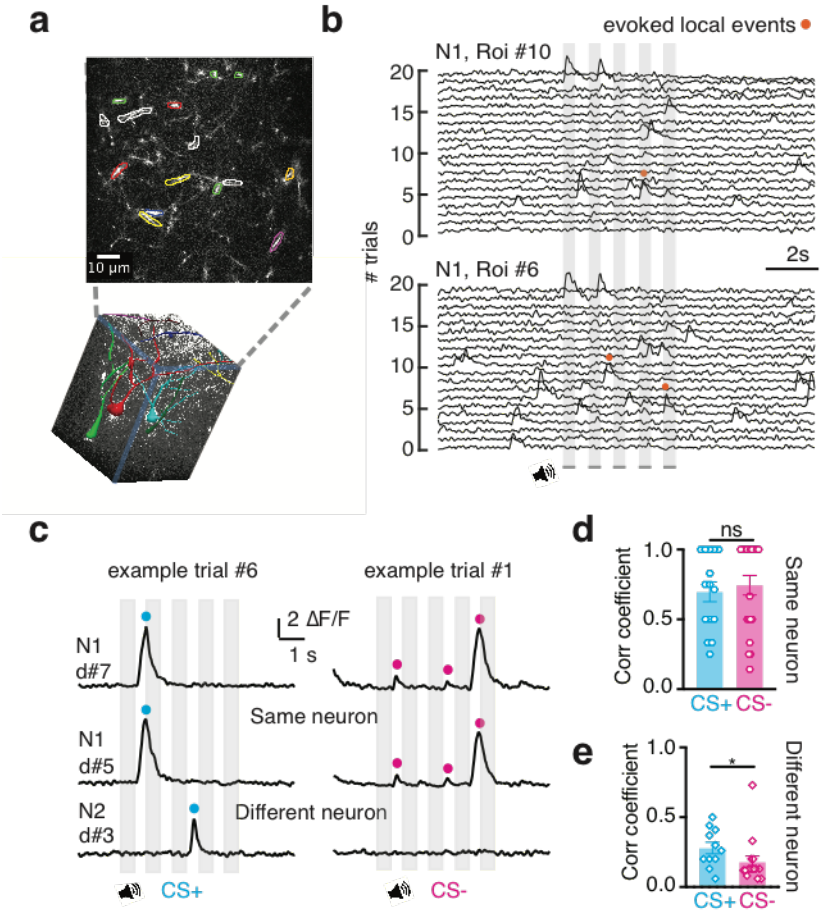

Figure 4.6 | Correlated Ca^{2+} activity is increased in tuft dendrites during CS+. a, 3D reconstruction of L2/3 pyramidal neurons in an example field of view. Inset, Tuft dendrite ROIs are colour coded according to the reconstructed neuron they belong to. **b**, Ca^{2+} transients were recorded in tuft dendrites from the same reconstructed neuron (Roi#10 and Roi#6; N1). Orange dots, local evoked Ca^{2+} transients.

c, Example of auditory evoked Ca^{2+} transients from 3 separate dendritic ROIs recorded during a single trial of CS+ (right) or CS- (left) presentation. Same neuron (N1), Roi dendrite #7 and #5. Different neuron (N2), Roi dendrite #3. **d**, Ca^{2+} responses in tuft dendrites from the same neuron are highly correlated during CS+ and CS-. Mann-Whitney test. **e**, Ca^{2+} responses in tuft dendrites from different neurons are more correlated during CS+ than CS-. Mann-Whitney test. All values represent mean ± SEM.

CHAPTER 4

DISCUSSION

The dendrites of pyramidal neurons encode sensory information and perception [22,50,56,57]. Whether sensory processing in dendrites is altered by fear learning was previously unknown. Using two-photon Ca^{2+} imaging and patch clamp electrophysiology in L2/3 pyramidal neurons within the auditory cortex, we found that fear learning increase the somatic output, with more action potentials evoked in response to CS+. This was associated with an enhancement of auditory-evoked Ca^{2+} responses in tuft, but not basal, dendrites following fear learning. These results contribute to a growing body of evidence illustrating the auditory cortex is involved in auditory-fear learning [97,98,168], where neurons are also changed morphologically [97,169] and functionally [81,95,96,98,160].

We demonstrate that following fear learning, auditory-evoked Ca^{2+} transients were remodelled in tuft dendrites with larger, but less frequent, Ca^{2+} responses during CS+. These results suggest that the local fine tuning of the microcircuitry within the auditory cortex is involved in fear learning, resulting in the emergence of sparse-coding mechanisms in tuft dendrites [90]. Fear learning specifically altered the tuft dendritic response to the first tone in a train of tones during CS+. This is presumably mediated by the fear pathway during fear conditioning[160] which would induce plasticity at the site of feedback input in tuft dendrites [97].

Following fear learning, changes in network activity were also evident when assessing the correlated activity within and between L2/3 pyramidal neurons. Recent studies illustrate that dendritic Ca^{2+} responses typically occur globally throughout an entire dendritic arbour [54,170,171]. Indeed, during both auditory stimuli (CS+ and CS-), tuft dendrites from the same neuron had highly correlated auditory-evoked activity. However, although the tuft dendrites of different neurons had an overall low correlation in Ca^{2+} activity, there was a significant increase in correlated tuft dendritic activity in different neurons during CS+. This suggests a functional change in the underlying microcircuit, which corresponds with the morphological changes

previously reported [97] and further supports the fine tuning of the microcircuit within the auditory cortex following fear learning [99]. These changes in the correlation in neural circuitry could create a more efficient representation of the associated auditory signal during fear learning, which would facilitate the transfer of relevant information to other areas [7].

Although a clear tonotopy is present in the auditory cortex at a large scale, such organisation is not always preserved at the fine scale [11]. Indeed, recordings from naïve mice, showed similar level of frequency encoding in both tuft dendrites and somatic output. In addition, to control for any difference of tone representation within the recording area across mice, the frequencies of the CS+ and CS- stimuli were counterbalanced.

Similar to previous studies [96,172], fear learning enhanced the auditory-evoked somatic action potentials in cortical pyramidal neurons. We illustrate that such changes are not accompanied by measurable differences in the synaptic inputs, as there was no effect of fear conditioning on the auditory-evoked subthreshold voltage response. Changes in neuronal output without changes in subthreshold activity has previously been reported during sensory encoding [50,173] and are indicative of the generation of dendritic spikes [43,149]. Indeed, blocking NMDA channels caused a dramatic decrease in auditory-evoked Ca^{2+} activity, suggesting the reported Ca^{2+} transients in this study were NMDA spikes. We suggest that the enhanced tuft dendritic response following fear learning directly led to an increase in the somatic output of L2/3 pyramidal neurons as 1) there was no change in the sensory-evoked responses in basal dendrites indicating the increase in action potentials following fear learning did not simply increase tuft dendritic signalling through backpropagation [125], 2) there was no measurable change in the sensory-evoked subthreshold response indicating there was not a dramatic change in synaptic input, 3) application of the NMDA channel blocker to the upper cortical layers abolished the increased response of the somatic output at the first tone. Furthermore, in naïve mice, where

there was no plasticity of dendritic activity, the somatic output was not different between the auditory stimuli.

The ability to adapt behavioural responses to the external environment relies on the flexibility of sensory representation that can be constantly updated through learning [91]. A previous study, has shown contrasting results, with no change in sensory representation in awake animals following fear learning [95]. Such contrast with our results could be due to the different methodology used for recording somatic activity as well as in the behavioral protocol. In addition, although anaesthesia reduce overall feedback activity, many other factors can influence the brain state and recordings in the awake animal [30].

Considering other recent evidence of plasticity within L1 of the auditory cortex [99], we propose that our findings highlight a plasticity mechanism within tuft dendrites of L2/3 pyramidal neurons. Feedback information to the upper cortical layers is increased following learning [1] and since tuft dendrites are typically the target of feedback information [41], we observed a change in the auditory-evoked Ca^{2+} response in tuft, but not basal, dendrites following fear conditioning. These results illustrate that changes in sensory encoding can be compartmentalized in different dendritic regions and might be localised to L1, as previously reported [99]. Tuft and basal dendrites might help shifting the balance between feedback and feedforward information onto a single neuron to guarantee a flexibility of the sensory representation. This is in direct contrast to the long held hypothesis that, despite extensive dendritic arbours, neurons may function as a simple one-compartment model (for a review, see [174]. Therefore, the compartmentalization of input can have a specific local influence and neurons can be viewed as having two or more layers [175].

In summary, we identified learning-dependent changes in the processing of auditory stimuli in the tuft dendrites and somatic output of L2/3 pyramidal neurons. We suggest that the localised

plasticity of L2/3 pyramidal neurons may provide a cellular mechanism for the control of somatic output during learning.

METHODS

All experiments were conducted in strict accordance with the Code of Practice for the Care and Use of Animals for Scientific Purposes (National Health and Medical Research Council, Australia) and guidelines given by the veterinary office at the Florey Institute of Neuroscience and Mental Health.

Auditory Fear Conditioning. Mice (C57BL/6; P42-70) were exposed to an auditory fear conditioning protocol. Mice were placed in fear conditioning chambers (MedAssociates) for 2 minutes of habituation before trains of tones were presented at 1Hz (pure tones: 5 or 15 kHz; 5x 500 ms duration – 500 ms ISI). The auditory trains were presented either with (CS+) or without (CS-) a 0.6 mA footshock for six times each, in a block design (CS+ following the CS- block). The onset of the footshock coincided with the onset of the last tone in the train of tones. After 24 hours, CS+ and CS- were presented again in a different context (8 repetitions each, duration 10 s) and freezing behavior was recorded and compared. Freezing scores were automatically measured by the software (MedAssociates) as the percentage of freezing during auditory stimulus presentation, corrected with the average values of the first two minutes of habituation, to adjust for baseline level of freezing. Mice that failed to discriminate between the CS- and CS+ (< 30% difference) were excluded from further experiments and recordings.

Virus injections. Mice (C57BL/6; P30-42) were anaesthetised with isoflurane (3% in 0.75 L/min O_2) and body temperature was maintained at 36-37 °C. Eye ointment was applied to prevent dehydration. Meloxicam (1-3mg/kg, Ilium) was intraperitonially injected at the beginning of the surgery. The skin was disinfected with ethanol 70% and betadine and a small slit was made in the skin to expose the skull. A small craniotomy (<0.5 mm) was made over the left auditory cortex (2.5 mm posterior to bregma and 4.5 mm lateral from midline) and the dura was left intact. To obtain sparse labelling of L2/3 pyramidal neurons, a mix of the Cre-dependent Ca^{2+} indicator, GCaMP6f (AAV1.Syn.Flex.GCaMP6f.WPRE.SV40, UPenn) and

diluted Cre (1:6000; AAV1.hSyn.Cre.WPRE.hGH, UPenn) was injected at a dorso-ventral distance of 450 µm with a microcapillary pipette. Finally, the skin was sutured and the mouse put back into their cage for a minimum of 3 weeks to allow expression of GCaMP6f, before two photon imaging.

Auditory Stimulation. During two-photon Ca^{2+} imaging and whole-cell patch clamp recordings, auditory stimulation was provided through a speaker (8Ω,5W; digikey) positioned on the right side of the mouse at about 8-10 cm from the ear. The auditory stimuli were custom made and delivered with an Arduino processing board at ~70 dB.

Two-photon Ca^{2+} imaging and image analysis. Mice previously transfected with GCaMP6f, using the sparse-labelling protocol, were initially anaesthetised with isoflurane (3% in 0.75 L/min O_2) before urethane anaesthesia (intraperitoneal, 1.6 g/kg, Sigma) was administered. After removing the skin and cleaning the skull with NaOH (3%), a craniotomy was performed (3 mm diameter) over the virus injection site in the auditory cortex (left hemisphere). A circular coverslip (3 mm diameter, size #1) was placed over the craniotomy, and sealed with glue. A custom-made metal head-bar (0.5g) was also attached to the skull using dental cement (paladur, Heraeus). For dendritic imaging, GCaMP6f was excited at 940 nm (~30 mW at the back aperture) with a titanium sapphire laser (140 fs pulse width; SpectraPhysics MaiTai Deepsee) and imaged on a Sutter MoM through a 16x Nikon objective (0.8 NA). Emitted light was passed through a dichroic filter (565dcxr, Chroma Technology) and short-pass filtered (ET525/70-2p, Chroma Technology) before being detected by a GaAsP photomultiplier tube (Hamamatsu). Images were acquired at a frequency of 30 Hz (512 x 512 pixels) using ScanImage software. Ca^{2+} transients were recorded from tuft and basal dendrites of L2/3 pyramidal neurons within the auditory cortex at a depth of 30-80 µm and 150-250 µm respectively, from the pia surface. The images were motion corrected when necessary and region of interests (ROIs) were manually selected using ImageJ software before fluorescence signal extraction. Ca^{2+} responses

were smoothed using a Savitzky-Golay filter (2nd order polynomial and 7 sample window) and the ΔF/F was measured by subtracting the median value of the baseline (5 seconds) fluorescence signal for each trial. All Ca^{2+} signal processing was performed with custom written Matlab scripts. For display purposes only, neuron images were Gamma corrected.

Ca^{2+} analysis. Auditory evoked Ca^{2+} transients were identified by applying a threshold measured as 3 standard deviation of the baseline (5 seconds before stimulus onset). The peak amplitude, onset and duration were then measured using custom Matlab scripts. Unless otherwise stated, data is presented as the mean response and error bars represent the standard error. The percentage of trials with Ca^{2+} transients was measured as the number of events for each dendrite divided by the number of trials. The mass average Ca^{2+} transients are an average of all the Ca^{2+} traces in trials which were active during the auditory stimulation, divided by the overall number of active ROIs. To measure the Ca^{2+} response to each tone in the train of conditioned stimuli, Ca^{2+} transients were allocated to a particular tone according to the onset of the Ca^{2+} transient (i.e. where it first crossed the event threshold). 3D reconstruction and tracing of tuft dendrites was performed using the software, NeuTube. Correlation coefficients were measured as the total number of Ca^{2+} transients occurring during a trial divided by the total number of branches. All Ca^{2+} analysis were performed with custom written Matlab scripts.

Whole-cell recordings under anaesthesia. Mice (C57BL/6; P42-63) were initially anaesthetised with isoflurane (3% in 0.75 L/min O_2) before urethane anaesthesia (intraperitoneal, 1.6 g/kg, Sigma) was administered. Anaesthesia was monitored throughout the experiment, and a top-up dose of 10% of the initial urethane dose was administered when necessary. Body temperature was maintained at 36-37 °C. Lidocaine (20mg/ml, Ilium) was injected around the surgical site on the scalp and the head was stabilized in a stereotaxic frame by a head-plate attached to the skull with dental cement (paladur, Heraeus). A craniotomy was performed over the left auditory cortex (~1.5 x 1.5 mm^2), centered at -2.5 mm from bregma

and 5 mm lateral from midline. The dura was surgically removed and the brain was constantly bathed with normal rat ringer (135 mM NaCl, 5.4 mM KCl, 1.8 mM CaCl2, 1 mM MgCl2, 5 mM HEPES) throughout the experiment. Whole-cell *in vivo* patch clamp recordings were performed using a patch pipette (resistance 6-9 MΩ) filled with an intracellular solution containing 115 mM potassium gluconate, 20mM KCl, 10 mM sodium phosphocreatine, 10 mM HEPES, 4 mM Mg-ATP, 0.3 mM Na-GTP, adjusted to pH 7.3-7.4 with KOH. The patch pipette was inserted into the brain at an angle of 30°- 40° relative to the cortical surface, to a depth of ~200 μm (to target layer 2/3 neurons). The pipette was then advanced in steps of 1 μm (to a maximum distance of 300 μm in the hypotenuse trajectory) until a neuron was encountered. Whole-cell voltage recordings were performed from the soma using Dagan BVC-700A amplifiers and were filtered at 10 kHz. Once a whole-cell recording was obtained, the voltage response to incremental current steps (50 pA; 800 ms) was recorded to characterize the neuron. Custom-written Igor software was used for the acquisition and of whole-cell recordings.

Data analysis. For whole cell recordings, the evoked subthreshold response was analysed as the integral or peak of the evoked voltage envelope (for each tone) using a custom written script in Igor and Matlab. The resting membrane potential was usually -60mV, and the peak amplitude is reported as the membrane voltage value at the peak of the voltage envelope. The firing rate was measured in a 500 ms window from each auditory tone onset.

Drug application. During two-photon imaging, the cranial window was partially removed to apply APV on the brain surface (10 mM, Tocris). The glass coverslip was then immediately resealed to perform imaging. During *in vivo* whole-cell patch clamp recordings, APV (200 μM; Tocris) was topically applied over the craniotomy and current clamp recordings were performed.

Statistical analysis. Data were tested for normality and parametric or non-parametric test were used accordingly using the software GraphPad-Prism. All data are reported as mean value ± SEM.

EXTENDED DATA

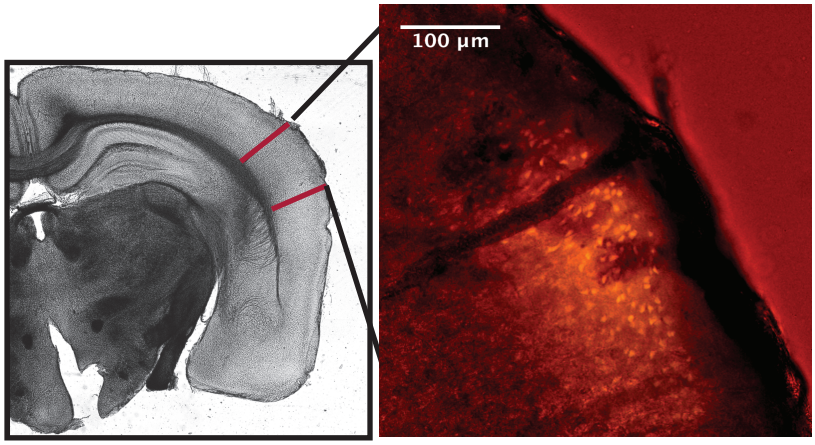

Supplementary Figure 4.1 | Identification of the whole cell patch clamp recordings site in the auditory cortex. During a whole cell patch clamp experiments in vivo, the recording pipettes was filled with byocitin to locate the recording region post-hoc. After perfusion, brain slices were collected at the vibratome and analysed with fluorescent microscopy to find the location of the recordings. Right: cortical location of the recording site was identified as the auditory cortex with the Paxinos Atlas. Inset (right): byocitin-filled neurons in the auditory cortex.

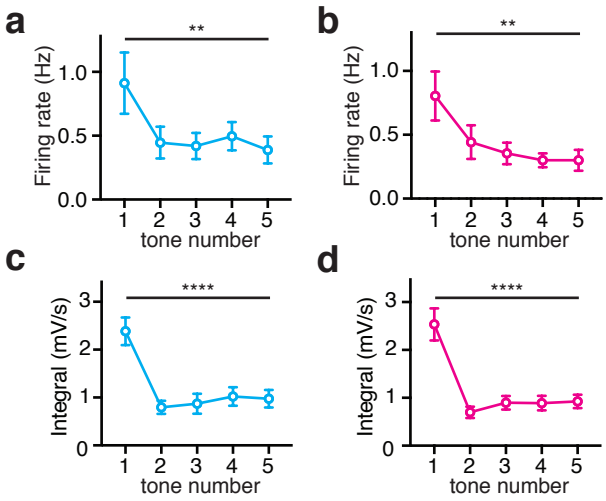

Supplementary Figure 4.2 | Somatic output and voltage response to the first tone is increased in both CS+ and CS-. a and **b,** Firing rate in response to each tone in the CS+ (**a**) and CS- (**b**) auditory stimuli. The first tone evoked significantly more action potentials compared to the following ones. Krustal-Wallis test. **c** and **d**, Integral of the voltage response to each tone in the CS+ (**c**) and CS- (**d**) auditory stimuli. The first tone evoked a significantly larger voltage response compared to the following ones. Krustal-Wallis test.

Plots show mean ± SEM.

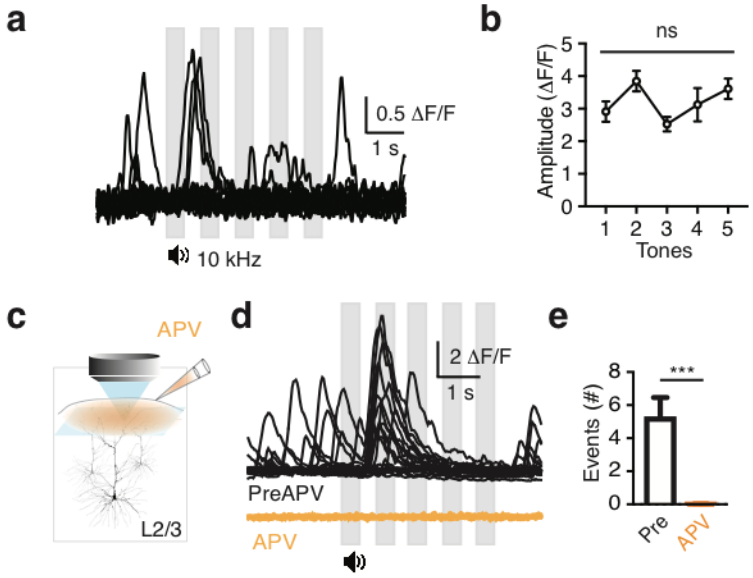

Supplementary Figure 4.3 | Ca^{2+} responses to a reference stimulus and local block of NMDA channels in tuft dendrites. a, Tuft dendrites Ca^{2+} activity in response to a reference train of tones (10 kHz), never presented to the mice before. **b**, The peak amplitudes in response to each tone were not significantly different. Krustal-Wallis test. **c**, Schematic of experimental design. The NMDA channel antagonist, APV, was topically applied onto the cortical surface during two-photon Ca^{2+} imaging of tuft dendrites. **d**, Example auditory-evoked Ca^{2+} responses in a tuft dendrite before (top, black) and after (bottom, orange) the local cortical application of APV. **e**, Percentage of auditory stimuli which evoked Ca^{2+} responses pre (black; 5.2 ± 1 %, n = 59 dendrites, 3 mice) and post APV (orange; 0.01 ± 0 %, p = 0.0001, Mann-Whitney test; n = 55 dendrites, 3 mice). Plots represent mean ± SEM.

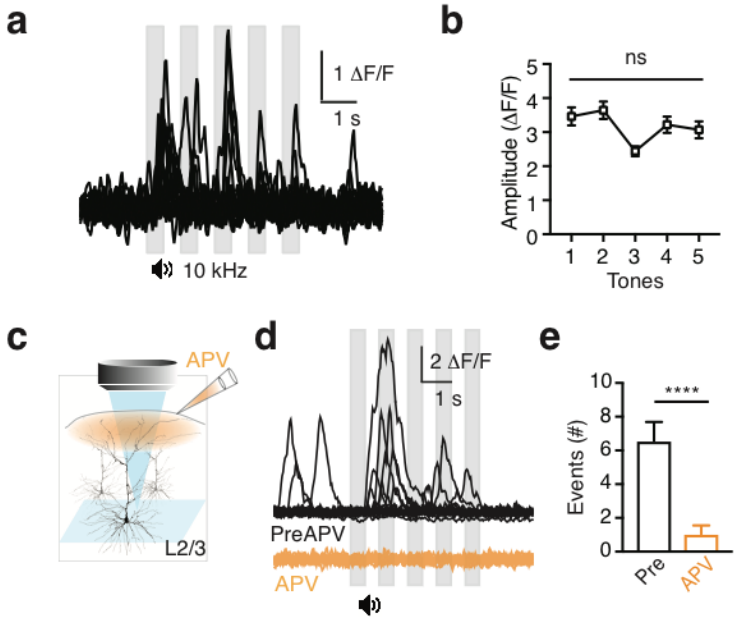

Supplementary Figure 4.4 | Ca^{2+} responses to a reference stimulus and local block of NMDA channels in basal dendrites. **a**, Basal dendrites Ca^{2+} activity in response to a reference train of tones (10 kHz), never presented to the mice before. **b**, The peak amplitudes in response to each tone were not significantly different. Krustal-Wallis test. **c**, Schematic of experimental design. The NMDA channel antagonist, APV, was locally applied onto the cortical surface during two-photon Ca^{2+} imaging of basal dendrites. **d**, Example auditory-evoked Ca^{2+} responses in a basal dendrites before (top, black) and after (bottom, orange) the local cortical application of APV. **e**, Percentage of auditory stimuli which evoked Ca^{2+} responses pre (black; 6.5 ± 1 %) and post APV (orange; 1.0 ± 0.5 %; p =0.0001, Mann Whitney test; n = 48 dendrites, 3 mice. Plots show mean ± SEM.

CHAPTER 5

DYNAMICS OF DENDRITIC ACTIVITY DURING LEARNING OF AN AUDITORY DISCRIMINATION TASK

CHAPTER 5

In this chapter I investigate the dynamic changes occurring in dendritic activity during learning in awake behaving mice. Bear in mind that, because of the low number of subjects (see methods), at this stage, this is to be considered a pilot study. The results shown here will be the starting point for future experiments designed to address the involvement of cortical dendrites during perceptual learning. However, interesting comments and observations can already be made from the following results.

INTRODUCTION

Perceptual learning occurs when sensory signalling is optimised during the acquisition of a sensory-based task. As the rules of the task are learnt and the behavior is consolidated, the underlying neural activity is shaped to be reliable and stable[7,176]. Frequency discrimination learning induces plasticity of sensory representations[87,88]. Learning of a visual discrimination task enhances neuronal stimulus selectivity and increases stimulus discriminability in the primary visual cortex[89]. Further evidence in the somatosensory (barrel) cortex also illustrate that behavioral performance and sensory encoding, both in single neurons and in the population, are stabilised during learning[67]. In the auditory cortex, engagement during an auditory discrimination task suppresses neural activity[177] and recruits smaller neural ensemble to better encode the behavioral choice[83]. Despite a wealth of evidence showing that perceptual learning involves the auditory cortex[88,178-183], the mechanisms underlying the changes in auditory-sensory representations remain unclear. Notably, one study has highlighted that the reorganisation of auditory cortical maps during perceptual learning is controlled by top down modulation[182]. Indeed, learning increases the impact of top-down signalling in sensory areas[1] via long range projections in layer 1 that synapse onto tuft dendrites of pyramidal neurons. An important question that remains unanswered is whether dendritic activity is also modulated during perceptual learning.

CHAPTER 5

In the previous chapter I illustrated that tuft dendrites in the auditory cortex encode auditory information and undergoes local plastic changes following fear learning. Previous studies have also identified the encoding of reward in tuft dendrites following learning of a sensory-based task [161] and localised plastic changes in tuft dendrites during motor learning[112]. Importantly, dendrites have a relevant role during behavior as their modulation can shift the perceptual threshold for the detection of a sensory stimulus[56] . In addition, dendritic signalling can encode complex features of the stimulus and support a mixed network representation[57]. Further data presented in this thesis (Chapter 3) also shows that dendritic integration of multisensory inputs is correlated with enhanced behavioral responses during the performance of a sensory-based task. Here, we investigated the dynamics of dendritic activity as mice learned to perform a sensory-based task. We used 2 photon microscopy to chronically image the same population of dendrites within the auditory cortex, sparsely expressing GCaMP, during learning of an auditory discrimination task.

RESULTS

To investigate the role of dendrites during learning of an auditory discrimination task we sparsely transfected layer 2/3 pyramidal neurons within the auditory cortex with a genetically encoded Ca^{2+} sensor (see methods for details) and performed two photon Ca^{2+} imaging from tuft dendrites at a depth 20-80 μm from the surface of the brain (Figure 5.1a). We established an auditory discrimination task using pure tones (5 or 15 kHz, 500 ms) as either Go or No-Go signals (Figure 5.1b). Mice were trained to lick a water port in response to the presentation of the auditory Go signal. If the licking response was within 1s of the auditory stimulus (response window), mice received a sugar water reward (5-10 μl). During No-Go trials, mice were required to withhold licking during the response window to avoid a timeout punishment (see methods). Overall, mice learnt to discriminate Go and No-Go signals to a threshold of 75%

correct responses in 7 days (n = 4 mice; Figure 5.1c). We first imaged dendritic activity during Go and No-Go signals from the naïve mouse, prior to training (n = 70 dendrites from 4 mice) and compared the population dynamics in the selected field of views (Figure 5.1d). There was no difference in the amplitude of the evoked Ca^{2+} activity between Go and No-Go signals (Go: 2.89 ± 0.28 ΔF/F; No-Go: 3.25 ± 0.29 ΔF/F; p = 0.20; Figure 5.1e and h). Although a small subset of dendrites were active prior to the stimulus (Figure 5.1d), the numbers were too low at this stage for further investigation. Mice were then trained daily in the auditory discrimination task and the same population of dendrites (i.e. same field of view) was followed during learning (n = 75 dendrites from 4 mice; Figure 5.1f). Also here, Go and No-Go signals evoked similar activity (Go: 2.38 ± 0.28 ΔF/F; No-Go: 2.96 ± 0.36 ΔF/F; p = 0.30; Figure 5.1g and h). However, comparing tuft activity in naïve and behaving (expert) mice showed significant differences. Overall, the number of Ca^{2+} transients evoked by the auditory stimuli were significantly decreased in expert mice compared to naïve in both the Go trials (expert: 3 ± 0.6 %; naïve, 8 ± 1 %; p= 0.0001; n = 75/70 dendrites from 4 mice) and No-Go trials (expert: 3 ± 0.5 %; naïve, 9 ± 1 %; p= 0.0001; n = 75/70 dendrites from 4 mice; Figure 5.1i). These results illustrate that dendrites in the auditory cortex encode sounds differently when engaged in a task compared to passive listening. Specifically, the data highlights that task engagement suppresses sensory-evoked dendritic activity in the auditory cortex.

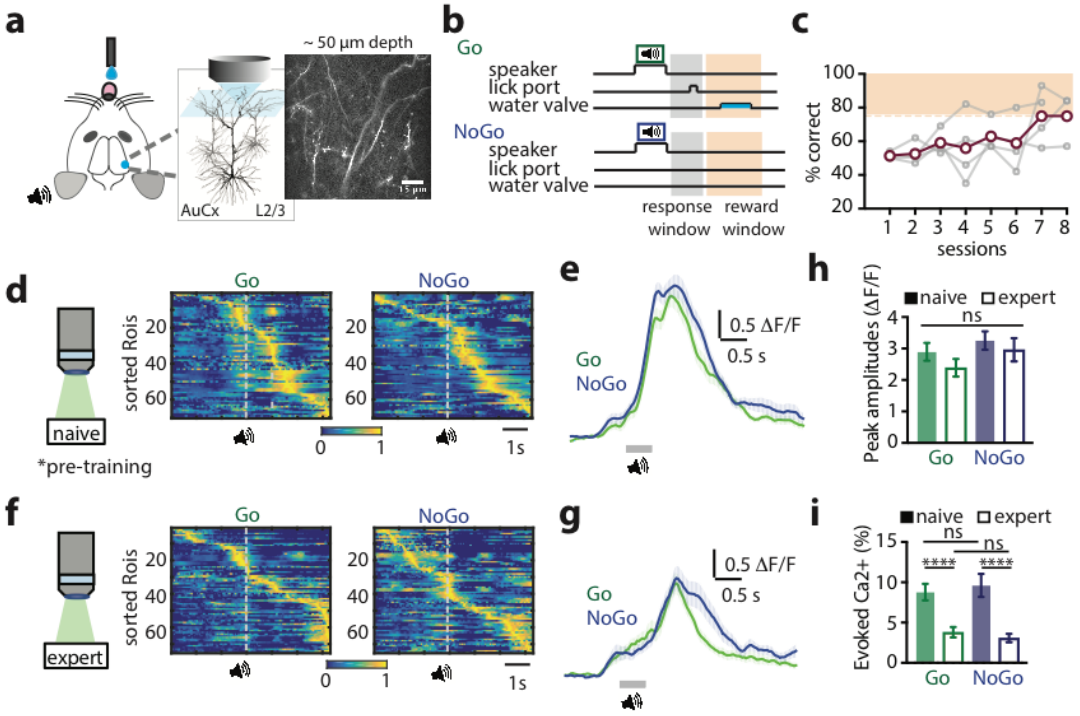

Figure 5.1 | Imaging dendritic dynamics during an auditory discrimination task.

a Schematic of the imaging protocol. Tuft dendrites of L2/3 pyramidal neurons (sparsely expressing GCamp6f or GCamp7f) were imaged with two photon microscopy. **b** Behavioral protocol of the sound discrimination task. Go cue is rewarded when mice licks during the response window. **c** Mass learning curves of 4 mice during the acquisition of the task. Orange line show the learning threshold of 75% correct answers. **d** Heatmaps of overall dendritic activity and **e** averages of sound-evoked responses (active trials) in dendrites imaged from naïve mice (passive listening), prior to training. **f** Heatmaps of overall dendritic activity and **g** averages of sound-evoked responses (active trials) in dendrites imaged during the task in expert mice. **h** Peak amplitudes of the auditory evoked Ca^{2+} transients across recording conditions. **i** Percentage of auditory evoked Ca^{2+} transients across recording conditions. Statistical significance was determined with Mann Whitney test at a p value < 0.05 (*). Error bars show mean ± SEM.

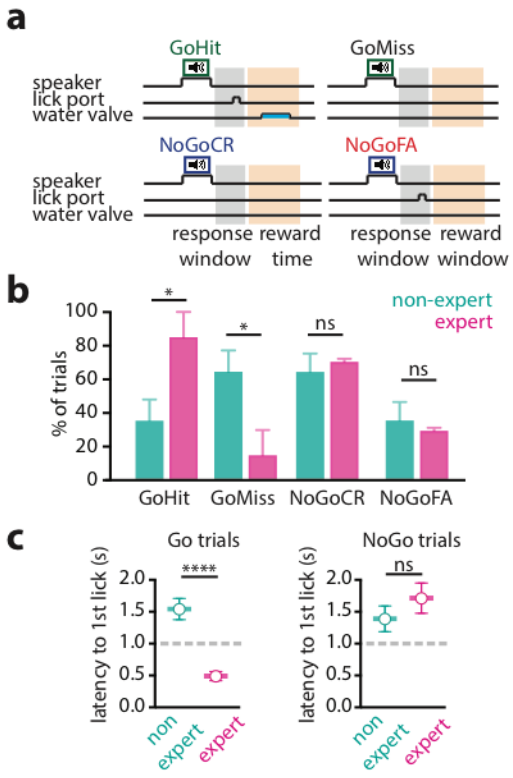

Figure 5.2 | Analysis of trial types and lick latencies. a, Schematic of possible behavioural outcome during the sound discrimination task. **b**, Behavioral performance of mice (n = 4) divided by trial type in non-expert (teal) and expert (magenta) condition. **c**, Latency to first lick for Go trials (left) and No-Go trials (right) comparing non-expert (teal) and expert (magenta) conditions. The grey-dotted line shows the response window. Error bars show mean ± SEM.

These dynamics may be instrumental to the performance of the task and could help shaping sensory representation of the auditory stimuli during learning. To better address this issue, we analysed the behavioral data according to the task outcome. A Go trial can result in a Hit, when the mouse correctly licks for reward after the auditory cue, or a Miss, when the mouse fails to do so. A No-Go trial can result in a correct rejection (CR), when the mouse does not respond following the appropriate auditory cue, or a false alarm (FA), when the mouse fails to do so and instead licks the water port following the auditory No-Go cue (Figure 5.2a). During Go trials, mice have a low percentage of correct Hits (non-expert: 35.5 ± 12.7%) in the first training session which rapidly increases with learning (expert: 85 ± 15%; p = 0.04; n = 4 mice; Figure 5.2b). In contrast, false alarm and correct rejections remains stable throughout learning, with no significant difference in rates of CR (non-expert: 64.4 ± 11 %; expert: 70.4 ± 1.8 %; p = 0.61) and FA (non-expert, 35.5 ± 11 %; 29.5 ± 1.8 %; p = 0.61; n = 4 mice; Figure 5.2b).

Furthermore, the onset of licking bouts after the presentation of the auditory cue became significantly faster during Go trials in expert mice (non-expert, 1.54 ± 0.16 s; expert, 0.49 ± 0.07 s; p = 0.0001; n = 4 mice; Figure 5.2c). In contrast, lick latencies during No-Go trials did not differ significantly between non-expert and expert conditions (1.38 ± 0.20 s vs 1.71 ± 0.23 s; p = 0.91; n = 4 mice; Figure 5.2c). These data illustrate that learning is highlighted by modification of the behavioral response specifically during Go Trials in the expert mouse.

Since learning alters the behavioral response during task performance, we then sought to answer whether dendrites encoded the sounds differently according to trial types. Dendritic activity during Hit trials was remodelled during perceptual learning. Although the peak amplitude of the auditory evoked Ca^{2+} transients was overall similar (non-expert: 3.59 ± 0.53 ΔF/F; n = 20 transients; vs expert: 2.52 ± 0.27 ΔF/F; n = 38 transients; p = 0.14; 72/75 dendrites from 4 mice; Figure 5.3a, b) more events occurred across dendrites in the expert mouse (non-expert: 2 ± 0.8 %; n = 72 dendrites from 4 mice; vs expert: 4 ± 0.7 %; n = 75 dendrites from 4 mice; p = 0.01; Figure 5.3c). In contrast, sound driven Ca^{2+} transients in dendrites during CR trials were stable during learning as the peak amplitudes (non-expert: 3.38 ± 0.38 ΔF/F; n = 39 Ca^{2+} transients; vs expert: 3.32 ± 0.43 ΔF/F; n = 32 Ca^{2+} transients; p = 0.65; 72/75 dendrites from 4 mice; Figure 5.3d, e), and the evoked frequency during learning was not significantly different (non-expert: 4 ± 0.6 %; n = 72 dendrites from 4 mice; vs expert: 3 ± 0.6 %; n = 75 dendrites from 4 mice; p = 0.12; Figure 5.3f). Interestingly, dendritic activity changed also in FA trials during learning (Figure 5.3g, h). Here, auditory evoked Ca^{2+} transients had significantly smaller amplitudes (non-expert: 4.40 ± 0.60 ΔF/F; n = 21 Ca^{2+} transients; vs expert: 2.09 ± 0.42 ΔF/F; n = 15 Ca^{2+} transients; p= 0.09; 72/75 dendrites from 4 mice; Figure 5.3i) in the expert condition, however, they did not differ in efficacy (non-expert: 4 ± 1 %; n = 72 dendrites from 4 mice; vs expert: 3 ± 0.9 %; n = 75 dendrites from 4 mice; p = 0.24; Figure

5.3f). These results suggest that tuft dendrites in the auditory cortex encode trial outcome and that their sensory encoding is shaped by learning in a way which could be instrumental to the performance of the auditory discrimination task.

How do these learning-induced changes emerge in single dendrites? To start addressing this question we tracked single dendrites during learning by identifying dendrites in our fields of view across the recording sessions from naïve to expert (Figure 5.4).

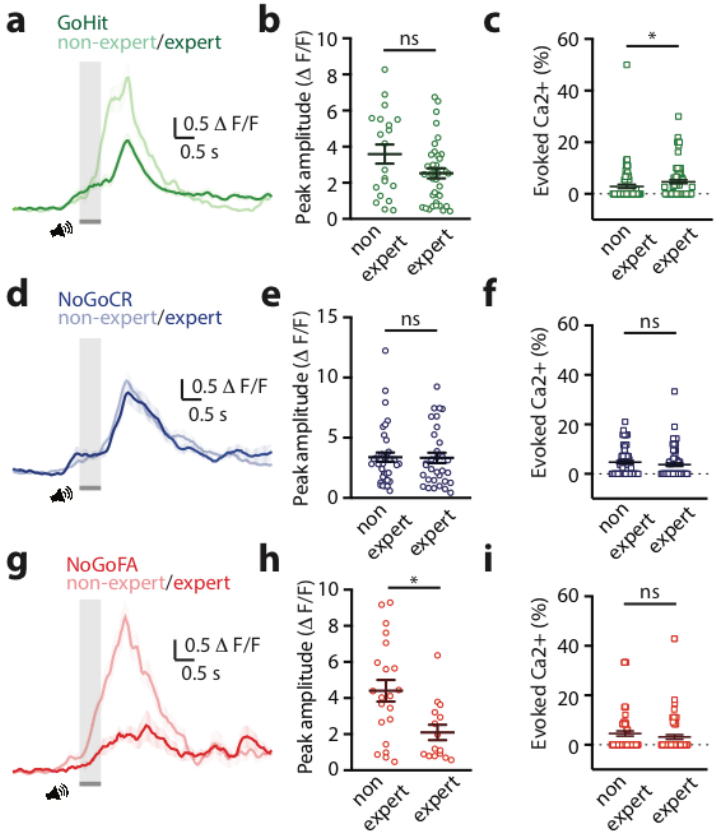

Figure 5.3 | Learning during the sound discrimination task induces specific changes of sensory-evoked activity in tuft dendrites. a Average traces of sensory evoked dendritic Ca^{2+} transients (active trials) during Hit trials in non-expert (light green) and expert mice (dark green). b Peak amplitudes of the sound -evoked Ca^{2+} transients.

c Percentage of the sensory evoked Ca^{2+} transients detected across Hit trials in non-expert and expert conditions. expert mouse. **d** Average trace of sensory evoked dendritic Ca^{2+} transients (active trials) during CR trials in non-expert (light blue) and expert mice (dark blue). **e** peak amplitudes of the evoked Ca^{2+} transients. **f** Efficacy of evoked Ca^{2+} transients in CR trials compared between the non-expert and the expert mouse. **g** average trace of sensory evoked dendritic Ca^{2+} transients (active trials) during FA trials in non-expert (light red) and expert mice (dark red). **h** Peak amplitudes of the evoked compared across learning. **f** Percentage of the sensory evoked Ca^{2+} transients in FA trials during the non-expert and expert sessions. Error bars show mean ± SEM.

Comparing patterns of activity in non-expert and expert mice, single dendrites altered their activity (Figure 5.4a and b). Interestingly, in the expert mouse, during Hit trials, most dendrites increased the number of evoked Ca^{2+} transients during the reward period (11/14 tracked dendrites; Figure 5.4c). The peak amplitude of these reward-evoked Ca^{2+} events in tracked dendrites were significantly larger in expert mice compared to non-expert mice (non-expert: 0.75 ± 0.20 ΔF/F ; expert: 1.83 ± 0.30 ΔF/F; p = 0.0009; n= 14 dendrites from 3 mice; Figure 5.4d). These data show that changes in dendritic encoding during learning can occur in single dendrites. Furthermore, such modulation of dendritic signalling might underlie reinforcement during rewarded trials and be important for the performance of the task. Future experiments will expand on this and further address the causal role of dendritic encoding in task performance through optical or pharmacological manipulation.

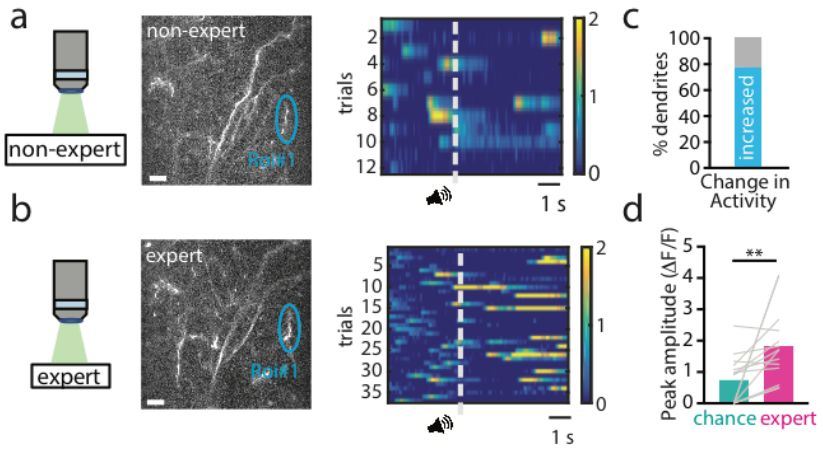

Figure 5.4 | Tracking single dendrites across recording sessions. a, b (left) Same field of view showing dendrites recorded across different conditions: non-expert (**a**) and expert (**b**). Cyan show an example ROIs of dendrite tracked across days. Scale bars = 10 ηm. **a, b** (right) Heatmaps (PSTH) of single dendrites in the example ROIs from non-expert (**a**) and expert (**b**) during Hit trials. **d** percentage of tracked dendrites that showed increased activity after learning (11/14 tracked dendrites). **e** peak amplitudes of the tracked dendrites comparing non-expert and expert activity after reward delivery. Statistics in **e**: Wilcoxon matched-pairs

CHAPTER 5

DISCUSSION

Cortical dendrites encode sensory information[22,50,53], have an important role in sensory perception[56,57] and are a substrate for plasticity mechanisms[61,108,110,128,184,185]. Whether perceptual learning changes dendritic encoding is currently unknown and is the focus of this study. To address this question, we performed longitudinal 2-photon Ca^{2+} imaging of dendritic activity in the auditory cortex during the acquisition of an auditory discrimination task.

Imaging dendrites in naïve mice, as they are passive listening to auditory cues, showed a striking difference in the activity patterns during sound-driven behavior. Specifically, dendrites showed a strong reduction in stimulus encoding as during the task performance, less Ca^{2+} transients were evoked in response to the auditory cues. Previous studies have also reported inhibition during behavior [84,85,177]. This mechanism could highlight the emergence of a coding mechanism that reduce the network components to optimise signalling[83,90]. An additional interpretation is that feedforward signalling is the default mode for dendritic encoding in the naïve mouse, while learning of the auditory discrimination task recruits top-down inputs from other brain regions such as the posterior parietal cortex (PPC)[186,187] or the pre-frontal cortex (PFC)[188,189].

In our data, learning has a stronger effect on the Go trials compared with No-Go trials, as shown by the performance and lick latencies (Figure 5.2b and c). This could reflect the mice strategy and their motivational drive. To learn the task, there are two main strategies that mice can take: 1) Mice do not lick spontaneously at early phases of training, therefore leading to a low Hit and FA rate, and high CR and Miss. However, as they learn the task, they start licking more and more in response to the Go cue. In this case, the Go signal acquires relevance while the No-Go continues to be simply ignored. 2) Mice learn that they can receive a reward and therefore they would immediately lick to both cues and then slowly learning to discriminate by suppressing licking in the No-Go trials. In this case, both Go and No-Go signals would require

important changes during learning. Since, in our experiments, mice learn to alter their response to the Go signal whereas the responses during No-Go trials remained the same, it appears as though mice typically learn using strategy #1. The low number of subjects did not allow for further analysis at this stage. In addition, it is also possible that mice use individual strategies. Perceptual learning increases the efficacy of sensory signalling[7,89,176]. In this study, we found that auditory-evoked activity in dendrites during correct performance in Go trials differed following learning of an auditory discrimination task. In contrast, dendritic activity during correct performance in No-Go trials remained stable during learning. Considering the behavioral results, this specificity might underlie changes that are instrumental to the performance of the task. Although the amplitude of the auditory-evoked Ca^{2+} transients did not differ, their efficacy was significantly increased during Hit trials, suggesting a more reliable representation. Tracking dendrites across sessions also showed that more activity is evoked during the reward epoch in expert mice. The fact that these changes occur in tuft dendrites supports the idea that they could reflect a selective increase in the impact of top down modulation during learning[1]. The optimisation of signal processing could be achieved through reinforcement of the Go cue during Hit trials, as a result of reward delivery[179]. Interestingly, recent studies have highlighted the emergence of reward signalling in tuft dendrites during learning[58]. Although we have not currently investigated this aspect in our study, it will be object of future analysis and experiments.

These data suggest that active and passive listening are differently encoded in tuft dendrites of the auditory cortex. In addition, they add evidence to the idea that learning selectively increases top down modulation in sensory areas. This was reflected by the specific changes in auditory evoked activity in tuft dendrites of the expert mouse. NMDA spikes in tuft dendrites can affect the dendrite-to-soma coupling during sensory processing[50]. Although we have not investigated the nature of the Ca^{2+} transients recorded in this study, considering our previous results

(Chapter 3 and 4), we also expect them to be NMDA dependent. Enhancing the efficacy of sensory-evoked NMDA dependent dendritic activity could provide a mechanism to increase the effect of feedback input on the neural output. In this way, the modulation of dendrites during learning could play an important, active, role in increasing the reliability of sensory representations. Further experiments await to address this question.

Acknowledgments

I would like to thank George Stuyt who kindly performed virus injection and chronic window surgeries in two of the mice included in this study.

METHODS

All experiments were conducted in strict accordance with the Code of Practice for the Care and Use of Animals for Scientific Purposes (National Health and Medical Research Council, Australia) and guidelines given by the veterinary office of The Florey Institute of Neuroscience and Mental Health.

Mice. C57BL/6 were used for behavioral training and two photon Ca^{2+} imaging. One cohort of mice (n = 2 mice) had previously undergone behavioral training on a different task and used GCaMP7f (AAV1.Syn.Flex.GCaMP7f.WPRE.SV40). The other cohort (n = 2 mice) was infected with GCaMP6f (AAV1.Syn.Flex.GCaMP6f.WPRE.SV40). The two Ca^{2+} indicator have very similar properties and data were therefore pooled together.

Virus injections. Mice (C57BL/6; P30 - 55) were anaesthetised with isoflurane (1 - 3 % in 0.75 L/min O2) and body temperature was maintained at 36 - 37 °C. Eye ointment was applied to prevent dehydration and meloxicam (1 - 3mg/kg, Ilium) was intraperitoneally injected for anti-inflammatory action. The skin was disinfected with ethanol 70 % and betadine before a cut was made to expose the skull. A small craniotomy (0.7 x 0.7 mm) was then made over the auditory cortex and a mix of Cre-dependent genetic Ca^{2+} indicator and diluted Cre (AAV1.hSyn.Cre.WPRE.hGH) was injected in L2/3 (-2.5 mm from bregma and 4.5 mm from midline, 450 µm along the dorsoventral axis) to achieve sparse labelling. After slowly retracting the microcapillary pipette, the skin was sutured and the mouse was able to recover for at least 3 days prior to any further experimental procedures.

Head-post implantation and cranial window surgery. To surgically implant the head-post and cranial window for recordings in the awake state, mice were anaesthetized with isoflurane (1 – 3 % in 0.75 L/min O2) and intraperitonially injected with Meloxicam (1 – 3 mg/kg, Ilium). Throughout the surgery, body temperature was maintained at 36 - 37 °C. Lidocaine (20mg/ml, Ilium) was topically injected around the surgical site before the skin was cut to expose the

skull. A craniotomy was performed (3 mm diameter) over the virus injection site, in the auditory cortex. A circular coverslip (3 mm diameter, size #1) was placed over the craniotomy, and sealed with glue and dental cement before the remaining skull surface was covered with inert silicon (kwik-cast, WPI). A custom-made metal head-bar was also attached to the skull using dental cement (C&B Metabond®, Parkell) for head-fixation. Mice were returned to their home cage for at least 3 days before behavioral training commenced.

Behavioral protocol. Mice were water restricted (5 - 2 cycle, 1 ml/day on restriction days; ad libitum access to food). After > 2 days of water restriction, mice were gradually habituated to head fixation and the microscope setup. Auditory stimulation (pure tones: 5 - 15 kHz, 75 dB, 500 ms) was generated using an Arduino micro-processing boards (Arduino Uno) and delivered through electrostatic speakers (Tucker-Davis Technology - ES1) placed approximately 5 - 10 cm away from the contralateral ear. Behavioral training started the day after the naïve imaging session. One of the two sound cue was randomly assigned as Go or No-Go signals (counterbalanced in the 2 cohort). After Go cue presentation mice have to lick in a window of 1 second to receive a sugar reward (5-10 µl, sugar/water: 10%). In No-Go trials mice have to suppress licking during the same time window to avoid a time out punishment (4-8 seconds). Trials presentation were equal in percentage (50% Go and 50% No-Go) since day one of training. Mice were considered expert once they consistently reached 75 % of correct responses on 2 consecutive sessions. The behavioral training protocol was custom-written and presented using BPod (Sanworks), and MATLAB (MathWorks) was used to collect data and analysis.

Two-photon Ca^{2+} imaging. For dendritic imaging, GCaMP6f or GCaMP7f was excited at 940nm (~30 mW at the back aperture) with a titanium sapphire laser (140 fs pulse width; SpectraPhysics MaiTai Deepsee) and imaged on a Sutter MoM through a 16x Nikon objective (0.8 NA). Emitted light was passed through a dichroic filter (565dcxr, Chroma Technology)

and short-pass filtered (ET525/70-2p, Chroma Technology) before being detected by a GaAsP photomultiplier tube (Hamamatsu). Images were acquired at a frequency of 30 Hz (512 x 512 pixels) using ScanImage software. Ca^{2+} transients were recorded from tuft dendrites of layer 2/3 pyramidal neurons within the auditory cortex at a depth of 30-80 μm from the pia surface. The images where motion corrected and region of interest (ROI) where manually drawn on ImageJ before fluorescence signal extraction. Ca^{2+} responses were smoothed using a Savitzky-Golay filter (2^{nd} order polynomial and 7 sample window) and the ΔF/F was measured by subtracting the median of the baseline to the fluorescence signal for each trial. All Ca^{2+} signal processing was performed with custom written Matlab scripts.

Ca^{2+} transients analysis. Auditory evoked Ca^{2} transients were identified by applying a threshold of 3 standard deviation of the baseline. An event was detected when this threshold was crossed in a window of 1 second from stimulus onset. The peak amplitudes of this detected events were then measured in a window of 2 seconds from auditory stimulation. The percentage of trials with Ca^{2} transients was measured as the number of events for each dendrite divided by the number of trials. The mass traces shown represents the mass average of all the active trials across the population of dendrites (where an auditory evoked calcium transient was detected during the entire auditory stimulation). Error bars show SEM.

Data analysis. All statistical analysis was performed using GraphPad (Prism). Normality of the dataset was determined, and parametric or non-parametric test were chosen accordingly. Statistic tests used are Mann Whitney test or Wilcoxon matched pair signed-rank test with significance determined at $p < 0.05$.

CHAPTER 6

GENERAL DISCUSSION

CHAPTER 6

SUMMARY OF THE MAIN RESULTS

This thesis investigates the modulation of cortical dendrites during sensory perception and learning. In Chapter 3 we show that L2/3 pyramidal neurons in the forepaw area of the primary somatosensory cortex receive cross-modal inputs from the auditory cortex. Pairing auditory inputs with tactile stimulation increased the evoked rate and amplitude of the Ca^{2+} events occurring in tuft dendrites of L2/3 pyramidal . Importantly, auditory inputs led to an increase in the somatic action potential output and increased reaction speed during a tactile-based goal-directed behavior. In addition, this mechanism was specific to L2/3, but not L5, pyramidal neurons (Figure 6.1 a). In Chapter 4 we identified learning-dependent changes in dendritic sensory processing in L2/3 pyramidal neurons that were localised to tuft, but not basal, dendrites. Similar to what was observed in Chapter 3, the localised enhanced activity in tuft dendrites was correlated to an increase in somatic action potentials following fear learning (Figure 6.1 b). In Chapter 5, we investigated experience-dependent changes in dendritic activity during the acquisition of an auditory discrimination task. Here, we show that dendrites of layer 2/3 pyramidal neurons are involved in perceptual learning by specifically increasing the efficacy of tuft dendritic activity during correct rewarded trials (Figure 6.1 c).

Although each chapter explored different aspects of dendritic modulation during memory and behavior, there are many commonalities in the results. This suggests that the mechanisms described could be shared across sensory cortices and are of great importance to the overall computation performed by cortical L2/3 pyramidal neurons.

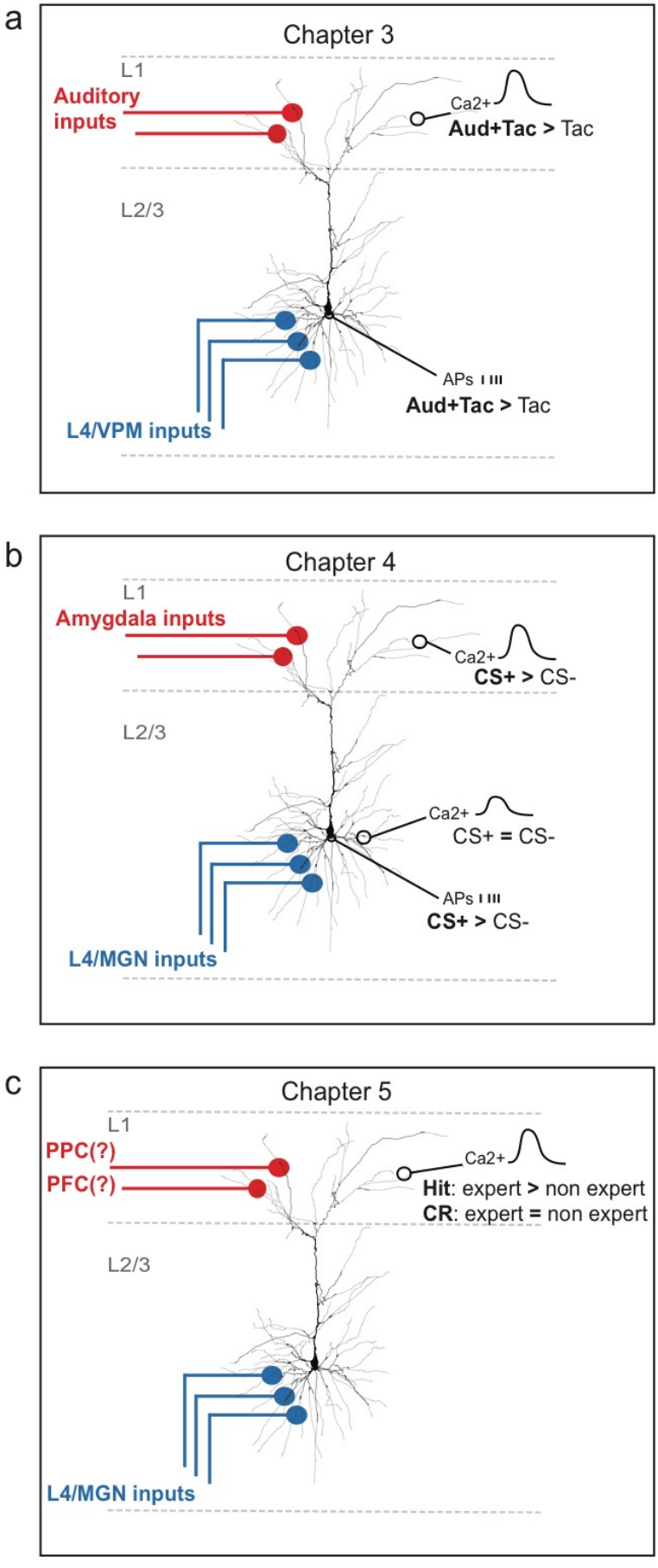

Figure 6.1 | Summary of the main results.

a Auditory inputs onto tuft dendrites of L2/3 pyramidal neurons of the somatosensory cortex, evoked large Ca^{2+} events and increased dendritic activity. Somatic APs were also increased when auditory and tactile stimulation were combined. **b** Fear conditioning increased CS+ encoding in tuft dendrites but not in basal dendrites. APs were also increased in response to CS+. **c** Perceptual learning during an auditory discrimination task increased the efficiency of auditory encoding in tuft dendrites only in correctly rewarded trials.

Compartmentalisation of dendritic processing

L2/3 pyramidal neurons receive different streams of information onto different dendritic compartments[41]. Tuft dendrites, which are found in layer 1 of the cortex, are the target of long-range projections from other cortical and subcortical areas. These inputs arriving onto tuft dendrites are referred to as feedback inputs as they usually carry information about the internal brain state. Tuft dendrites are located far from the soma and are therefore more electrically isolated than basal dendrites which project radially from the soma. Basal dendrites receive a large amount of synaptic inputs from primary thalamic nuclei and other local pyramidal neurons as part of the feedforward pathway. The inputs onto basal dendrites usually carry direct information about sensory features of the external environment[41]. Basal dendrites are also much closer and electrically connected to the soma compared to tuft dendrites. For example, action potentials that are generated at the soma, can typically propagate faithfully into basal dendrites[51]. Although they receive different input streams of information, both tuft and basal dendrites can generate NMDA dependent dendritic events[50,149,150]. This suggest that dendrites process and encode different types of sensory information, allowing pyramidal neurons to multiplex computations within different dendritic compartments.

Taken together, the results in each Chapter of this thesis illustrates that tuft and basal dendrites provide neurons with domains that can perform different computations. In Chapter 4, we found specific changes in activity following fear conditioning in tuft, but not basal, dendrites, suggesting that fear learning specifically shapes the processing of sensory information within tuft dendrites. Interestingly, feedback projections from the amygdala into layer 1 of the auditory cortex have been shown to remodel dendritic spines on tuft dendrites of cortical pyramidal neurons[97] . These results are of great importance since the amygdala undergoes plasticity after fear conditioning[190-192] [159,172,192,193] and is known to be a key player in the changes that occur during fear learning[194]. In contrast, basal dendrites remained unaltered

following fear conditioning, presumably because they primarily receive feedforward sensory information which represents the (unchanged) sensory signals from the external world. Future experiments should investigate whether the modulation tuft dendritic activity in the auditory cortex is indeed mediated by amygdalocortical projections.

Also, in Chapter 3 we show evidence of compartmentalisation. Tuft dendrites of layer 2/3 pyramidal neurons within the primary somatosensory cortex had a high level of Ca^{2+} activity evoked by broadband auditory stimulation. Surprisingly this auditory-evoked Ca^{2+} activity was even larger than activation of the primary sense via tactile stimulation. Similar to what was highlighted by the specific learning-dependent changes in tuft dendrites of the auditory cortex (Chapter 3), we suggest that the activity in tuft dendrites within the somatosensory cortex reflected the long-range feedback inputs from the auditory cortex. In Chapter 5, comparable to the changes in tuft dendrites following fear conditioning, we show that tuft dendrites within layer 1 of the auditory cortex also undergoes changes in sensory processing during perceptual learning. This modulation was selective to auditory-evoked activity during correct performance in an auditory discrimination task, suggesting the involvement of a specific pathway. Here too, we believe that feedback inputs might be responsible for the changes of sensory encoding in tuft dendrites. To prove the importance of feedback modulation, we would need to establish whether basal dendrites undergo similar changes during perceptual learning. Future experiments will address the role of basal dendrites during the performance of the auditory discrimination task to provide further evidence that tuft and basal dendrites can encode different types of information in parallel. In addition, it would be important to trace and identify the neurons where the dendrites originate from. This information would complement and solidify the results presented in both Chapter 3 and Chapter 4.

Taken together, these findings enhance our knowledge of the computations performed by pyramidal neurons during learning. Indeed, the ability to process different streams of

information in each sub-compartment could provide a flexible switch for sensory processing at a cellular level[32,195]. This hypothesis is supported by our data, as we show that different dendritic compartments can be modified independently. Furthermore, our results challenge the long-standing hypothesis that neurons act as a single - one point - processing element. We show that individual pyramidal neurons are multi-layered structures with complex and independent integrative properties[175]. Theoretical models also support our results, illustrating that the input-output transformation of a pyramidal neuron in vivo requires the multiplexed processing of sensory inputs – a process which can be achieved via local dendritic computations[196,197]. Ever since the early description of active dendritic properties[44], the importance of dendritic compartmentalisation in the processing of sensory input has been debated. However, due to advances in imaging systems, it has only recently been possible to directly address this question[16]. The ability to finally look at these processes in vivo has shed light on how pyramidal neurons can actively integrate the wealth of synaptic inputs they receive on their dendrites.

Different role of cortical layers in sensory processing

A long-standing question in neuroscience involves understanding the function of each cortical layer during sensory perception. Indeed, we know that each cortical layer is composed of different cell types, local connections and long-range inputs[4,5,198]. Despite a general idea of what computations are performed within each layer of the cortex during sensory perception, how these computations are achieved remains largely unknown[4]. Although we have not directly addressed this question in this body of work, several results in our studies shed some light on this issue.

Strikingly, we found diversity in the encoding of sensory information in pyramidal neurons from different cortical layers (Chapter 3). Specifically, we illustrated that the auditory cortex is monosynaptically connected to L2/3 pyramidal neurons of the somatosensory cortex via

long-range projections in L1. Interestingly, L5 pyramidal neurons did not receive direct connections from the auditory cortex via L1. Although we found that tuft dendrites of L5 pyramidal neurons were occasionally responsive to auditory stimuli, they did not integrate auditory and tactile inputs. Contrary to L2/3 pyramidal neurons, combining auditory and tactile stimulation did not have an influence of on the somatic output of L5 pyramidal neurons. This striking difference could be explained by many factors such as the diverse morphology and compartmentalisation of L5 and L2/3 pyramidal neurons[144,199]. In L5 pyramidal neurons, the soma and its tuft dendrites, which stratify in L1, are quite spatially distant from each other. As a consequence, signals generated at different dendritic locations need to travel a long way to influence each other. Therefore, tuft dendrites of L5 pyramidal neurons are more electrically isolated respect to tuft dendrites of L2/3 pyramidal neurons[144,199]. In addition, inputs on L5 pyramidal neurons have a different organisation compared to L2/3 pyramidal neurons[41]. Each dendritic compartment within a L5 pyramidal neuron receives different types of synaptic inputs (i.e. feedforward and feedback). Therefore, L5 pyramidal neurons display less global organisation of their inputs[40], supporting the theory that L5 pyramidal neurons are composed of independent, weakly coupled, compartments[144]. Moreover, there are also differences in the local circuit components that contact L2/3 and L5 pyramidal neurons[2]. Therefore, different mechanisms might be involved in the integration of multisensory inputs within L2/3 and L5 pyramidal neurons, which could explain why we observed differences in our results. Importantly, the data presented in Chapter 2 further supports the idea of a diversification of functions and computations across the cortical layers. In Chapter 4, we illustrate that sensory encoding in tuft dendrites within the auditory cortex are modulated following fear conditioning. However, this was not the case for the basal dendrites. In Chapter 5, we again observed changes in sensory encoding occurring in tuft dendrites of the auditory cortex during perceptual learning. Collectively, these results confirm that layer 1 of the cortex is an important hub for

the processing of feedback inputs and that tuft dendrites, which reside in layer 1, can locally perform different types of computations. The data also highlights a cellular mechanism, the NMDA spike, which enables synaptic input onto tuft dendrites to influence somatic output[37,50]. Indeed, in Chapter 3 and 4, the changes we observed in tuft dendrites was correlated with an increase in the somatic output of L2/3 pyramidal neurons. This illustrates that the upper layers of the cortex are a substrate for the changes in neural activity occurring during learning and can act as flexible module during sensory processing. We believe that sensory representations in the upper layers of the cortex can be constantly updated by current and past experiences, through the integration of long-range inputs. In addition, the upper layers of the cortex can also provide control over the cortical output of L5 through gain modulation[132,200,201].

The data presented in this thesis support the idea that cortical layers have specialised and distinct functions. They also propose a mechanism within the upper layers of the cortex, involving active dendritic integration, that could form a flexible module for the continuous refinement of internal representations.

A cellular mechanism for the modulation of somatic output

The pyramidal neuron is the fundamental element for associating information in the cortex. This is due to its morphology and position within the cortical layers, as it receives compartmentalised and localised inputs onto its dendrites[32,41]. However, this compartmentalisation raises a technical issue. Dendritic events in distal tuft dendrites have a very small effect on the membrane potential at the soma[46]. Since the membrane potential fluctuations at the soma is what ultimately determines the generation of an action potential, how can synaptic inputs onto tuft dendrites have an effect on the pyramidal neuron activity? Active dendritic properties help to overcome this issue as they provide a mechanism to increase the somato-dendritic coupling[42]. Local NMDA spiking in L2/3 tuft dendrites increase the

action potential response to sensory inputs[50]. Importantly, it does so without directly altering the somatic membrane potential. This means that even if the inputs that reach the soma are constant, distal inputs on tuft dendrites can modulate the somatic output through active integration. This mechanism could be a key feature for the flexible encoding of sensory information in pyramidal neurons. Indeed, a simultaneous action potential at the soma and an NMDA dendritic spike in tuft dendrites, can boost the output of the cell, allowing input to tuft dendrites to transiently modulate somatic activity[37]. In our results, we found evidence in support of this mechanism in L2/3 pyramidal neurons. In Chapter 3, pairing auditory and tactile inputs had no effect on the subthreshold response of L2/3 pyramidal neurons recoded in the somatosensory cortex using whole cell patch clamp electrophysiology. However, the somatic action potential was increased during paired audio-tactile stimulation compared to the tactile response alone. Solely auditory stimulation did not evoke action potentials suggesting that the supra-linear increase could occur through modulation of tuft dendrites activity via feedback inputs. Indeed, we found that L2/3 pyramidal neurons in the somatosensory cortex received monosynaptic inputs from the auditory cortex onto tuft dendrites that can evoke large Ca^{2+} events during auditory stimulation. In addition, when tactile and auditory stimulation were combined, Ca^{2+} activity in tuft dendrites was increased. These data illustrate that distal auditory inputs on tuft dendrites of L2/3 pyramidal neuron can modulate sensory encoding in the somatosensory cortex via a cellular mechanism that involves dendritic integration.

In this thesis, we also supplied evidence that activity in tuft dendrites could provide a way to modulate somatic output following fear learning. Feedback signalling of long-range projections within cortical L1 is increased during learning[1]. Tuft dendrites of L2/3 pyramidal neurons are also found in L1 and receive most of their inputs from long-range axonal projections. In this thesis, both Chapter 4 and 5 illustrate that also sensory encoding in tuft dendrites of L2/3 pyramidal neurons is enhanced during learning. In Chapter 4 we further

show that the learning-dependent enhancement of tuft activity was also reflected in the somatic output. Here, we reported an increase in action potentials in response to conditioned stimuli following fear learning. However, similar to the influence of auditory input on sensory encoding in the somatosensory cortex (Chapter 3), we also did not observe any change in the subthreshold somatic voltage response to the conditioned stimuli following fear learning. In addition, activity in basal dendrites was unchanged by fear conditioning suggesting that the feedforward pathway was not altered following fear learning. Taken together, these results demonstrate that changes of sensory encoding within tuft dendrites can provide a way to modulate the somatic output following fear learning.

In both Chapter 3 and 4, we also assessed the nature of the recorded dendritic events by locally applying the NDMA channel blocker APV. APV significantly reduced sensory evoked Ca^{2+} transients in tuft dendrites of both the auditory cortex (Chapter 4) and somatosensory cortex (Chapter 3) illustrating that they are NMDA dependent dendritic events. In Chapter 4 we also addressed the effect of NMDA block on action potential generation following fear learning. APV had a strong effect on the somatic output, significantly reducing action potential generation in response to the conditioned stimuli and abolishing the difference in CS+ and CS- evoked activity.

All together, these data illustrate that active processing in tuft dendrites can provide a way to increase the somato-dendritic coupling of L2/3 pyramidal neurons and modulate the somatic output during sensory processing. This mechanism could be important to bind together different streams of information and flexibly link together the upper layers of the cortex.

Technical considerations of imaging dendritic activity

The active properties of cortical dendrites have been extensively studied in vitro and only in the last decade have found their way to be addressed in vivo. Advances in genetic fluorophores

[17,202,203] and two photon Ca^{2+} imaging have provided a great set of tools to investigate dendritic activity in awake behaving mice[16,18]. However, these achievements do not come without challenges. It is important to note that genetic calcium indicators typically represent supra-threshold events. In addition, although calcium sensors have now achieved the ability to detect single action potentials[202,203], calcium activity in dendrites can follow other constraints due to the difference in morphology of the two compartments. The differences of calcium propagation in dendrites and soma should be kept in mind when looking at dendritic imaging data and comparing it with somatic data.

Another important factor to consider is the spatial dimension and distribution of dendrites. In Chapter 4 we traced dendrites in the field of view to their soma, to analyse correlated activity in dendrites from the same neuron or from different ones. This analysis allowed us to identify an increase in correlated activity between dendrites of different neurons following fear conditioning, suggesting a refinement of the network during fear learning. However, it is sometimes challenging to identify the neurons from which dendrites originates in the field of view as the soma might be outside of the accessible imaging region. In addition, with the common imaging techniques it is not possible to simultaneously monitor the entirety of the dendrites belonging to a single neuron. This information would be important in order to characterise the properties of a dendritic event and the relationship between local and global computations in a pyramidal neuron. However, techniques are constantly advancing[170]. For example, the use of a piezo-stepper system to swiftly switch the imaging focus can allow the simultaneous recording of somatic and dendritic activity from the same pyramidal neuron[54,55,204].

In conclusion, the development of voltage sensors[205,206] and new imaging techniques[207-210] will be of great benefit for advancing our understanding of active dendritic properties in vivo and the computations performed by the pyramidal neuron during sensory perception and behavior.

CHAPTER 6

CONCLUSIONS

Cortical dendrites of pyramidal neurons are an appealing substrate for sensory perception. Their position in the laminar structure of the cortex and their intrinsic active properties suggest they could play an important role in integrating internal information (feedback) with the current sensory experience (feedforward). In this thesis, we took advantage of the organisation principles of inputs onto L2/3 pyramidal neurons to address the role of dendrites in integrating different sensory information. Previously, it had been reported that L1 could be an important hub for the local integration of cross modal inputs[20], however, no previous study has investigated whether tuft dendrites play an active role during multisensory integration. The work presented in this thesis shows that tuft dendrites within L1 of the somatosensory cortex differentially encode tactile (feedforward) and auditory (feedback) information and support the integration of multisensory inputs. This thesis also addressed the effect of learning on dendritic activity in vivo. Although plasticity mechanisms have been widely investigated in dendrites in vitro[62,105,108,110,111,128,185,211,212], only a few other studies have identified learning-dependent changes in dendritic activity in vivo[112,61]. Furthermore, following from recent findings illustrating the importance of the auditory cortex during fear learning[81,98,99], our study additionally identified changes of tuft dendritic activity in the auditory cortex following fear conditioning. Finally, throughout this thesis, we presented evidence of compartmentalised modulation of dendritic activity, which provides a cellular mechanism to gate the action potential output of L2/3 pyramidal neurons.

Active dendrites remain a complex mystery that we are slowly starting to unravel. The findings presented in this thesis could help build an in-depth understanding of the role and the computations performed by cortical pyramidal neurons during sensory perception.

In conclusion, I hope that this work will provide even the smallest contribution towards the solution of the gigantic, mysterious, puzzle that is the brain.

THESIS REFERENCES

1 Makino, H. & Komiyama, T. Learning enhances the relative impact of top-down processing in the visual cortex. *Nat Neurosci* **18**, 1116-1122, doi:10.1038/nn.4061 (2015).

2 Palmer, L., Murayama, M. & Larkum, M. Inhibitory Regulation of Dendritic Activity in vivo. *Front Neural Circuits* **6**, 26, doi:10.3389/fncir.2012.00026 (2012).

3 Fregnac, Y. & Bathellier, B. Cortical Correlates of Low-Level Perception: From Neural Circuits to Percepts. *Neuron* **88**, 110-126, doi:10.1016/j.neuron.2015.09.041 (2015).

4 Adesnik, H. & Naka, A. Cracking the Function of Layers in the Sensory Cortex. *Neuron* **100**, 1028-1043, doi:10.1016/j.neuron.2018.10.032 (2018).

5 Harris, K. D. & Mrsic-Flogel, T. D. Cortical connectivity and sensory coding. *Nature* **503**, 51-58, doi:10.1038/nature12654 (2013).

6 Panzeri, S., Harvey, C. D., Piasini, E., Latham, P. E. & Fellin, T. Cracking the Neural Code for Sensory Perception by Combining Statistics, Intervention, and Behavior. *Neuron* **93**, 491-507, doi:10.1016/j.neuron.2016.12.036 (2017).

7 Makino, H., Hwang, E. J., Hedrick, N. G. & Komiyama, T. Circuit Mechanisms of Sensorimotor Learning. *Neuron* **92**, 705-721, doi:10.1016/j.neuron.2016.10.029 (2016).

8 Carcea, I. & Froemke, R. C. Cortical Plasticity, Excitatory–Inhibitory Balance, and Sensory Perception. **207**, 65-90, doi:10.1016/b978-0-444-63327-9.00003-5 (2013).

9 Hubel, D. H. & Wiesel, T. N. Receptive fields of single neurones in the cat's striate cortex. *J Physiol* **148**, 574-591, doi:10.1113/jphysiol.1959.sp006308 (1959).

10 Hubel, D. H. & Wiesel, T. N. Receptive fields, binocular interaction and functional architecture in the cat's visual cortex. *J Physiol* **160**, 106-154, doi:10.1113/jphysiol.1962.sp006837 (1962).

11 Bandyopadhyay, S., Shamma, S. A. & Kanold, P. O. Dichotomy of functional organization in the mouse auditory cortex. *Nat Neurosci* **13**, 361-368, doi:10.1038/nn.2490 (2010).

12 Rothschild, G., Nelken, I. & Mizrahi, A. Functional organization and population dynamics in the mouse primary auditory cortex. *Nat Neurosci* **13**, 353-360, doi:10.1038/nn.2484 (2010).

13 Wehr, M. & Zador, A. M. Synaptic mechanisms of forward suppression in rat auditory cortex. *Neuron* **47**, 437-445, doi:10.1016/j.neuron.2005.06.009 (2005).

14 Luna, R., Hernandez, A., Brody, C. D. & Romo, R. Neural codes for perceptual discrimination in primary somatosensory cortex. *Nat Neurosci* **8**, 1210-1219, doi:10.1038/nn1513 (2005).

15 Prsa, M., Morandell, K., Cuenu, G. & Huber, D. Feature-selective encoding of substrate vibrations in the forelimb somatosensory cortex. *Nature* **567**, 384-388, doi:10.1038/s41586-019-1015-8 (2019).

16 Helmchen, F. & Denk, W. Deep tissue two-photon microscopy. *Nature Methods* **2**, 932-940, doi:10.1038/nmeth818 (2005).

17 Tian, L., Hires, S. A. & Looger, L. L. Imaging neuronal activity with genetically encoded calcium indicators. *Cold Spring Harb Protoc* **2012**, 647-656, doi:10.1101/pdb.top069609 (2012).

18 Tian, L. *et al.* Imaging neural activity in worms, flies and mice with improved GCaMP calcium indicators. *Nat Methods* **6**, 875-881, doi:10.1038/nmeth.1398 (2009).

19 Bieler, M. *et al.* Rate and Temporal Coding Convey Multisensory Information in Primary Sensory Cortices. *eNeuro* **4**, doi:10.1523/ENEURO.0037-17.2017 (2017).

20 Ibrahim, L. A. *et al.* Cross-Modality Sharpening of Visual Cortical Processing through Layer-1-Mediated Inhibition and Disinhibition. *Neuron* **89**, 1031-1045, doi:10.1016/j.neuron.2016.01.027 (2016).

21 Petreanu, L. *et al.* Activity in motor–sensory projections reveals distributed coding in somatosensation. *Nature* **489**, 299-303, doi:10.1038/nature11321 (2012).

22 Xu, N. L. *et al.* Nonlinear dendritic integration of sensory and motor input during an active sensing task. *Nature* **492**, 247-251, doi:10.1038/nature11601 (2012).

23 Cooke, S. F., Komorowski, R. W., Kaplan, E. S., Gavornik, J. P. & Bear, M. F. Visual recognition memory, manifested as long-term habituation, requires synaptic plasticity in V1. *Nature Neuroscience* **18**, 262-271, doi:10.1038/nn.3920 (2015).

24 Grosso, A., Cambiaghi, M., Concina, G., Sacco, T. & Sacchetti, B. Auditory cortex involvement in emotional learning and memory. *Neuroscience* **299**, 45-55, doi:10.1016/j.neuroscience.2015.04.068 (2015).

25 Keller, G. B., Bonhoeffer, T. & Hubener, M. Sensorimotor mismatch signals in primary visual cortex of the behaving mouse. *Neuron* **74**, 809-815, doi:10.1016/j.neuron.2012.03.040 (2012).

26 Zhang, S. *et al.* Selective attention. Long-range and local circuits for top-down modulation of visual cortex processing. *Science* **345**, 660-665, doi:10.1126/science.1254126 (2014).

27 Ayaz, A., Saleem, A. B., Scholvinck, M. L. & Carandini, M. Locomotion controls spatial integration in mouse visual cortex. *Curr Biol* **23**, 890-894, doi:10.1016/j.cub.2013.04.012 (2013).

28 Dipoppa, M. *et al.* Vision and Locomotion Shape the Interactions between Neuron Types in Mouse Visual Cortex. *Neuron* **98**, 602-615.e608, doi:10.1016/j.neuron.2018.03.037 (2018).

29 Saleem, A. B., Ayaz, A., Jeffery, K. J., Harris, K. D. & Carandini, M. Integration of visual motion and locomotion in mouse visual cortex. *Nature Neuroscience* **16**, 1864-1869, doi:10.1038/nn.3567 (2013).

30 Stringer, C. *et al.* Spontaneous behaviors drive multidimensional, brainwide activity. *Science* **364**, 255, doi:10.1126/science.aav7893 (2019).

31 Stringer, C., Pachitariu, M., Steinmetz, N., Carandini, M. & Harris, K. D. High-dimensional geometry of population responses in visual cortex. *Nature* **571**, 361-365, doi:10.1038/s41586-019-1346-5 (2019).

32 Larkum, M. A cellular mechanism for cortical associations: an organizing principle for the cerebral cortex. *Trends Neurosci* **36**, 141-151, doi:10.1016/j.tins.2012.11.006 (2013).

33 Morgenstern, N. A., Bourg, J. & Petreanu, L. Multilaminar networks of cortical neurons integrate common inputs from sensory thalamus. *Nat Neurosci* **19**, 1034-1040, doi:10.1038/nn.4339 (2016).

34 Larkum, M. E. The yin and yang of cortical layer 1. *Nature Neuroscience* **16**, 114-115, doi:10.1038/nn.3317 (2013).

35 Lee, A. J. *et al.* Canonical Organization of Layer 1 Neuron-Led Cortical Inhibitory and Disinhibitory Interneuronal Circuits. *Cereb Cortex* **25**, 2114-2126, doi:10.1093/cercor/bhu020 (2015).

36 Bastos, A. M. *et al.* Canonical microcircuits for predictive coding. *Neuron* **76**, 695-711, doi:10.1016/j.neuron.2012.10.038 (2012).

37 Larkum, M. E., Senn, W. & Luscher, H. R. Top-down dendritic input increases the gain of layer 5 pyramidal neurons. *Cereb Cortex* **14**, 1059-1070, doi:10.1093/cercor/bhh065 (2004).

38 Manita, S. *et al.* A Top-Down Cortical Circuit for Accurate Sensory Perception. *Neuron* **86**, 1304-1316, doi:10.1016/j.neuron.2015.05.006 (2015).

39 DeFelipe, J. & Fariñas, I. The pyramidal neuron of the cerebral cortex: Morphological and chemical characteristics of the synaptic inputs. *Progress in Neurobiology* **39**, 563-607, doi:10.1016/0301-0082(92)90015-7 (1992).

40 Petreanu, L., Mao, T., Sternson, S. M. & Svoboda, K. The subcellular organization of neocortical excitatory connections. *Nature* **457**, 1142-1145, doi:10.1038/nature07709 (2009).

41 Petreanu, L., Mao, T., Sternson, S. M. & Svoboda, K. The subcellular organization of neocortical excitatory connections. *Nature* **457**, 1142-1145, doi:10.1038/nature07709 (2009).

42 Larkum, M. E., Zhu, J. J. & Sakmann, B. Dendritic mechanisms underlying the coupling of the dendritic with the axonal action potential initiation zone of adult rat layer 5 pyramidal neurons. *J Physiol* **533**, 447-466, doi:10.1111/j.1469-7793.2001.0447a.x (2001).

43 Major, G., Larkum, M. E. & Schiller, J. Active properties of neocortical pyramidal neuron dendrites. *Annu Rev Neurosci* **36**, 1-24, doi:10.1146/annurev-neuro-062111-150343 (2013).

44 Johnston, D., Magee, J. C., Colbert, C. M. & Cristie, B. R. Active properties of neuronal dendrites. *Annu Rev Neurosci* **19**, 165-186, doi:10.1146/annurev.ne.19.030196.001121 (1996).

45 Magee, J. C. Dendritic integration of excitatory synaptic input. *Nat Rev Neurosci* **1**, 181-190, doi:10.1038/35044552 (2000).

46 Stuart, G. J. & Spruston, N. Dendritic integration: 60 years of progress. *Nat Neurosci* **18**, 1713-1721, doi:10.1038/nn.4157 (2015).

47 Larkum, M. E., Kaiser, K. M. & Sakmann, B. Calcium electrogenesis in distal apical dendrites of layer 5 pyramidal cells at a critical frequency of back-propagating action potentials. *Proc Natl Acad Sci U S A* **96**, 14600-14604, doi:10.1073/pnas.96.25.14600 (1999).

48 Stuart, G., Spruston, N., Sakmann, B. & Häusser, M. Action potential initiation and backpropagation in neurons of the mammalian CNS. *Trends in Neurosciences* **20**, 125-131, doi:10.1016/s0166-2236(96)10075-8 (1997).

49 Stuart, G. J. & Hausser, M. Dendritic coincidence detection of EPSPs and action potentials. *Nat Neurosci* **4**, 63-71, doi:10.1038/82910 (2001).

50 Palmer, L. M. *et al.* NMDA spikes enhance action potential generation during sensory input. *Nat Neurosci* **17**, 383-390, doi:10.1038/nn.3646 (2014).

51 Nevian, T., Larkum, M. E., Polsky, A. & Schiller, J. Properties of basal dendrites of layer 5 pyramidal neurons: a direct patch-clamp recording study. *Nat Neurosci* **10**, 206-214, doi:10.1038/nn1826 (2007).

52 Polsky, A., Mel, B. & Schiller, J. Encoding and decoding bursts by NMDA spikes in basal dendrites of layer 5 pyramidal neurons. *J Neurosci* **29**, 11891-11903, doi:10.1523/JNEUROSCI.5250-08.2009 (2009).

53 Smith, S. L., Smith, I. T., Branco, T. & Hausser, M. Dendritic spikes enhance stimulus selectivity in cortical neurons in vivo. *Nature* **503**, 115-120, doi:10.1038/nature12600 (2013).

54 Beaulieu-Laroche, L., Toloza, E. H. S., Brown, N. J. & Harnett, M. T. Widespread and Highly Correlated Somato-dendritic Activity in Cortical Layer 5 Neurons. *Neuron* **103**, 235-241 e234, doi:10.1016/j.neuron.2019.05.014 (2019).

55 Voigts, J. & Harnett, M. T. Somatic and Dendritic Encoding of Spatial Variables in Retrosplenial Cortex Differs during 2D Navigation. *Neuron* **105**, 237-245 e234, doi:10.1016/j.neuron.2019.10.016 (2020).

56 Takahashi, N., Oertner, T. G., Hegemann, P. & Larkum, M. E. Active cortical dendrites modulate perception. *Science* **354**, 1587-1590, doi:10.1126/science.aah6066 (2016).

57 Ranganathan, G. N. *et al.* Active dendritic integration and mixed neocortical network representations during an adaptive sensing behavior. *Nature Neuroscience* **21**, 1583-1590, doi:10.1038/s41593-018-0254-6 (2018).

58 Lacefield, C. O., Pnevmatikakis, E. A., Paninski, L. & Bruno, R. M. Reinforcement Learning Recruits Somata and Apical Dendrites across Layers of Primary Sensory Cortex. *Cell Rep* **26**, 2000-2008 e2002, doi:10.1016/j.celrep.2019.01.093 (2019).

59 Sheffield, M. E. J., Adoff, M. D. & Dombeck, D. A. Increased Prevalence of Calcium Transients across the Dendritic Arbor during Place Field Formation. *Neuron* **96**, 490-504 e495, doi:10.1016/j.neuron.2017.09.029 (2017).

60 Schmidt-Hieber, C. & Hausser, M. Cellular mechanisms of spatial navigation in the medial entorhinal cortex. *Nat Neurosci* **16**, 325-331, doi:10.1038/nn.3340 (2013).

61 Bittner, K. C., Milstein, A. D., Grienberger, C., Romani, S. & Magee, J. C. Behavioral time scale synaptic plasticity underlies CA1 place fields. *Science* **357**, 1033-1036, doi:10.1126/science.aan3846 (2017).

62 Magee, J. C. & Johnston, D. A synaptically controlled, associative signal for Hebbian plasticity in hippocampal neurons. *Science* **275**, 209-213, doi:10.1126/science.275.5297.209 (1997).

63 Gambino, F. *et al.* Sensory-evoked LTP driven by dendritic plateau potentials in vivo. *Nature* **515**, 116-119, doi:10.1038/nature13664 (2014).

64 Hong, Y. K., Lacefield, C. O., Rodgers, C. C. & Bruno, R. M. Sensation, movement and learning in the absence of barrel cortex. *Nature* **561**, 542-546, doi:10.1038/s41586-018-0527-y (2018).

65 Brecht, M. The Body Model Theory of Somatosensory Cortex. *Neuron* **94**, 985-992, doi:10.1016/j.neuron.2017.05.018 (2017).

66 Diamond, M. E. & Arabzadeh, E. Whisker sensory system - from receptor to decision. *Prog Neurobiol* **103**, 28-40, doi:10.1016/j.pneurobio.2012.05.013 (2013).

67 Peron, S. P., Freeman, J., Iyer, V., Guo, C. & Svoboda, K. A Cellular Resolution Map of Barrel Cortex Activity during Tactile Behavior. *Neuron* **86**, 783-799, doi:10.1016/j.neuron.2015.03.027 (2015).

68 Kleinfeld, D., Ahissar, E. & Diamond, M. E. Active sensation: insights from the rodent vibrissa sensorimotor system. *Curr Opin Neurobiol* **16**, 435-444, doi:10.1016/j.conb.2006.06.009 (2006).

69 Sachidhanandam, S., Sreenivasan, V., Kyriakatos, A., Kremer, Y. & Petersen, C. C. Membrane potential correlates of sensory perception in mouse barrel cortex. *Nat Neurosci* **16**, 1671-1677, doi:10.1038/nn.3532 (2013).

70 Petersen, C. C. The functional organization of the barrel cortex. *Neuron* **56**, 339-355, doi:10.1016/j.neuron.2007.09.017 (2007).

71 Bjerre, A. S. & Palmer, L. M. Probing Cortical Activity During Head-Fixed Behavior. *Front Mol Neurosci* **13**, 30, doi:10.3389/fnmol.2020.00030 (2020).

72 Micallef, A. H., Takahashi, N., Larkum, M. E. & Palmer, L. M. A Reward-Based Behavioral Platform to Measure Neural Activity during Head-Fixed Behavior. *Front Cell Neurosci* **11**, 156, doi:10.3389/fncel.2017.00156 (2017).

73 Nikbakht, N., Tafreshiha, A., Zoccolan, D. & Diamond, M. E. Supralinear and Supramodal Integration of Visual and Tactile Signals in Rats: Psychophysics and Neuronal Mechanisms. *Neuron* **97**, 626-639 e628, doi:10.1016/j.neuron.2018.01.003 (2018).

74 Olcese, U., Iurilli, G. & Medini, P. Cellular and synaptic architecture of multisensory integration in the mouse neocortex. *Neuron* **79**, 579-593, doi:10.1016/j.neuron.2013.06.010 (2013).

75 Ghazanfar, A. A. & Schroeder, C. E. Is neocortex essentially multisensory? *Trends Cogn Sci* **10**, 278-285, doi:10.1016/j.tics.2006.04.008 (2006).

76 Henschke, J. U., Noesselt, T., Scheich, H. & Budinger, E. Possible anatomical pathways for short-latency multisensory integration processes in primary sensory cortices. *Brain Struct Funct* **220**, 955-977, doi:10.1007/s00429-013-0694-4 (2015).

77 Iurilli, G. *et al.* Sound-driven synaptic inhibition in primary visual cortex. *Neuron* **73**, 814-828, doi:10.1016/j.neuron.2011.12.026 (2012).

78 Rohe, T. & Noppeney, U. Distinct Computational Principles Govern Multisensory Integration in Primary Sensory and Association Cortices. *Curr Biol* **26**, 509-514, doi:10.1016/j.cub.2015.12.056 (2016).

79 Kato, H. K., Asinof, S. K. & Isaacson, J. S. Network-Level Control of Frequency Tuning in Auditory Cortex. *Neuron* **95**, 412-423 e414, doi:10.1016/j.neuron.2017.06.019 (2017).

80 Li, L. Y. *et al.* A feedforward inhibitory circuit mediates lateral refinement of sensory representation in upper layer 2/3 of mouse primary auditory cortex. *J Neurosci* **34**, 13670-13683, doi:10.1523/JNEUROSCI.1516-14.2014 (2014).

81 Dalmay, T. *et al.* A Critical Role for Neocortical Processing of Threat Memory. *Neuron* **104**, 1180-1194 e1187, doi:10.1016/j.neuron.2019.09.025 (2019).

82 Ceballo, S., Piwkowska, Z., Bourg, J., Daret, A. & Bathellier, B. Targeted Cortical Manipulation of Auditory Perception. *Neuron* **104**, 1168-1179.e1165, doi:10.1016/j.neuron.2019.09.043 (2019).

83 Francis, N. A. *et al.* Small Networks Encode Decision-Making in Primary Auditory Cortex. *Neuron* **97**, 885-897 e886, doi:10.1016/j.neuron.2018.01.019 (2018).

84 Schneider, D. M., Nelson, A. & Mooney, R. A synaptic and circuit basis for corollary discharge in the auditory cortex. *Nature* **513**, 189-194, doi:10.1038/nature13724 (2014).

85 Schneider, D. M., Sundararajan, J. & Mooney, R. A cortical filter that learns to suppress the acoustic consequences of movement. *Nature* **561**, 391-395, doi:10.1038/s41586-018-0520-5 (2018).

86 LeMessurier, A. M. & Feldman, D. E. Plasticity of population coding in primary sensory cortex. *Curr Opin Neurobiol* **53**, 50-56, doi:10.1016/j.conb.2018.04.029 (2018).

87 Recanzone, G. H., Merzenich, M. M., Jenkins, W. M., Grajski, K. A. & Dinse, H. R. Topographic reorganization of the hand representation in cortical area 3b owl monkeys trained in a frequency-discrimination task. *J Neurophysiol* **67**, 1031-1056, doi:10.1152/jn.1992.67.5.1031 (1992).

88 Recanzone, G. H., Schreiner, C. E. & Merzenich, M. M. Plasticity in the frequency representation of primary auditory cortex following discrimination training in adult owl monkeys. *The Journal of Neuroscience* **13**, 87-103, doi:10.1523/jneurosci.13-01-00087.1993 (1993).

89 Poort, J. *et al.* Learning Enhances Sensory and Multiple Non-sensory Representations in Primary Visual Cortex. *Neuron* **86**, 1478-1490, doi:10.1016/j.neuron.2015.05.037 (2015).

90 Gdalyahu, A. *et al.* Associative fear learning enhances sparse network coding in primary sensory cortex. *Neuron* **75**, 121-132, doi:10.1016/j.neuron.2012.04.035 (2012).

91 Kato, H. K., Gillet, S. N. & Isaacson, J. S. Flexible Sensory Representations in Auditory Cortex Driven by Behavioral Relevance. *Neuron* **88**, 1027-1039, doi:10.1016/j.neuron.2015.10.024 (2015).

92 Kass, M. D., Rosenthal, M. C., Pottackal, J. & McGann, J. P. Fear Learning Enhances Neural Responses to Threat-Predictive Sensory Stimuli. *Science* **342**, 1389-1392, doi:10.1126/science.1244916 (2013).

93 Li, W., Howard, J. D., Parrish, T. B. & Gottfried, J. A. Aversive learning enhances perceptual and cortical discrimination of indiscriminable odor cues. *Science* **319**, 1842-1845, doi:10.1126/science.1152837 (2008).

94 Grewe, B. F. *et al.* Neural ensemble dynamics underlying a long-term associative memory. *Nature* **543**, 670-675, doi:10.1038/nature21682 (2017).

95 Gillet, S. N., Kato, H. K., Justen, M. A., Lai, M. & Isaacson, J. S. Fear Learning Regulates Cortical Sensory Representations by Suppressing Habituation. *Frontiers in Neural Circuits* **11**, doi:10.3389/fncir.2017.00112 (2018).

96 Weinberger, N. M. Specific long-term memory traces in primary auditory cortex. *Nat Rev Neurosci* **5**, 279-290, doi:10.1038/nrn1366 (2004).

97 Yang, Y. *et al.* Selective synaptic remodeling of amygdalocortical connections associated with fear memory. *Nat Neurosci* **19**, 1348-1355, doi:10.1038/nn.4370 (2016).

98 Letzkus, J. J. *et al.* A disinhibitory microcircuit for associative fear learning in the auditory cortex. *Nature* **480**, 331-335, doi:10.1038/nature10674 (2011).

99 Abs, E. *et al.* Learning-Related Plasticity in Dendrite-Targeting Layer 1 Interneurons. *Neuron* **100**, 684-699 e686, doi:10.1016/j.neuron.2018.09.001 (2018).

100 Lovett-Barron, M. *et al.* Dendritic inhibition in the hippocampus supports fear learning. *Science* **343**, 857-863, doi:10.1126/science.1247485 (2014).

101 Dan, Y. & Poo, M. M. Spike timing-dependent plasticity: from synapse to perception. *Physiol Rev* **86**, 1033-1048, doi:10.1152/physrev.00030.2005 (2006).

102 Dan, Y. & Poo, M. M. Spike timing-dependent plasticity of neural circuits. *Neuron* **44**, 23-30, doi:10.1016/j.neuron.2004.09.007 (2004).

103 Caporale, N. & Dan, Y. Spike timing-dependent plasticity: a Hebbian learning rule. *Annu Rev Neurosci* **31**, 25-46, doi:10.1146/annurev.neuro.31.060407.125639 (2008).

104 Stuart, G. J. & Sakmann, B. Active propagation of somatic action potentials into neocortical pyramidal cell dendrites. *Nature* **367**, 69-72, doi:10.1038/367069a0 (1994).

105 Frick, A., Magee, J. & Johnston, D. LTP is accompanied by an enhanced local excitability of pyramidal neuron dendrites. *Nat Neurosci* **7**, 126-135, doi:10.1038/nn1178 (2004).

106 Kampa, B. M., Letzkus, J. J. & Stuart, G. J. Dendritic mechanisms controlling spike-timing-dependent synaptic plasticity. *Trends Neurosci* **30**, 456-463, doi:10.1016/j.tins.2007.06.010 (2007).

107 Letzkus, J. J., Kampa, B. M. & Stuart, G. J. Learning rules for spike timing-dependent plasticity depend on dendritic synapse location. *J Neurosci* **26**, 10420-10429, doi:10.1523/JNEUROSCI.2650-06.2006 (2006).

108 Kampa, B. M., Letzkus, J. J. & Stuart, G. J. Requirement of dendritic calcium spikes for induction of spike-timing-dependent synaptic plasticity. *J Physiol* **574**, 283-290, doi:10.1113/jphysiol.2006.111062 (2006).

109 Remy, S. & Spruston, N. Dendritic spikes induce single-burst long-term potentiation. *Proc Natl Acad Sci U S A* **104**, 17192-17197, doi:10.1073/pnas.0707919104 (2007).

110 Brandalise, F., Carta, S., Helmchen, F., Lisman, J. & Gerber, U. Dendritic NMDA spikes are necessary for timing-dependent associative LTP in CA3 pyramidal cells. *Nat Commun* **7**, 13480, doi:10.1038/ncomms13480 (2016).

111 Sandler, M., Shulman, Y. & Schiller, J. A Novel Form of Local Plasticity in Tuft Dendrites of Neocortical Somatosensory Layer 5 Pyramidal Neurons. *Neuron* **90**, 1028-1042, doi:10.1016/j.neuron.2016.04.032 (2016).

112 Cichon, J. & Gan, W. B. Branch-specific dendritic Ca(2+) spikes cause persistent synaptic plasticity. *Nature* **520**, 180-185, doi:10.1038/nature14251 (2015).

113 Meijer, G. T., Pie, J. L., Dolman, T. L., Pennartz, C. M. A. & Lansink, C. S. Audiovisual Integration Enhances Stimulus Detection Performance in Mice. *Front Behav Neurosci* **12**, 231, doi:10.3389/fnbeh.2018.00231 (2018).

114 Raposo, D., Sheppard, J. P., Schrater, P. R. & Churchland, A. K. Multisensory decision-making in rats and humans. *J Neurosci* **32**, 3726-3735, doi:10.1523/JNEUROSCI.4998-11.2012 (2012).

115 Wimmer, R. D. *et al.* Thalamic control of sensory selection in divided attention. *Nature* **526**, 705-709, doi:10.1038/nature15398 (2015).

116 Winters, B. D. & Reid, J. M. A distributed cortical representation underlies crossmodal object recognition in rats. *J Neurosci* **30**, 6253-6261, doi:10.1523/JNEUROSCI.6073-09.2010 (2010).

117 Meredith, M. A. & Stein, B. E. Visual, auditory, and somatosensory convergence on cells in superior colliculus results in multisensory integration. *J Neurophysiol* **56**, 640-662, doi:10.1152/jn.1986.56.3.640 (1986).

118 Driver, J. Enhancement of selective listening by illusory mislocation of speech sounds due to lip-reading. *Nature* **381**, 66-68, doi:10.1038/381066a0 (1996).

119 Stein, B. E. & Stanford, T. R. Multisensory integration: current issues from the perspective of the single neuron. *Nat Rev Neurosci* **9**, 255-266, doi:10.1038/nrn2331 (2008).

120 Gamanut, R. *et al.* The Mouse Cortical Connectome, Characterized by an Ultra-Dense Cortical Graph, Maintains Specificity by Distinct Connectivity Profiles. *Neuron* **97**, 698-715 e610, doi:10.1016/j.neuron.2017.12.037 (2018).

121 Falchier, A., Clavagnier, S., Barone, P. & Kennedy, H. Anatomical evidence of multimodal integration in primate striate cortex. *J Neurosci* **22**, 5749-5759, doi:20026562 (2002).

122 Bizley, J. K., Nodal, F. R., Bajo, V. M., Nelken, I. & King, A. J. Physiological and anatomical evidence for multisensory interactions in auditory cortex. *Cerebral cortex* **17**, 2172-2189, doi:10.1093/cercor/bhl128 (2007).

123 Attinger, A., Wang, B. & Keller, G. B. Visuomotor Coupling Shapes the Functional Development of Mouse Visual Cortex. *Cell* **169**, 1291-1302 e1214, doi:10.1016/j.cell.2017.05.023 (2017).

124 Larkum, M. E., Zhu, J. J. & Sakmann, B. A new cellular mechanism for coupling inputs arriving at different cortical layers. *Nature* **398**, 338-341, doi:10.1038/18686 (1999).

125 Helmchen, F., Svoboda, K., Denk, W. & Tank, D. W. In vivo dendritic calcium dynamics in deep-layer cortical pyramidal neurons. *Nat Neurosci* **2**, 989-996, doi:10.1038/14788 (1999).

126 Stuart, G., Schiller, J. & Sakmann, B. Action potential initiation and propagation in rat neocortical pyramidal neurons. *J Physiol* **505 (Pt 3)**, 617-632 (1997).

127 Golding, N. L., Staff, N. P. & Spruston, N. Dendritic spikes as a mechanism for cooperative long-term potentiation. *Nature* **418**, 326-331, doi:10.1038/nature00854 (2002).

128 Losonczy, A., Makara, J. K. & Magee, J. C. Compartmentalized dendritic plasticity and input feature storage in neurons. *Nature* **452**, 436-441, doi:10.1038/nature06725 (2008).

129 Lavzin, M., Rapoport, S., Polsky, A., Garion, L. & Schiller, J. Nonlinear dendritic processing determines angular tuning of barrel cortex neurons in vivo. *Nature* **490**, 397-401, doi:10.1038/nature11451

nature11451 [pii] (2012).

130 Harnett, M. T., Xu, N. L., Magee, J. C. & Williams, S. R. Potassium channels control the interaction between active dendritic integration compartments in layer 5 cortical pyramidal neurons. *Neuron* **79**, 516-529, doi:10.1016/j.neuron.2013.06.005 (2013).

131 Ranganathan, G. N. *et al.* Active dendritic integration and mixed neocortical network representations during an adaptive sensing behavior. *Nat Neurosci* **21**, 1583-1590, doi:10.1038/s41593-018-0254-6 (2018).

132 Quiquempoix, M. *et al.* Layer 2/3 Pyramidal Neurons Control the Gain of Cortical Output. *Cell Rep* **24**, 2799-2807 e2794, doi:10.1016/j.celrep.2018.08.038 (2018).

133 Lefort, S., Tomm, C., Floyd Sarria, J. C. & Petersen, C. C. The excitatory neuronal network of the C2 barrel column in mouse primary somatosensory cortex. *Neuron* **61**, 301-316, doi:10.1016/j.neuron.2008.12.020 (2009).

134 Petreanu, L., Huber, D., Sobczyk, A. & Svoboda, K. Channelrhodopsin-2-assisted circuit mapping of long-range callosal projections. *Nat Neurosci* **10**, 663-668, doi:10.1038/nn1891 (2007).

135 Yamashita, T. *et al.* Diverse Long-Range Axonal Projections of Excitatory Layer 2/3 Neurons in Mouse Barrel Cortex. *Front Neuroanat* **12**, 33, doi:10.3389/fnana.2018.00033 (2018).

136 Oh, S. W. *et al.* A mesoscale connectome of the mouse brain. *Nature* **508**, 207-214, doi:10.1038/nature13186 (2014).

137 Dewson, J. H., 3rd, Cowey, A. & Weiskrantz, L. Disruptions of auditory sequence discrimination by unilateral and bilateral cortical ablations of superior temporal gyrus in the monkey. *Experimental neurology* **28**, 529-548 (1970).

138 Winans, S. S. Visual form discrimination after removal of the visual cortex in cats. *Science* **158**, 944-946 (1967).

139 Felleman, D. J. & Van Essen, D. C. Distributed hierarchical processing in the primate cerebral cortex. *Cerebral cortex* **1**, 1-47 (1991).

140 Kuypers, H. G., Szwarcbart, M. K., Mishkin, M. & Rosvold, H. E. Occipitotemporal Corticocortical Connections in the Rhesus Monkey. *Experimental neurology* **11**, 245-262 (1965).

141 Higley, M. J. & Contreras, D. Balanced excitation and inhibition determine spike timing during frequency adaptation. *J Neurosci* **26**, 448-457, doi:10.1523/JNEUROSCI.3506-05.2006 (2006).

142 Priebe, N. J. & Ferster, D. Mechanisms underlying cross-orientation suppression in cat visual cortex. *Nat Neurosci* **9**, 552-561, doi:10.1038/nn1660 (2006).

143 Williams, S. R. Spatial compartmentalization and functional impact of conductance in pyramidal neurons. *Nat Neurosci* **7**, 961-967, doi:10.1038/nn1305 (2004).

144 Beaulieu-Laroche, L. *et al.* Enhanced Dendritic Compartmentalization in Human Cortical Neurons. *Cell* **175**, 643-651 e614, doi:10.1016/j.cell.2018.08.045 (2018).

145 Morrill, R. J. & Hasenstaub, A. R. Visual Information Present in Infragranular Layers of Mouse Auditory Cortex. *J Neurosci* **38**, 2854-2862, doi:10.1523/JNEUROSCI.3102-17.2018 (2018).

146 Hooks, B. M. *et al.* Organization of cortical and thalamic input to pyramidal neurons in mouse motor cortex. *J Neurosci* **33**, 748-760, doi:10.1523/JNEUROSCI.4338-12.2013 (2013).

147 Palmer, L. M. *et al.* The cellular basis of GABA(B)-mediated interhemispheric inhibition. *Science* **335**, 989-993, doi:335/6071/989 [pii]
10.1126/science.1217276 (2012).

148 Schiller, J., Schiller, Y., Stuart, G. & Sakmann, B. Calcium action potentials restricted to distal apical dendrites of rat neocortical pyramidal neurons. *J Physiol* **505 (Pt 3)**, 605-616 (1997).

149 Larkum, M. E., Nevian, T., Sandler, M., Polsky, A. & Schiller, J. Synaptic integration in tuft dendrites of layer 5 pyramidal neurons: a new unifying principle. *Science* **325**, 756-760, doi:325/5941/756 [pii]
10.1126/science.1171958 (2009).

150 Schiller, J., Major, G., Koester, H. J. & Schiller, Y. NMDA spikes in basal dendrites of cortical pyramidal neurons. *Nature* **404**, 285-289, doi:10.1038/35005094 (2000).

151 Polsky, A., Mel, B. W. & Schiller, J. Computational subunits in thin dendrites of pyramidal cells. *Nat Neurosci* **7**, 621-627, doi:10.1038/nn1253
nn1253 [pii] (2004).

152 Boly, M. *et al.* Preserved feedforward but impaired top-down processes in the vegetative state. *Science* **332**, 858-862, doi:332/6031/858 [pii]
10.1126/science.1202043 (2011).

153 Guo, Z. V. *et al.* Flow of cortical activity underlying a tactile decision in mice. *Neuron* **81**, 179-194, doi:10.1016/j.neuron.2013.10.020
S0896-6273(13)00924-0 [pii] (2014).

154 Siemann, J. K. *et al.* A novel behavioral paradigm to assess multisensory processing in mice. *Front Behav Neurosci* **8**, 456, doi:10.3389/fnbeh.2014.00456 (2014).

155 Tang, C. C. *et al.* Decreased firing of striatal neurons related to licking during acquisition and overtraining of a licking task. *J Neurosci* **29**, 13952-13961, doi:10.1523/JNEUROSCI.2824-09.2009 (2009).

156 Vecchia, D. *et al.* Temporal Sharpening of Sensory Responses by Layer V in the Mouse Primary Somatosensory Cortex. *Curr Biol*, doi:10.1016/j.cub.2020.02.004 (2020).

157 Holtmaat, A. *et al.* Long-term, high-resolution imaging in the mouse neocortex through a chronic cranial window. *Nat Protoc* **4**, 1128-1144, doi:10.1038/nprot.2009.89
nprot.2009.89 [pii] (2009).

158 Wiegert, J. S., Mahn, M., Prigge, M., Printz, Y. & Yizhar, O. Silencing Neurons: Tools, Applications, and Experimental Constraints. *Neuron* **95**, 504-529, doi:10.1016/j.neuron.2017.06.050 (2017).

159 Herry, C. & Johansen, J. P. Encoding of fear learning and memory in distributed neuronal circuits. *Nat Neurosci* **17**, 1644-1654, doi:10.1038/nn.3869 (2014).

160 Quirk, G. J., Repa, C. & LeDoux, J. E. Fear conditioning enhances short-latency auditory responses of lateral amygdala neurons: parallel recordings in the freely behaving rat. *Neuron* **15**, 1029-1039, doi:10.1016/0896-6273(95)90092-6 (1995).

161 Lacefield, C. O., Pnevmatikakis, E. A., Paninski, L. & Bruno, R. M. Reinforcement Learning Recruits Somata and Apical Dendrites across Layers of Primary Sensory Cortex. *Cell Reports* **26**, 2000-2008.e2002, doi:10.1016/j.celrep.2019.01.093 (2019).

162 Bakin, J. S. & Weinberger, N. M. Classical conditioning induces CS-specific receptive field plasticity in the auditory cortex of the guinea pig. *Brain Res* **536**, 271-286, doi:10.1016/0006-8993(90)90035-a (1990).

163 Edeline, J. M., Pham, P. & Weinberger, N. M. Rapid development of learning-induced receptive field plasticity in the auditory cortex. *Behav Neurosci* **107**, 539-551, doi:10.1037//0735-7044.107.4.539 (1993).

164 Moczulska, K. E. *et al.* Dynamics of dendritic spines in the mouse auditory cortex during memory formation and memory recall. *Proc Natl Acad Sci U S A* **110**, 18315-18320, doi:10.1073/pnas.1312508110 (2013).

165 Bannister, A. P. Inter- and intra-laminar connections of pyramidal cells in the neocortex. *Neurosci Res* **53**, 95-103, doi:10.1016/j.neures.2005.06.019 (2005).

166 Schiller, J. & Schiller, Y. NMDA receptor-mediated dendritic spikes and coincident signal amplification. *Curr Opin Neurobiol* **11**, 343-348, doi:S0959-4388(00)00217-8 [pii] (2001).

167 Palmer, L. M. Dendritic integration in pyramidal neurons during network activity and disease. *Brain Res Bull* **103**, 2-10, doi:10.1016/j.brainresbull.2013.09.010 (2014).

168 Romanski, L. M. & LeDoux, J. E. Equipotentiality of thalamo-amygdala and thalamo-cortico-amygdala circuits in auditory fear conditioning. *The Journal of Neuroscience* **12**, 4501-4509, doi:10.1523/jneurosci.12-11-04501.1992 (1992).

169 Lai, C. S. W., Adler, A. & Gan, W. B. Fear extinction reverses dendritic spine formation induced by fear conditioning in the mouse auditory cortex. *Proc Natl Acad Sci U S A* **115**, 9306-9311, doi:10.1073/pnas.1801504115 (2018).

170 Kerlin, A. *et al.* Functional clustering of dendritic activity during decision-making. *Elife* **8**, doi:10.7554/eLife.46966 (2019).

171 Francioni, V., Padamsey, Z. & Rochefort, N. L. High and asymmetric somato-dendritic coupling of V1 layer 5 neurons independent of visual stimulation and locomotion. *Elife* **8**, doi:10.7554/eLife.49145 (2019).

172 Quirk, G. J., Armony, J. L. & LeDoux, J. E. Fear Conditioning Enhances Different Temporal Components of Tone-Evoked Spike Trains in Auditory Cortex and Lateral Amygdala. *Neuron* **19**, 613-624, doi:10.1016/s0896-6273(00)80375-x (1997).

173 Jia, H., Rochefort, N. L., Chen, X. & Konnerth, A. Dendritic organization of sensory input to cortical neurons in vivo. *Nature* **464**, 1307-1312, doi:10.1038/nature08947 (2010).

174 Häusser, M. & Mel, B. Dendrites: bug or feature? *Current Opinion in Neurobiology* **13**, 372-383, doi:10.1016/s0959-4388(03)00075-8 (2003).

175 Poirazi, P., Brannon, T. & Mel, B. W. Pyramidal Neuron as Two-Layer Neural Network. *Neuron* **37**, 989-999, doi:10.1016/s0896-6273(03)00149-1 (2003).

176 Chu, M. W., Li, W. L. & Komiyama, T. Balancing the Robustness and Efficiency of Odor Representations during Learning. *Neuron* **92**, 174-186, doi:10.1016/j.neuron.2016.09.004 (2016).

177 Otazu, G. H., Tai, L. H., Yang, Y. & Zador, A. M. Engaging in an auditory task suppresses responses in auditory cortex. *Nat Neurosci* **12**, 646-654, doi:10.1038/nn.2306 (2009).

178 Alain, C., Snyder, J. S., He, Y. & Reinke, K. S. Changes in auditory cortex parallel rapid perceptual learning. *Cereb Cortex* **17**, 1074-1084, doi:10.1093/cercor/bhl018 (2007).

179 Blake, D. T., Heiser, M. A., Caywood, M. & Merzenich, M. M. Experience-dependent adult cortical plasticity requires cognitive association between sensation and reward. *Neuron* **52**, 371-381, doi:10.1016/j.neuron.2006.08.009 (2006).

180 Brown, M., Irvine, D. R. & Park, V. N. Perceptual learning on an auditory frequency discrimination task by cats: association with changes in primary auditory cortex. *Cereb Cortex* **14**, 952-965, doi:10.1093/cercor/bhh056 (2004).

181 Fritz, J. B., Elhilali, M. & Shamma, S. A. Differential dynamic plasticity of A1 receptive fields during multiple spectral tasks. *J Neurosci* **25**, 7623-7635, doi:10.1523/JNEUROSCI.1318-05.2005 (2005).

182 Polley, D. B., Steinberg, E. E. & Merzenich, M. M. Perceptual learning directs auditory cortical map reorganization through top-down influences. *J Neurosci* **26**, 4970-4982, doi:10.1523/JNEUROSCI.3771-05.2006 (2006).

183 Rutkowski, R. G. & Weinberger, N. M. Encoding of learned importance of sound by magnitude of representational area in primary auditory cortex. *Proc Natl Acad Sci U S A* **102**, 13664-13669, doi:10.1073/pnas.0506838102 (2005).

184 Holthoff, K., Kovalchuk, Y. & Konnerth, A. Dendritic spikes and activity-dependent synaptic plasticity. *Cell Tissue Res* **326**, 369-377, doi:10.1007/s00441-006-0263-8 (2006).

185 Holthoff, K., Kovalchuk, Y., Yuste, R. & Konnerth, A. Single-shock LTD by local dendritic spikes in pyramidal neurons of mouse visual cortex. *J Physiol* **560**, 27-36, doi:10.1113/jphysiol.2004.072678 (2004).

186 Mohan, H. *et al.* Sensory representation of an auditory cued tactile stimulus in the posterior parietal cortex of the mouse. *Sci Rep* **8**, 7739, doi:10.1038/s41598-018-25891-x (2018).

187 Zhong, L. *et al.* Causal contributions of parietal cortex to perceptual decision-making during stimulus categorization. *Nat Neurosci* **22**, 963-973, doi:10.1038/s41593-019-0383-6 (2019).

188 Pinto, L. & Dan, Y. Cell-Type-Specific Activity in Prefrontal Cortex during Goal-Directed Behavior. *Neuron* **87**, 437-450, doi:10.1016/j.neuron.2015.06.021 (2015).

189 Le Merre, P. *et al.* Reward-Based Learning Drives Rapid Sensory Signals in Medial Prefrontal Cortex and Dorsal Hippocampus Necessary for Goal-Directed Behavior. *Neuron* **97**, 83-91 e85, doi:10.1016/j.neuron.2017.11.031 (2018).

190 Rogan, M. T., Staubli, U. V. & LeDoux, J. E. Fear conditioning induces associative long-term potentiation in the amygdala. *Nature* **390**, 604-607, doi:10.1038/37601 (1997).

191 Bissiere, S., Humeau, Y. & Luthi, A. Dopamine gates LTP induction in lateral amygdala by suppressing feedforward inhibition. *Nat Neurosci* **6**, 587-592, doi:10.1038/nn1058 (2003).

192 Mahanty, N. K. & Sah, P. Calcium-permeable AMPA receptors mediate long-term potentiation in interneurons in the amygdala. *Nature* **394**, 683-687, doi:10.1038/29312 (1998).

193 Sun, Y., Gooch, H. & Sah, P. Fear conditioning and the basolateral amygdala. *F1000Res* **9**, doi:10.12688/f1000research.21201.1 (2020).

194 Sah, P., Westbrook, R. F. & Luthi, A. Fear conditioning and long-term potentiation in the amygdala: what really is the connection? *Ann N Y Acad Sci* **1129**, 88-95, doi:10.1196/annals.1417.020 (2008).

195 Manita, S., Miyakawa, H., Kitamura, K. & Murayama, M. Dendritic Spikes in Sensory Perception. *Front Cell Neurosci* **11**, 29, doi:10.3389/fncel.2017.00029 (2017).

196 Ujfalussy, B. B., Makara, J. K., Lengyel, M. & Branco, T. Global and Multiplexed Dendritic Computations under In Vivo-like Conditions. *Neuron* **100**, 579-592 e575, doi:10.1016/j.neuron.2018.08.032 (2018).

197 Reyes, A. Influence of dendritic conductances on the input-output properties of neurons. *Annu Rev Neurosci* **24**, 653-675, doi:10.1146/annurev.neuro.24.1.653 (2001).

198 Harris, K. D. & Shepherd, G. M. The neocortical circuit: themes and variations. *Nat Neurosci* **18**, 170-181, doi:10.1038/nn.3917 (2015).

199 Gidon, A. *et al.* Dendritic action potentials and computation in human layer 2/3 cortical neurons. *Science* **367**, 83-87, doi:10.1126/science.aax6239 (2020).

200 Ferguson, K. A. & Cardin, J. A. Mechanisms underlying gain modulation in the cortex. *Nat Rev Neurosci* **21**, 80-92, doi:10.1038/s41583-019-0253-y (2020).

201 Pluta, S. R., Telian, G. I., Naka, A. & Adesnik, H. Superficial Layers Suppress the Deep Layers to Fine-tune Cortical Coding. *J Neurosci* **39**, 2052-2064, doi:10.1523/JNEUROSCI.1459-18.2018 (2019).

202 Dana, H. *et al.* High-performance calcium sensors for imaging activity in neuronal populations and microcompartments. *Nat Methods* **16**, 649-657, doi:10.1038/s41592-019-0435-6 (2019).

203 Chen, T. W. *et al.* Ultrasensitive fluorescent proteins for imaging neuronal activity. *Nature* **499**, 295-300, doi:10.1038/nature12354 (2013).

204 Grewe, B. F., Voigt, F. F., van 't Hoff, M. & Helmchen, F. Fast two-layer two-photon imaging of neuronal cell populations using an electrically tunable lens. *Biomed Opt Express* **2**, 2035-2046, doi:10.1364/BOE.2.002035 (2011).

205 Abdelfattah, A. S. *et al.* Bright and photostable chemigenetic indicators for extended in vivo voltage imaging. *Science* **365**, 699-704, doi:10.1126/science.aav6416 (2019).

206 Villette, V. *et al.* Ultrafast Two-Photon Imaging of a High-Gain Voltage Indicator in Awake Behaving Mice. *Cell* **179**, 1590-1608 e1523, doi:10.1016/j.cell.2019.11.004 (2019).

207 Wu, J. *et al.* Kilohertz two-photon fluorescence microscopy imaging of neural activity in vivo. *Nat Methods* **17**, 287-290, doi:10.1038/s41592-020-0762-7 (2020).

208 Kazemipour, A. *et al.* Kilohertz frame-rate two-photon tomography. *Nat Methods* **16**, 778-786, doi:10.1038/s41592-019-0493-9 (2019).

209 Lu, R. *et al.* Rapid mesoscale volumetric imaging of neural activity with synaptic resolution. *Nat Methods* **17**, 291-294, doi:10.1038/s41592-020-0760-9 (2020).

210 Bouchard, M. B. *et al.* Swept confocally-aligned planar excitation (SCAPE) microscopy for high speed volumetric imaging of behaving organisms. *Nat Photonics* **9**, 113-119, doi:10.1038/nphoton.2014.323 (2015).

211 Gordon, U., Polsky, A. & Schiller, J. Plasticity compartments in basal dendrites of neocortical pyramidal neurons. *J Neurosci* **26**, 12717-12726, doi:10.1523/JNEUROSCI.3502-06.2006 (2006).

212 Johnston, D. *et al.* Active dendrites, potassium channels and synaptic plasticity. *Philos Trans R Soc Lond B Biol Sci* **358**, 667-674, doi:10.1098/rstb.2002.1248 (2003).

APPENDIX

In this appendix I show the two main codes used to analyse the calcium imaging data. The codes were custom written by myself on MATLAB.

Calculation of the dF/F:

```
freqAcq = 30;
preStim = 6;
stimOn = round(freqAcq * preStim);
nRois = size(roimeans{1,1},1);
nTrials = size(roimeans,2)
dffmat = cell (nTrials,nRois);

for i = 1:nTrials
  Roistrace = cell2mat(roimeans(i));
  for j = 1:nRois
     ftrace = (Roistrace(j,:));
     fo = median(ftrace(1:stimOn));
     df = ftrace - fo;
     dff= sgolayfilt((df./fo),2,7);
     dffmat{i,j} = dff;
  end
end
```

Ca^{2+} events detection:

```
%% SET YOUR PARAMETERS HERE

stimOn = 120;
stimOff = 140;
peakdetect = 150;
eventduration = 15;
peakDistance = 30;
peakWidth = 1;
baseline = 1:stimOn;

%% MAIN LOOP

for i = 1:nRois
   for k = 1:nTrials

      rise_edge = 0;
      fall_edge = 0;

      ftrace = dffmat{k,i};                    threshold = 3 * (std(ftrace(baseline)));
sup_ftrace = ftrace > threshold;
      diff_sup_ftrace = diff(sup_ftrace
      rise_edge = find(diff_sup_ftrace == 1);          fall_edge = find(diff_sup_ftrace == -1);
       a = size(rise_edge); a = a(2);
       b = size(fall_edge); b = b(2);
       if a > b
         rise_edge = rise_edge(1:end-1);
       elseif b > a
         fall_edge(1) = [];
       end

      diff_sup_ftrace (rise_edge) = rise_edge;
      diff_sup_ftrace (fall_edge) = fall_edge;
      detect_event = (fall_edge - rise_edge) > eventduration ;       diff_sup_ftrace(rise_edge)
= detect_event;
      diff_sup_ftrace (fall_edge) = 0 ;


       if sum(detect_event) == 0
         diff_sup_ftrace  = zeros (1,size(ftrace,2));
       end
```

```
        spk = diff_sup_ftrace ;
              nspk = sum(spk(stimOn:stimOff));

        if nspk > nTrials
           disp('-->indexing problem, double check diff_sup_ftrace vector')
        end

        ampl=0;
        locs=0;

        if nspk > 0
           diff_sup_ftrace = ftrace;

          [ampl,locs] = findpeaks(ftrace(stimOn:peakdetect),'MinPeakheight',threshold
,'MinPeakDistance',peakDistance, 'MinPeakWidth',peakWidth,
'Annotate','extents','WidthReference','halfheight');


          figure;
          findpeaks(ftrace,'MinPeakheight',threshold,
'MinPeakDistance',peakDistance,'MinPeakWidth',peakWidth,'Annotate','extents','WidthRefer
ence','halfheight');
          hold on;
          plot (locs+ stimOn , ampl +0.1 , 'o','MarkerSize',10,'MarkerFaceColor','r');
          title(['Roi ', num2str(i) ' Trial ', num2str(k)]);

        end
end
end
```